

September 8, 2011

Document Control Desk
U. S. Nuclear Regulatory Commission
11555 Rockville Pike
Rockville, MD 20852

Attention: Andrew Hon

Subject: Project No. 704 – BWRVIP Response to NRC Request for Additional Information on BWRVIP-194

- References:
1. Letter from Joseph F. Williams (NRC) to Mr. Rick Libra (BWRVIP Chairman), "Acceptance Review of Boiling Water Reactor Vessel and Internals Project (BWRVIP)-194, Methodology for Demonstrating Steam Dryer Integrity for Power Uprate (TAC NO. ME0317)," dated June 30, 2009.
 2. Letter from Eric E. Bowman (NRC) to Mr. Rick Libra (BWRVIP Chairman), "Request for Additional Information Re: Boiling Water Reactor Vessel and Internals Project (BWRVIP)-194, Methodologies for Demonstrating Steam Dryer Integrity for Power Uprate (TAC NO. ME0317)," dated March 25, 2010.

Enclosed are:

1. Five (5) copies of LTR-A&SA-11-47-P, Responses to NRC Request for Additional Information on BWRVIP-194: BWR Vessel and Internals Project Methodologies for Demonstrating Steam Dryer Integrity for Power Uprate (Proprietary)
2. Two (2) copies of LTR-A&SA-11-47-NP, Responses to NRC Request for Additional Information on BWRVIP-194: BWR Vessel and Internals Project Methodologies for Demonstrating Steam Dryer Integrity for Power Uprate (Non-Proprietary)

The Requests for Additional Information (RAIs) were transmitted to the BWRVIP by the NRC letters referenced above. Each item in the RAI is repeated verbatim in the enclosed response followed by the BWRVIP response to that item.

Also enclosed is the Westinghouse Application for Withholding Proprietary Information from Public Disclosure CAW-11-3239, accompanying Affidavit, Proprietary Information Notice, and Copyright Notice.

As Item 1 contains information proprietary to Westinghouse Electric Company LLC, it is supported by an affidavit signed by Westinghouse, the owner of the information. The affidavit sets forth the basis on which the information may be withheld from public disclosure by the Commission and addresses with specificity the considerations listed in paragraph (b)(4) of Together . . . Shaping the Future of Electricity

PALO ALTO OFFICE

3420 Hillview Avenue, Palo Alto, CA 94304-1395 USA • 650.855.2000 • Customer Service 800.313.3774 • www.epri.com

Additional copies sent
to PM

G004
NAR

Section 2.390 of the Commission's regulations. Brackets are used to identify the proprietary information in the enclosed responses. An EPRI letter requesting that the proprietary responses be withheld from public disclosure is also enclosed.

Correspondence with respect to the copyright or proprietary aspects of the items listed above or the supporting Westinghouse affidavit should reference CAW-11-3239 and should be addressed to J. A. Gresham, Manager, Regulatory Compliance, Westinghouse Electric Company LLC, Suite 428, 1000 Westinghouse Drive, Cranberry Township, Pennsylvania 16066.

Sincerely,

A handwritten signature in black ink, appearing to read 'D. Czufin', with a stylized flourish at the end.

Dave Czufin
Exelon
Chairman, BWR Vessel and Internals Project

September 6, 2011

Document Control Desk
Office of Nuclear Reactor Regulation
U.S. Nuclear Regulatory Commission
Washington, DC 20555-0001

Subject: Request for Withholding of the following Proprietary Document:

Responses to NRC Request for Additional Information on
BWRVIP-194: BWR Vessel and Internals Project Methodologies for Demonstrating
Steam Dryer Integrity for Power Uprate

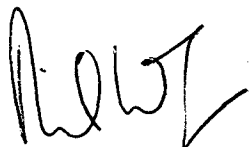
To Whom It May Concern:

This is a request under 10 C.F.R. §2.390(a)(4) that the U.S. Nuclear Regulatory Commission ("NRC") withhold from public disclosure the information identified in the enclosed Affidavit consisting of the proprietary information owned by Westinghouse Electric Company LLC, identified in the above ("Report"). Proprietary and non-proprietary versions of the Report and the Affidavit in support of this request are enclosed.

EPRI desires to disclose the Report in confidence as a means of exchanging technical information with the NRC. The Report is not to be divulged to anyone outside of the NRC or to any of its contractors, nor shall any copies be made of the Report provided herein. EPRI welcomes any discussions and/or questions relating to the information enclosed.

If you have any questions about the legal aspects of this request for withholding, please do not hesitate to contact me at (704) 704-595-2732. Questions on the content of the Report should be directed to **John Hosler** of EPRI at (704) 595-2720.

Sincerely,





Westinghouse Electric Company
Nuclear Services
1000 Westinghouse Drive
Cranberry Township, Pennsylvania 16066
USA

U.S. Nuclear Regulatory Commission
Document Control Desk
11555 Rockville Pike
Rockville, MD 20852

Direct tel: (412) 374-4643
Direct fax: (724) 720-0754
e-mail: greshaja@westinghouse.com
Proj Letter: LTR-A&SA-11-49

CAW-11-3239

September 2, 2011

APPLICATION FOR WITHHOLDING PROPRIETARY
INFORMATION FROM PUBLIC DISCLOSURE

Subject: LTR-A&SA-11-47-P, Responses to NRC Request for Additional Information on
BWRVIP-194: BWR Vessel and Internals Project Methodologies for Demonstrating Steam
Dryer Integrity for Power Uprate (Proprietary)

The proprietary information for which withholding is being requested in the above-referenced report is further identified in Affidavit CAW-11-3239 signed by the owner of the proprietary information, Westinghouse Electric Company LLC. The affidavit, which accompanies this letter, sets forth the basis on which the information may be withheld from public disclosure by the Commission and addresses with specificity the considerations listed in paragraph (b)(4) of 10 CFR Section 2.390 of the Commission's regulations.

Accordingly, this letter authorizes the utilization of the accompanying affidavit by Electric Power Research Institute (EPRI).

Correspondence with respect to the proprietary aspects of the application for withholding or the Westinghouse affidavit should reference this letter, CAW-11-3239, and should be addressed to J. A. Gresham, Manager, Regulatory Compliance, Westinghouse Electric Company LLC, Suite 428, 1000 Westinghouse Drive, Cranberry Township, Pennsylvania 16066.

Very truly yours,

A handwritten signature in black ink, appearing to read 'J. A. Gresham', written over a horizontal line.

J. A. Gresham, Manager
Regulatory Compliance

Enclosures

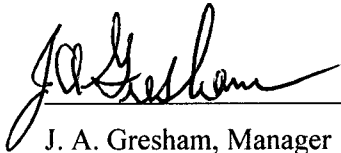
AFFIDAVIT

COMMONWEALTH OF PENNSYLVANIA:

ss

COUNTY OF BUTLER:

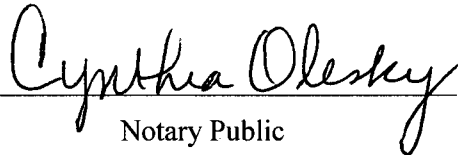
Before me, the undersigned authority, personally appeared J. A. Gresham, who, being by me duly sworn according to law, deposes and says that he is authorized to execute this Affidavit on behalf of Westinghouse Electric Company LLC (Westinghouse), and that the averments of fact set forth in this Affidavit are true and correct to the best of his knowledge, information, and belief:



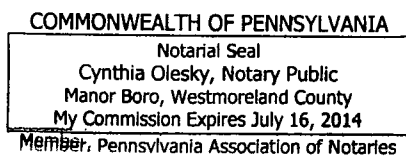
J. A. Gresham, Manager

Regulatory Compliance

Sworn to and subscribed before me
this 2nd day of September 2011



Notary Public



- (1) I am Manager, Regulatory Compliance, in Nuclear Services, Westinghouse Electric Company LLC (Westinghouse), and as such, I have been specifically delegated the function of reviewing the proprietary information sought to be withheld from public disclosure in connection with nuclear power plant licensing and rule making proceedings, and am authorized to apply for its withholding on behalf of Westinghouse.
- (2) I am making this Affidavit in conformance with the provisions of 10 CFR Section 2.390 of the Commission's regulations and in conjunction with the Westinghouse Application for Withholding Proprietary Information from Public Disclosure accompanying this Affidavit.
- (3) I have personal knowledge of the criteria and procedures utilized by Westinghouse in designating information as a trade secret, privileged or as confidential commercial or financial information.
- (4) Pursuant to the provisions of paragraph (b)(4) of Section 2.390 of the Commission's regulations, the following is furnished for consideration by the Commission in determining whether the information sought to be withheld from public disclosure should be withheld.
 - (i) The information sought to be withheld from public disclosure is owned and has been held in confidence by Westinghouse.
 - (ii) The information is of a type customarily held in confidence by Westinghouse and not customarily disclosed to the public. Westinghouse has a rational basis for determining the types of information customarily held in confidence by it and, in that connection, utilizes a system to determine when and whether to hold certain types of information in confidence. The application of that system and the substance of that system constitutes Westinghouse policy and provides the rational basis required.

Under that system, information is held in confidence if it falls in one or more of several types, the release of which might result in the loss of an existing or potential competitive advantage, as follows:

 - (a) The information reveals the distinguishing aspects of a process (or component, structure, tool, method, etc.) where prevention of its use by any of

Westinghouse's competitors without license from Westinghouse constitutes a competitive economic advantage over other companies.

- (b) It consists of supporting data, including test data, relative to a process (or component, structure, tool, method, etc.), the application of which data secures a competitive economic advantage, e.g., by optimization or improved marketability.
- (c) Its use by a competitor would reduce his expenditure of resources or improve his competitive position in the design, manufacture, shipment, installation, assurance of quality, or licensing a similar product.
- (d) It reveals cost or price information, production capacities, budget levels, or commercial strategies of Westinghouse, its customers or suppliers.
- (e) It reveals aspects of past, present, or future Westinghouse or customer funded development plans and programs of potential commercial value to Westinghouse.
- (f) It contains patentable ideas, for which patent protection may be desirable.

There are sound policy reasons behind the Westinghouse system which include the following:

- (a) The use of such information by Westinghouse gives Westinghouse a competitive advantage over its competitors. It is, therefore, withheld from disclosure to protect the Westinghouse competitive position.
- (b) It is information that is marketable in many ways. The extent to which such information is available to competitors diminishes the Westinghouse ability to sell products and services involving the use of the information.
- (c) Use by our competitor would put Westinghouse at a competitive disadvantage by reducing his expenditure of resources at our expense.

- (d) Each component of proprietary information pertinent to a particular competitive advantage is potentially as valuable as the total competitive advantage. If competitors acquire components of proprietary information, any one component may be the key to the entire puzzle, thereby depriving Westinghouse of a competitive advantage.
 - (e) Unrestricted disclosure would jeopardize the position of prominence of Westinghouse in the world market, and thereby give a market advantage to the competition of those countries.
 - (f) The Westinghouse capacity to invest corporate assets in research and development depends upon the success in obtaining and maintaining a competitive advantage.
- (iii) The information is being transmitted to the Commission in confidence and, under the provisions of 10 CFR Section 2.390, it is to be received in confidence by the Commission.
- (iv) The information sought to be protected is not available in public sources or available information has not been previously employed in the same original manner or method to the best of our knowledge and belief.
- (v) The proprietary information sought to be withheld in this submittal is that which is appropriately marked in “LTR-A&SA-11-47-P, Responses to NRC Request for Additional Information on BWRVIP-194: BWR Vessel and Internals Project Methodologies for Demonstrating Steam Dryer Integrity for Power Uprate” (Proprietary), for submittal to the Commission, being transmitted by EPRI letter and Application for Withholding Proprietary Information from Public Disclosure, to the Document Control Desk. The proprietary information as submitted by Westinghouse is that associated with Westinghouse’s request for NRC approval of BWRVIP-194, Revision 0, “BWRVIP-194: BWR Vessel and Internals Project, Methodologies for Demonstrating Steam Dryer Integrity for Power Uprate” and may be used only for that purpose.

This information is part of that which will enable Westinghouse to:

- (a) Obtain NRC approval of BWRVIP-194, Revision 0, "BWRVIP-194: BWR Vessel and Internals Project, Methodologies for Demonstrating Steam Dryer Integrity for Power Uprate"

Further this information has substantial commercial value as follows:

- (a) Westinghouse plans to sell the use of this information to its customers for purposes of performing steam dryer structural qualifications.
- (b) Westinghouse can sell support and defense of the use of this technology.
- (c) The information requested to be withheld reveals the distinguishing aspects of a methodology which is owned by Westinghouse.

Public disclosure of this proprietary information is likely to cause substantial harm to the competitive position of Westinghouse because it would enhance the ability of competitors to provide similar calculations and licensing defense services for commercial power reactors without commensurate expenses. Also, public disclosure of the information would enable others to use the information to meet NRC requirements for licensing documentation without purchasing the right to use the information.

The development of the technology described in part by the information is the result of applying the results of many years of experience in an intensive Westinghouse effort and the expenditure of a considerable sum of money.

In order for competitors of Westinghouse to duplicate this information, similar technical programs would have to be performed and a significant manpower effort, having the requisite talent and experience, would have to be expended.

Further the deponent sayeth not.

Proprietary Information Notice

Transmitted herewith are proprietary and/or non-proprietary versions of documents furnished to the NRC in connection with requests for generic and/or plant-specific review and approval.

In order to conform to the requirements of 10 CFR 2.390 of the Commission's regulations concerning the protection of proprietary information so submitted to the NRC, the information which is proprietary in the proprietary versions is contained within brackets, and where the proprietary information has been deleted in the non-proprietary versions, only the brackets remain (the information that was contained within the brackets in the proprietary versions having been deleted). The justification for claiming the information so designated as proprietary is indicated in both versions by means of lower case letters (a) through (f) located as a superscript immediately following the brackets enclosing each item of information being identified as proprietary or in the margin opposite such information. These lower case letters refer to the types of information Westinghouse customarily holds in confidence identified in Sections (4)(ii)(a) through (4)(ii)(f) of the affidavit accompanying this transmittal pursuant to 10 CFR 2.390(b)(1).

Copyright Notice

The reports transmitted herewith each bear a Westinghouse copyright notice. The NRC is permitted to make the number of copies of the information contained in these reports which are necessary for its internal use in connection with generic and plant-specific reviews and approvals as well as the issuance, denial, amendment, transfer, renewal, modification, suspension, revocation, or violation of a license, permit, order, or regulation subject to the requirements of 10 CFR 2.390 regarding restrictions on public disclosure to the extent such information has been identified as proprietary by Westinghouse, copyright protection notwithstanding. With respect to the non-proprietary versions of these reports, the NRC is permitted to make the number of copies beyond those necessary for its internal use which are necessary in order to have one copy available for public viewing in the appropriate docket files in the public document room in Washington, DC and in local public document rooms as may be required by NRC regulations if the number of copies submitted is insufficient for this purpose. Copies made by the NRC must include the copyright notice in all instances and the proprietary notice if the original was identified as proprietary.

LTR-A&SA-11-47-NP

Responses to NRC Request for Additional Information on
BWRVIP-194: BWR Vessel and Internals Project
Methodologies for Demonstrating Steam Dryer Integrity for
Power Uprate

This document is the property of and contains Proprietary Information owned by Westinghouse Electric Company LLC and/or its subcontractors and suppliers. It is transmitted to you in confidence and trust, and you agree to treat this document in strict accordance with the terms and conditions of the agreement under which it was provided to you.

Westinghouse Electric Company LLC
1000 Westinghouse Drive
Cranberry Township, Pennsylvania 16066

© 2011 Westinghouse Electric Company LLC
All Rights Reserved

NRC RAI BWRVIP194-EMCB-RAI-01

Section 6.3.5, Table 6-4, and Section 10.1, Table 10-1: Section 5.9.2 of the topical report describes []^{a,c}. ACM Rev. 4 bias and uncertainty values are based on benchmarking QC2 data []^{a,c}. The topical report should be revised to demonstrate the applicability of bias and uncertainty values established from the QC2 data []^{a,c}. If these QC2 bias and uncertainty values are not conservative, then a revised set of bias and uncertainty values for application to plants []^{a,c} should be provided.

BWRVIP Response to NRC RAI BWRVIP194-EMCB-RAI-01

The only noise reduction technique applied to the QC2 main steam line (MSL) strain gage data as part of the validation of the ACM Rev. 4 was []^{a,c}. Following the original model validation, additional noise reduction techniques were applied during plant-specific applications of ACM Rev. 4 that were not applied during the original validation, leading to questions related to the adequacy of the bias and uncertainty values determined for ACM Rev. 4.

In response to this RAI, the ACM model has been re-benchmarked using noise reduction techniques that will be used in future plant-specific applications of the model. In conjunction with the re-benchmark, []

[]^{a,c} In addition, the bias and uncertainty values to be applied at acoustic excitation frequencies have been revised. The new model (with corresponding bias and uncertainty values) is designated ACM Rev. 4.1. The re-benchmark was conducted using the same QC2 test (790 MWe) that was used for the original model validation with ACM Rev. 4. In addition, blind predictions and model data comparisons were also conducted against data from the QC2 840 MWe and 930 MWe tests.

Accordingly, the following changes will be made to the BWRVIP-194 report to replace the ACM Rev. 4 model with the ACM Rev. 4.1 model and all associated noise reduction techniques:

A. Section 5.9 Removal of Extraneous Noise from MSL Data will be replaced in its entirety by the following. Note that Section 5.9.1 Coherence Filtering now includes []

[]^{a,c} and Section 5.9.2 Noise Removal Example will now illustrate the noise removal techniques to be applied to MSL data going forward:

5.9 Removal of Extraneous Noise from MSL Data during Plant Application

a,c

5.9.1 Coherence Filtering

a,c

Westinghouse Non-Proprietary Class 3

a,c

a,c

5.9.2 Noise Removal Example

The effect of the various noise removal steps may be illustrated with the data from Plant A for its MSL A strain gage locations.

1. Low power, EIC, and CLTP strain gage data are collected on the main steam lines and converted to pressures, to obtain the plots shown in Figure 5-6 (low power), Figure 5-7 (EIC at CLTP power), and Figure 5-8 (CLTP power).
2. The low power and CLTP data are filtered []^{a,c} to obtain the plots shown in Figure 5-9 (low power) and Figure 5-10 (CLTP power).
3. The coherence filter is then applied, to obtain the plot shown in Figure 5-11. The coherence between the upper and lower MSL A strain gage locations, []^{a,c} is shown in Figure 5-12.

a,c

Figure 5-6: Low power pressure signals on MSL A for Plant A. Peaks at 60 and 180 Hz are electrical.



Figure 5-7: EIC pressure signals on MSL A for Plant A at CLTP. Peaks at 60 and 180 Hz are electrical; the peaks at 84 Hz and 135 Hz are from non-coherent electrical sources; and the peak at 150 Hz is the vane passing frequency.



Figure 5-8: CLTP pressure signals on MSL A for Plant A. Peaks at 60 and 180 Hz are electrical, the peak at 84 Hz is from a non-coherent electrical source, and the peak at 150 Hz is the vane passing frequency.



Figure 5-9: Filtered low power pressure signals on MSL A for Plant A (after filtering EIC, non-coherent electrical sources, and vane passing frequencies).



Figure 5-10: Filtered CLTP pressure signals on MSL A for Plant A (after filtering EIC, non-coherent electrical sources, and vane passing frequencies).



Figure 5-11: Coherence filtering applied to the filtered CLTP pressure signals on MSL A for Plant A.



Figure 5-12: Coherence between MSL A strain gage locations for Plant A.

- B. Section 5.10 References will delete Reference 5.3.
- C. Section 6, sixth line: "Revision 4" will be replaced by "Rev. 4.1".
- D. Section 6.1 Overview of ACM Rev. 4 Methodology will be replaced by 6.1 Overview of ACM Rev. 4.1 Methodology.
- E. Second from bottom paragraph on page 6-1, "Revision 4" will be replaced by "Rev. 4.1".
- F. Bottom paragraph on page 6-10, last line: "Revision 4" will be replaced by "Rev. 4.1".
- G. Bottom paragraph on page 6-11, first line: "(prior to Revision 4)" will be removed. Within this paragraph, line 6: "Revision 4" will be replaced by "Rev. 4.1".
- H. Above Figure 6-11 on page 6-14, the paragraph will be replaced in its entirety by the following:

[] a,c

I. Figure 6-11 will be replaced by the following figure:

[] a,c



a,c

Figure 6-11: Plots of the []^{a,c} determined from the QC2 data at 790 MWe for ACM Rev. 4.1 after application of all noise removal techniques.

J. Section 6.3.4 Combined Acoustic and Hydrodynamic Fluctuating Pressure Load Definition will be replaced in its entirety with the following:

6.3.4 Combined Acoustic and Hydrodynamic Fluctuating Pressure Load Definition

a,c

a,c

The solution process for all power levels is the following: (1) the eight strain gage measurements (from a time history of 120 seconds or more at 2000 samples/sec or higher) are obtained at a power level of []^{a,c}, and at CLTP, then converted to pressures, noise removed (removing AC electrical, extraneous electrical (EIC), and vane passing frequencies), and the coherence filter applied []^{a,c}; (2) the ACM is run to supply the driving acoustic pressures at the entrances to the four MSLs (as documented above) and (3) the Helmholtz model is used to paint the fluctuating pressures on the dryer surfaces (for a subsequent finite element model analysis of dryer stresses). []^{a,c} are incorporated into the result. Note that the frequency resolution of the prediction is less than $\Delta f = 0.083$ Hz, on the frequency range between 0 and 250 Hz.

K. Section 6.4 Key Modeling Parameters, second paragraph, will replace “Revision 4” with “Rev. 4.1” in two places. Table 6-1 will be expanded to include []^{a,c}, as tabulated and defined below:

Table 6-1: ACM Rev. 4.1 locked modeling parameters.

a,c

- L. Section 6.5 Validation of ACM Revision 4 will be replaced by 6.5 Validation of ACM Rev. 4.1 and “Revision 4” will be replaced by “Rev. 4.1” in multiple locations throughout this section.
- M. Section 6.5.1.1 Main Steam Line Instrumentation will now note that the analysis was conducted to 250 Hz.
- N. The first paragraph of Section 6.5.1.2 QC2 Tests used for Model Validation will be replaced by the following:

Table 6-3 summarizes the QC2 test from which data were used to assess the model and finalize the values for key parameters for ACM Rev. 4.1. Data taken at the power level of 790 MWe, test condition TC32B, at OLTP conditions, were used to finalize key parameters. Once these key parameters were established and locked, two “blind” model comparisons were made to data obtained at higher power levels (840 and 930 MWe) as discussed in Section 6.5.4.

- O. Section 6.5.2 ACM Revision 4 Model/Data Comparisons will be replaced in its entirety with the following:

6.5.2 ACM Rev. 4.1 Model/Data Comparisons

a,c

Westinghouse Non-Proprietary Class 3

[] a,c



Figure 6-16: ACM Rev. 4.1 predictions at 790 MWe at the dryer pressure sensors: peak maximum (top) and peak minimum (bottom) pressure levels, with data (black) and predictions (blue). Sensors P13, P14, P16, P23, and P27 are inside the dryer, while P26 is on a mast above the dryer.

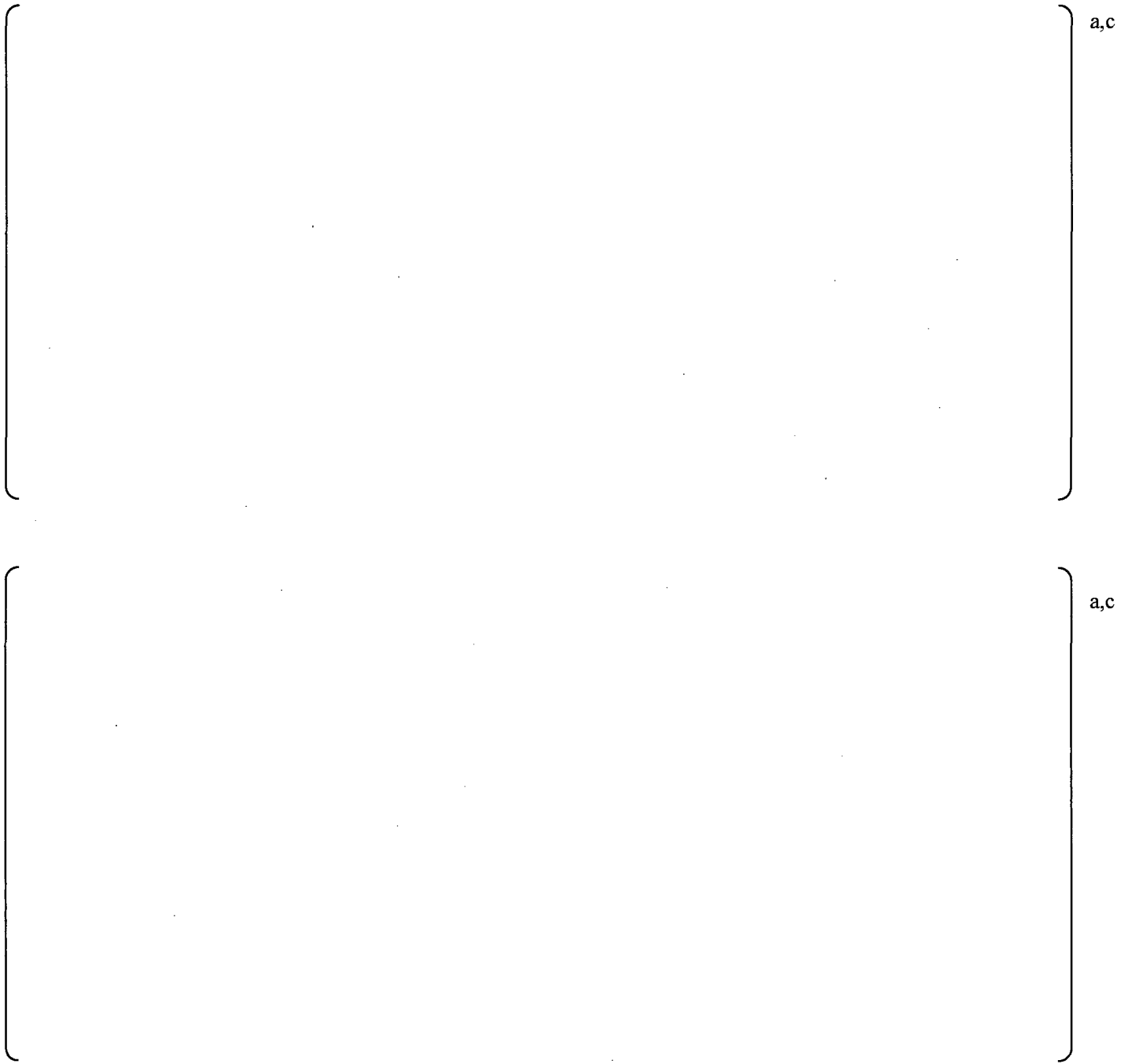


Figure 6-17: PSD comparison for 790 MWe for pressure sensor data (black curves) and ACM Rev. 4.1 predictions (blue curves), for sensors P20 (top) and P21 (bottom).

- P. Section 6.5.3 Evaluation of ACM Revision 4 Prediction Bias and Uncertainty will be replaced in its entirety with the following:

6.5.3 Evaluation of ACM Rev. 4.1 Prediction Bias and Uncertainty

As shown in the previous section, model comparisons with data demonstrate the high degree of correlation found in the application of ACM Rev. 4.1 to the QC2 steam dryer, steam dome, and main steam lines. Once predictions have been made, those predictions can be compared with the QC2 data to determine bias and uncertainty levels, to discern the applicable range of the model and where model uncertainty can be anticipated.

6.5.3.1 Bias and Uncertainty Evaluation

Bias is computed by taking the difference between the measured and predicted RMS pressure values for the sixteen pressure sensors on the outer bank hoods of the QC2 dryer (sensors P1 to P12 and P18 to P21), and dividing the mean of this difference by the mean of the predicted RMS. RMS is computed by integrating the PSD across the frequency range of interest and taking the square root

$$\text{BIAS} = \frac{\frac{1}{N} \sum (\text{RMS}_{\text{measured}} - \text{RMS}_{\text{predicted}})}{\frac{1}{N} \sum \text{RMS}_{\text{predicted}}} \quad (6.5.1)$$

where $\text{RMS}_{\text{measured}}$ is the RMS of the measured data and $\text{RMS}_{\text{predicted}}$ is the RMS of the predicted data. Summations are over the number of pressure sensors, or $N = 16$. The use of individual pressure sensors can be shown to be conservative with regard to the bias and uncertainty levels generated, when compared with the use of averaged pressure sensors, as was done in [6.4].

Uncertainty is defined as the fraction computed by the standard deviation

$$\text{UNCERTAINTY} = \frac{\sqrt{\frac{1}{N} \sum (\text{RMS}_{\text{measured}} - \text{RMS}_{\text{predicted}})^2}}{\frac{1}{N} \sum \text{RMS}_{\text{predicted}}} \quad (6.5.2)$$

ACM bias and uncertainty summary results for 790 MWe are compiled for specified frequency ranges of interest and summarized in Table 6-4. The bias and uncertainty values within ± 2 Hz of each of the three standpipe frequencies at QC2 (discussed in Section 4) are shown in Table 6-5. The values for Dresser 6×8, Electromatic, and Target Rock are computed from Equations (6.5.1) and (6.5.2) across the frequency intervals shown for each valve type.

Table 6-4: QC2 bias and uncertainty values for specified frequency intervals.



a,c

Table 6-5: QC2 bias and uncertainty values at standpipe excitation frequencies.



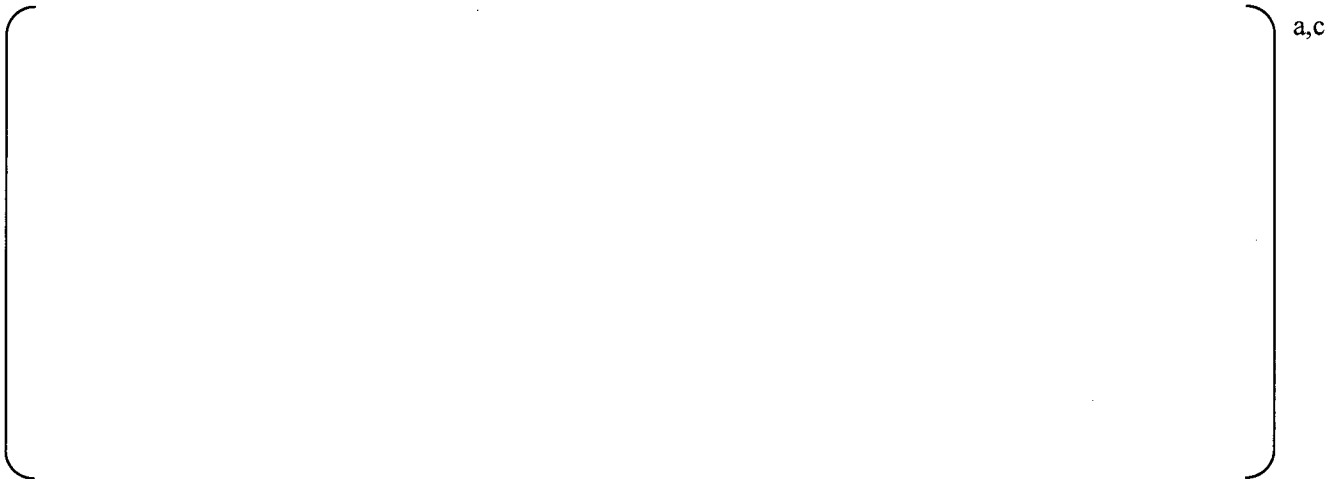
a,c

6.5.3.2 Total Bias and Uncertainty in ACM Rev. 4.1



A large, empty rectangular area enclosed by a thin black line with rounded corners. This area is intended for a table but is currently blank. To the right of the top-right corner of this area, the text 'a,c' is present.

Table 6-6: Total uncertainty on ACM Rev. 4.1 predictions at 790 MWe, with standpipe excitation between 149 and 156 Hz.



A large, empty rectangular area enclosed by a thin black line with rounded corners. This area is intended for a table but is currently blank. To the right of the top-right corner of this area, the text 'a,c' is present.

Application of the total uncertainty shown in Table 6-6 to ACM Rev. 4.1 predictions, and comparison with data, are shown in Figure 6-18 for peak pressures, and in Figure 6-19 for pressure sensors P20 and P21. [

]a,c

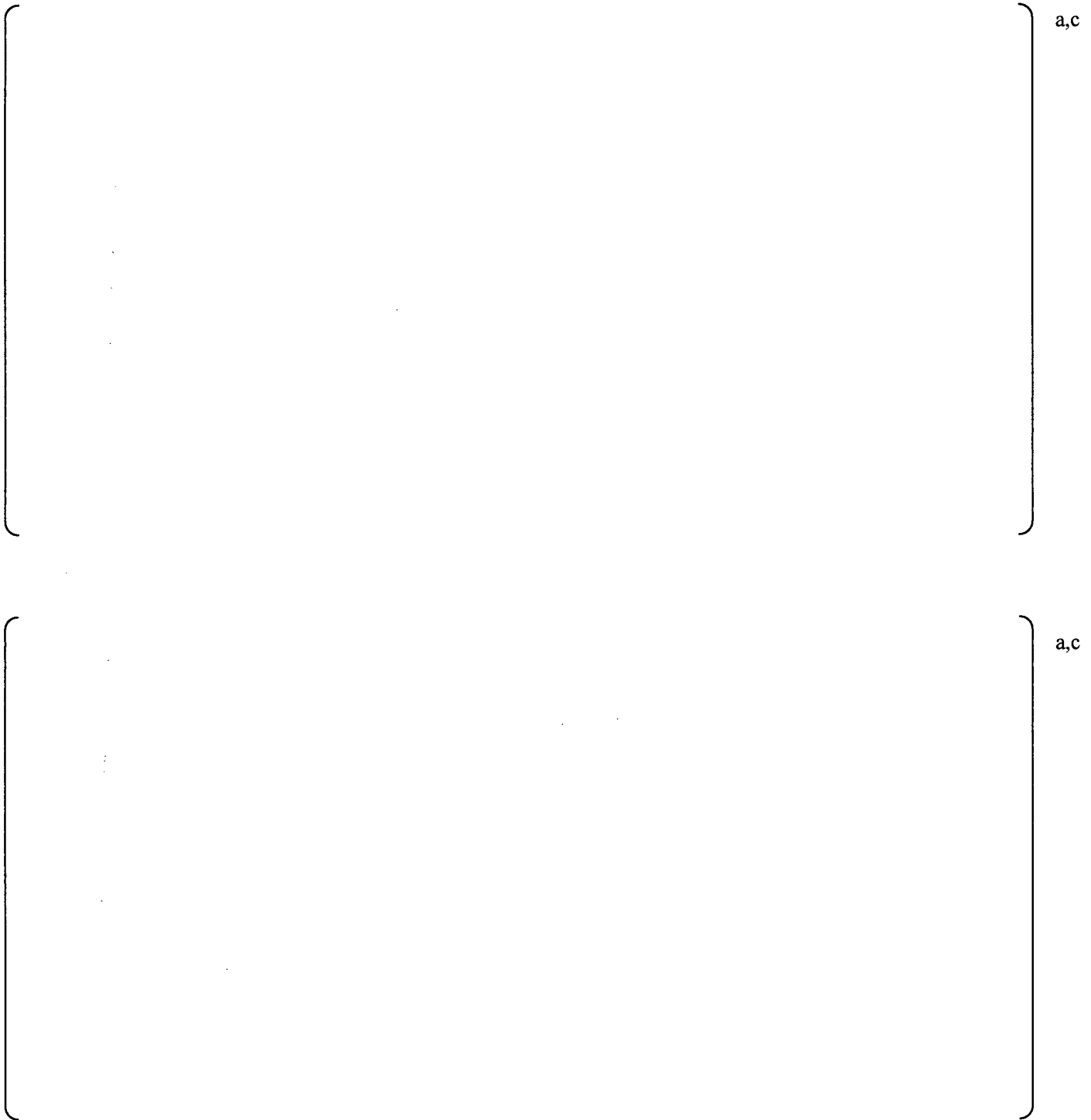


Figure 6-18: ACM Rev. 4.1 predictions at 790 MWe at the dryer pressure sensors: peak maximum (top) and peak minimum (bottom) pressure levels, with data (black), predictions (blue), and predictions with bias and uncertainty added (red). Sensors P13, P14, P16, P23, and P27 are inside the dryer, while P26 is on a mast above the dryer.

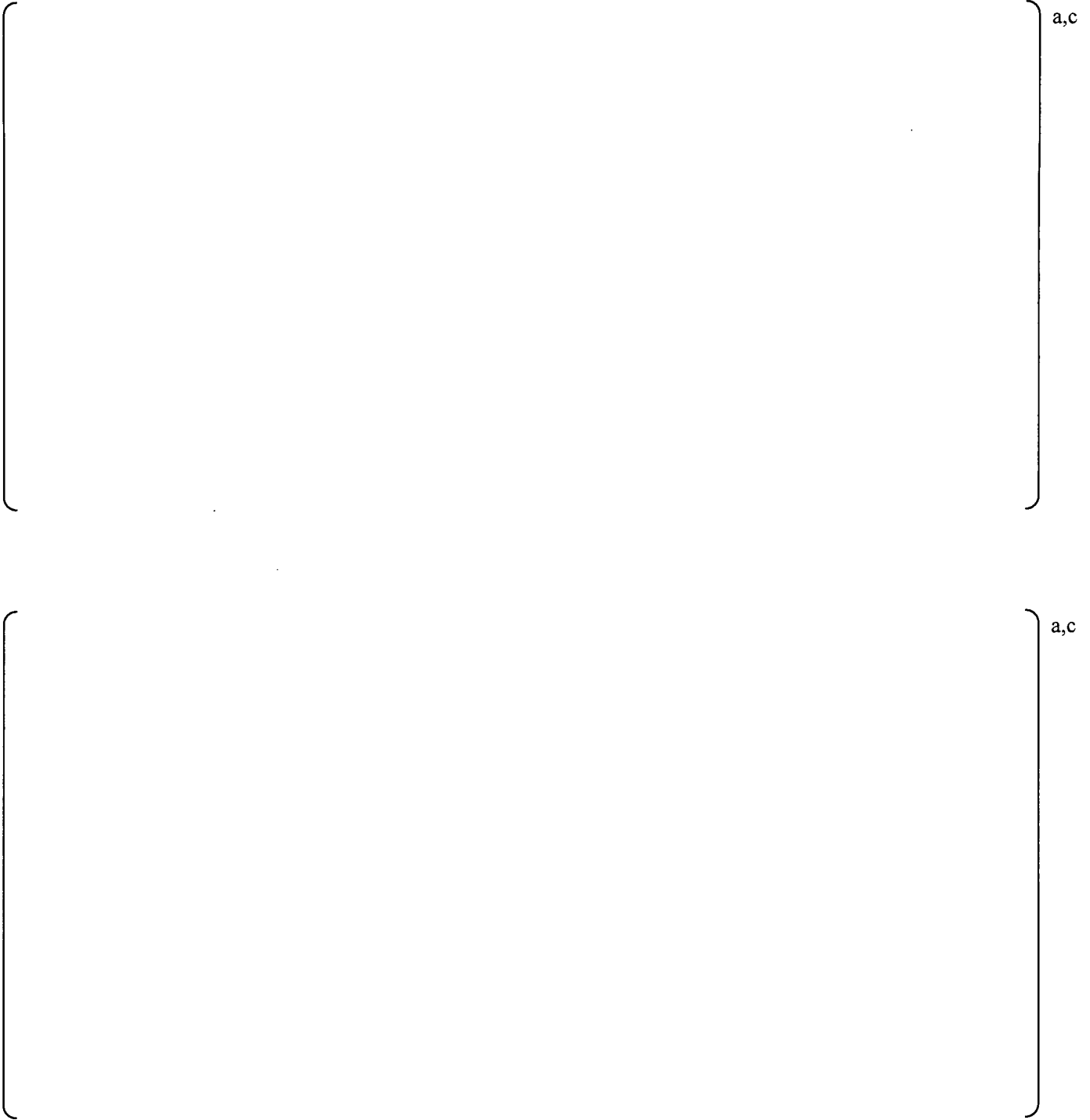


Figure 6-19: PSD comparison for 790 MWe for pressure sensor data (black curves) and ACM Rev. 4.1 predictions with bias and uncertainty added (red curves), for sensors P20 (top) and P21 (bottom).

Q. Section 6.5.4 Blind Benchmark will be replaced in its entirety with the following:

6.5.4 Blind Benchmarks

To provide further confidence in the adequacy of the ACM Rev. 4.1 model, two additional comparisons were made to other QC2 data sets at power conditions above OLTP, corresponding to 840 MWe and 930 MWe, as shown in Table 6-7. Comparisons of the Rev. 4.1 model with these data sets represent blind benchmarks, as the ACM Rev. 4.1 model has locked parameters.

Prior to each blind prediction, the MSL data were filtered as described in Section 5.9.

Table 6-7: QC2 blind benchmark test conditions

Exelon Test Condition	Electric Power Level (MWe)	Thermal Power Level (MWt)	MSL Flow Velocity (ft/sec)	Mach Number
TC35	840	2625	181	0.113
TC41 (EPU)	930	2887	206	0.129

A comparison of ACM Rev. 4.1 model predictions of maximum and minimum peak pressures to those measured at 840 and 930 MWe, after application of the total uncertainties summarized in Table 6-6, are shown in Figure 6-20 and Figure 6-21, respectively. Predictions of minimum and maximum peak pressures bound the QC2 dryer data except for sensors P7, P14, P16, P21, and P27.

[

] ^{a,c}

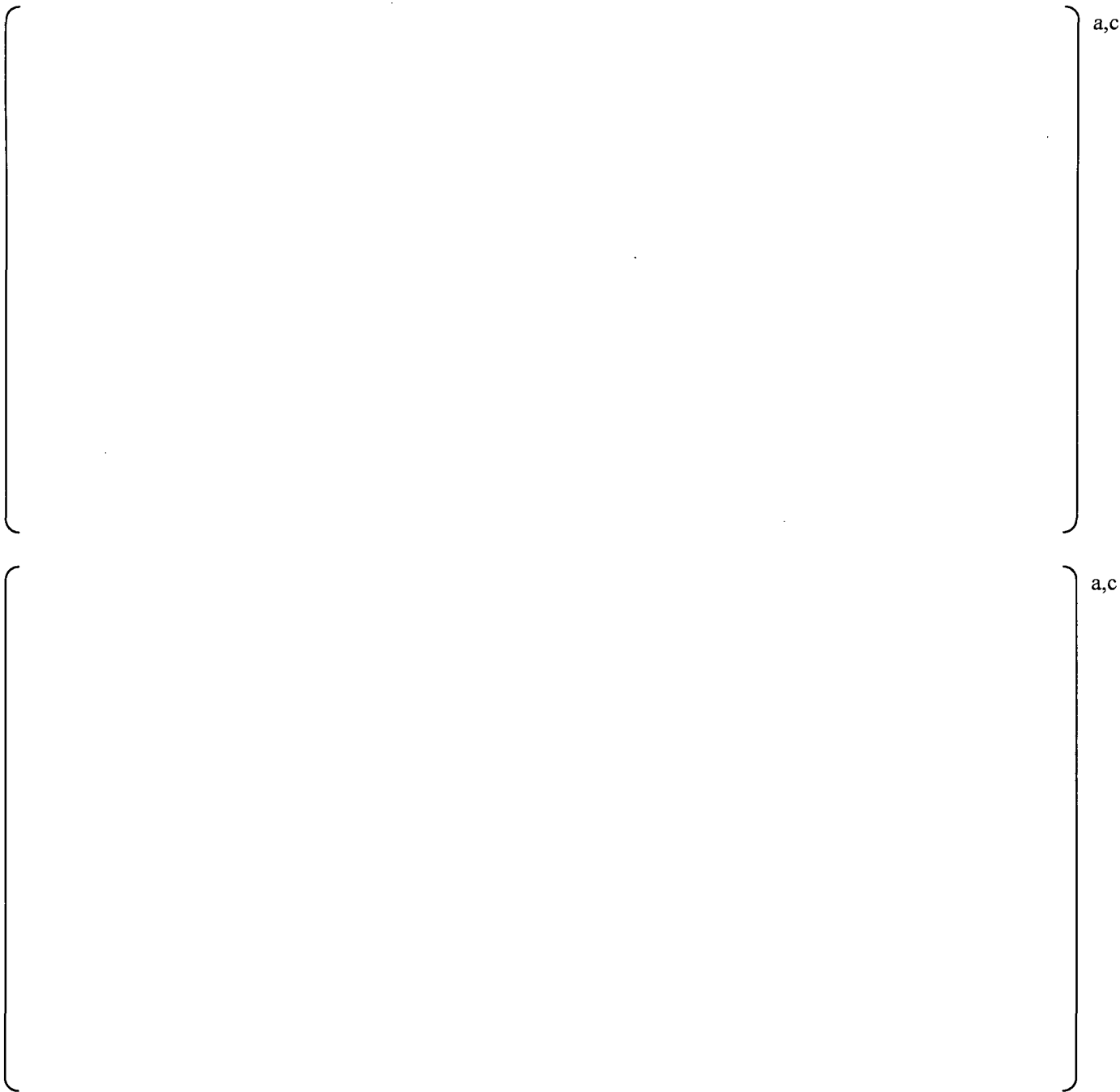


Figure 6-20: ACM Rev. 4.1 predictions at 840 MWe at the dryer pressure sensors: peak maximum (top) and peak minimum (bottom) pressure levels, with data (black) and predictions with bias and uncertainty added (red).

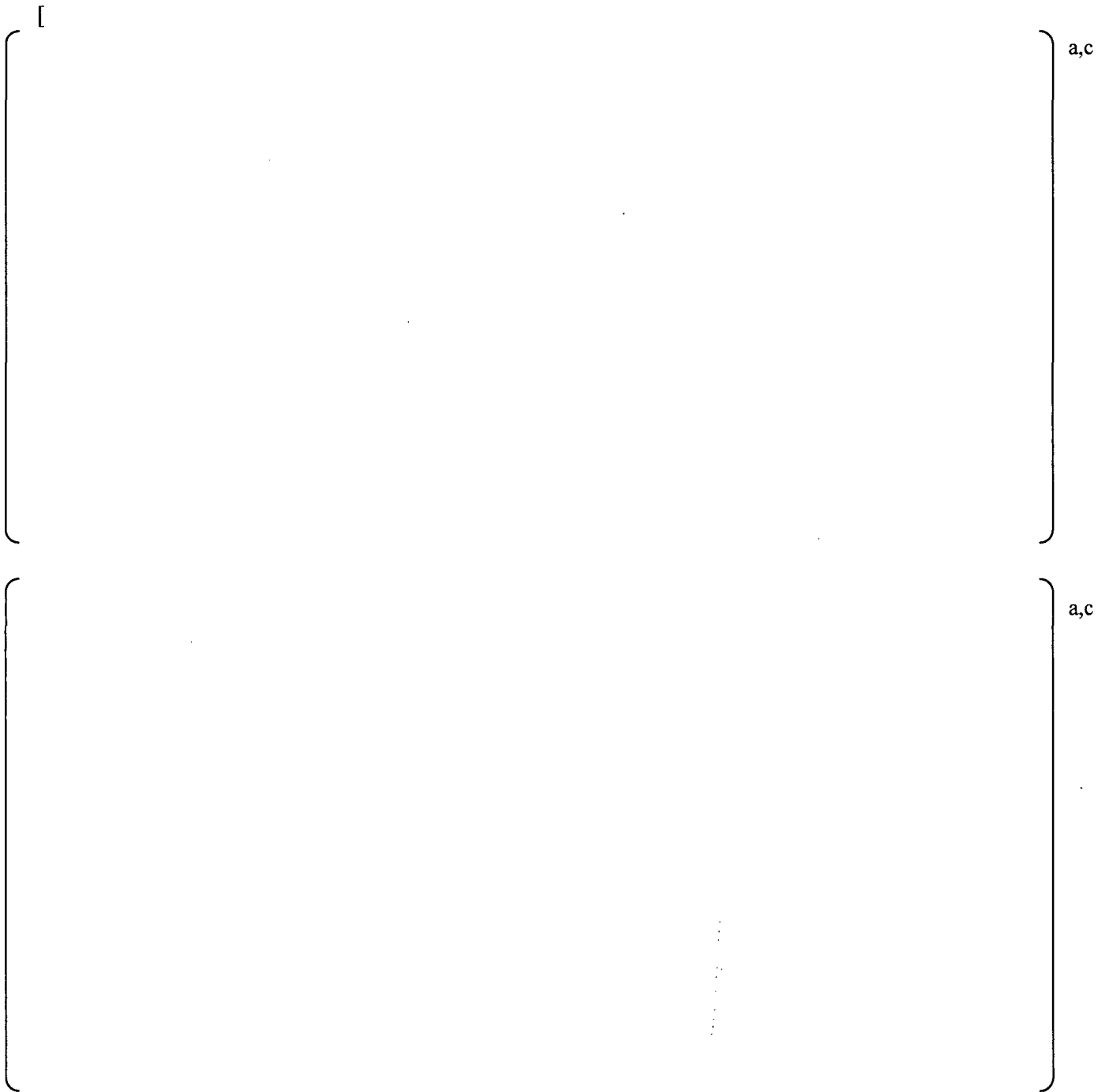


Figure 6-21: ACM Rev. 4.1 predictions at 930 MWe at the dryer pressure sensors: peak maximum (top) and peak minimum (bottom) pressure levels, with data (black) and predictions with bias and uncertainty added (red).

R. Section 6.6 Overall Bias and Uncertainty in ACM Revision 4 will be replaced in its entirety by the following:

6.6 Total Uncertainty in ACM Rev. 4.1

As discussed in Section 6.5.3, total uncertainty in each frequency range is defined as the bias plus the square root of the sum of the squares of the uncertainties for that frequency range. Bias is defined as the error in RMS pressure prediction at a given sensor (or group of sensors). A positive bias indicates a non-conservative prediction, and a negative bias indicates a conservative prediction. Uncertainties include SRSS model prediction uncertainty, strain gage measurement uncertainty, and pressure sensor measurement uncertainty.

a,c

The use of 16 individual outer bank hood pressure sensors is in contrast to the approach taken to determine bias and uncertainty values in previous power uprate submissions, where these signals were combined by averaging the individual pressure sensor signals over six regions oriented vertically on the outer bank hoods, such that six signals result: the average of P1, P2, and P3; P4, P5, and P6; P7, P8, and P9; P10, P11, and P12; P18 and P20; and P19 and P21.

The conservatism inherent in the use of the 790 MWe data using all 16 outer bank hood sensors individually without averaging may be seen in Figure 6-22. Here, the loading factors (defined as 1.0 + the total uncertainty in decimal form) determined using six average sensors (at 790 MWe, 840 MWe, and 930 MWe) are compared to the loading factors determined based on ACM Rev. 4.1 bias and uncertainty values for the 790 MWe data set using all 16 outer bank hood pressure sensors.



Figure 6-22: Comparison of the loading factor computed from bias and uncertainty values for the three power levels, based on six average sensors, to the loading factor computed from bias and uncertainty values for 790 MWe based on 16 sensors.



Table 6-5 gives the bias and uncertainty values within the standpipe excitation frequency interval for 790 MWe with 16 sensors. These results are reproduced in Table 6-8, along with the bias and uncertainty values for 790 MWe, 840 MWe, and 930 MWe six average sensors.

Table 6-8: QC2 bias and uncertainty values at the standpipe excitation frequency.

The table content is missing, represented by a large empty rectangular frame. Brackets on the right side of the frame indicate the table's extent, with labels 'a,c' at the top and bottom right corners.

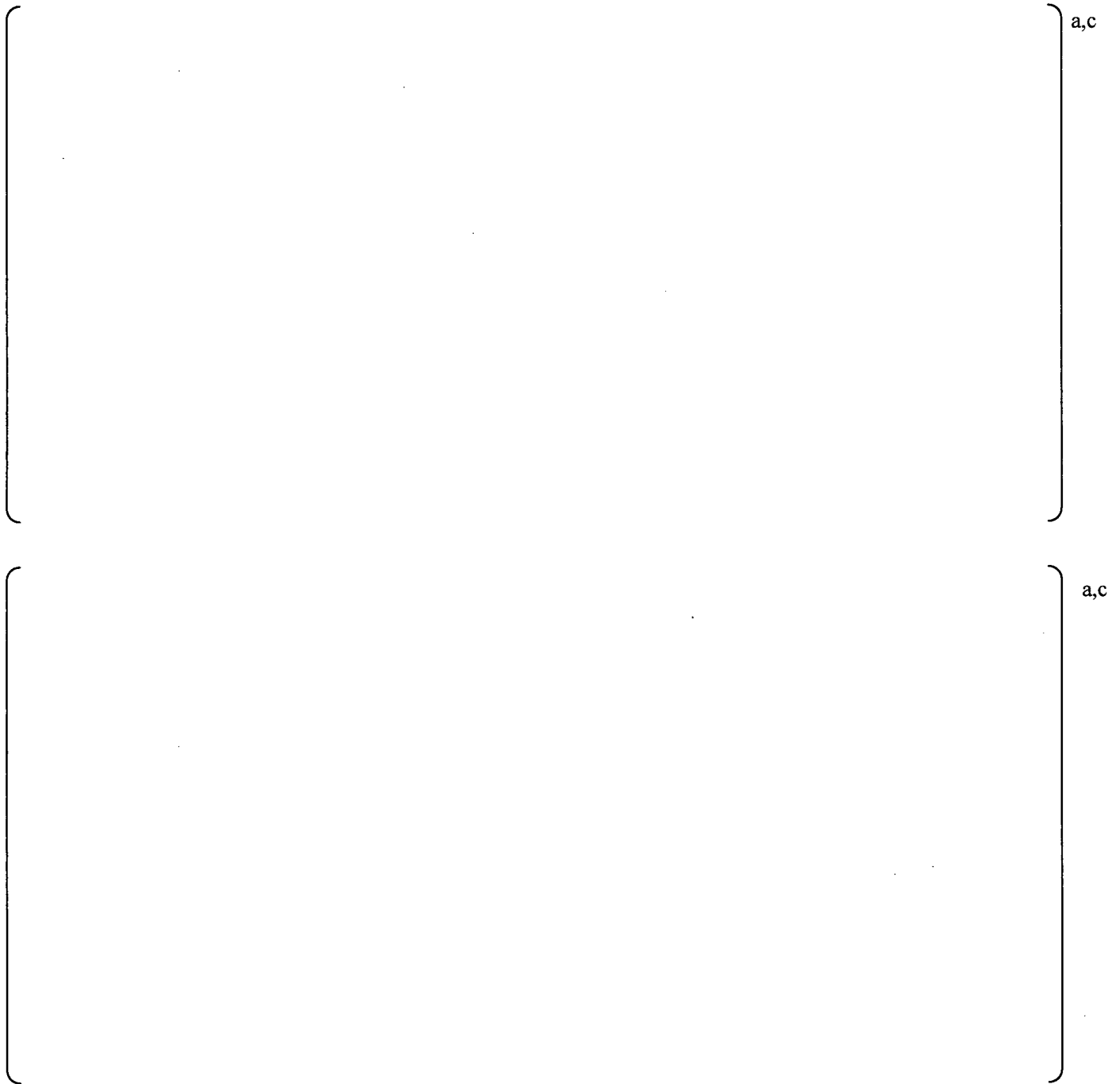


Figure 6-23: ACM Rev. 4.1 predictions at 790 MWe at the dryer pressure sensors: peak maximum (top) and peak minimum (bottom) pressure levels, with data (black), predictions (blue), and predictions with corrected bias and uncertainty added (red). Sensors P13, P14, P16, P23, and P27 are inside the dryer, while P26 is on a mast above the dryer.

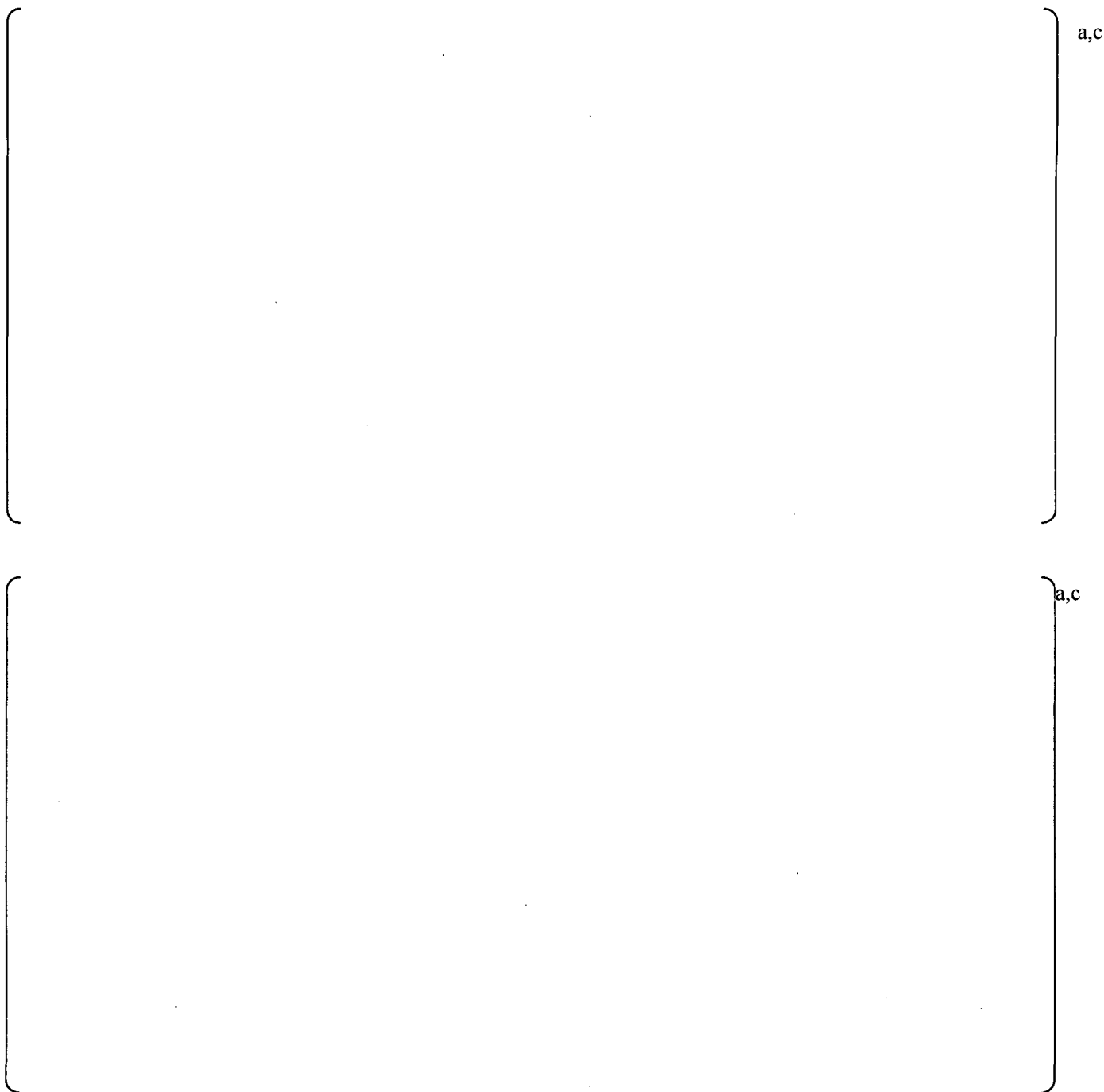


Figure 6-24: ACM Rev. 4.1 predictions at 840 MWe at the dryer pressure sensors: peak maximum (top) and peak minimum (bottom) pressure levels, with data (black) and predictions with corrected bias and uncertainty added (red).

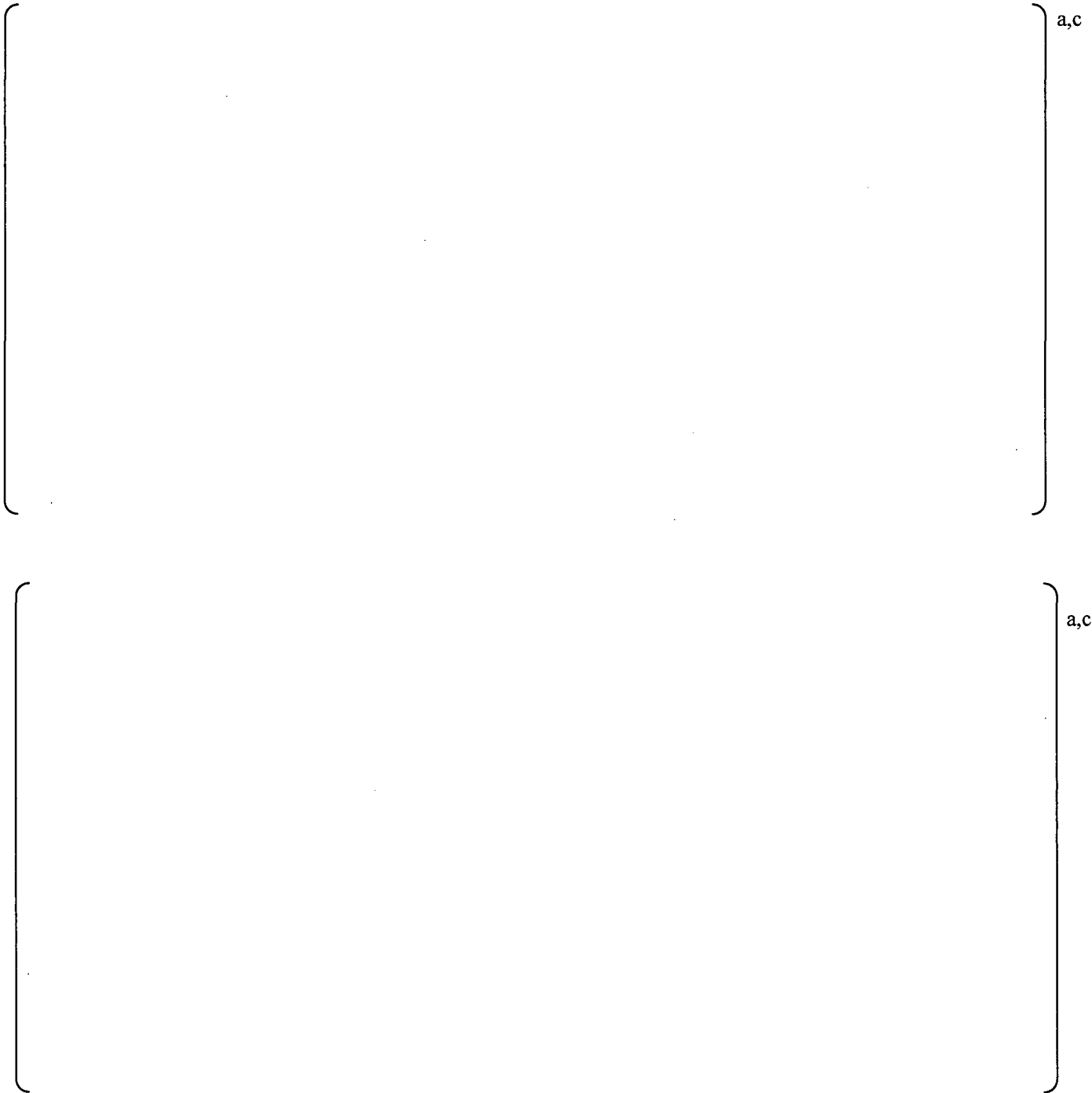


Figure 6-25: ACM Rev. 4.1 predictions at 930 MWe at the dryer pressure sensors: peak maximum (top) and peak minimum (bottom) pressure levels, with data (black) and predictions with corrected bias and uncertainty added (red).

Table 6-9: Final ACM Rev. 4.1 bias and uncertainty values for specified frequency intervals.



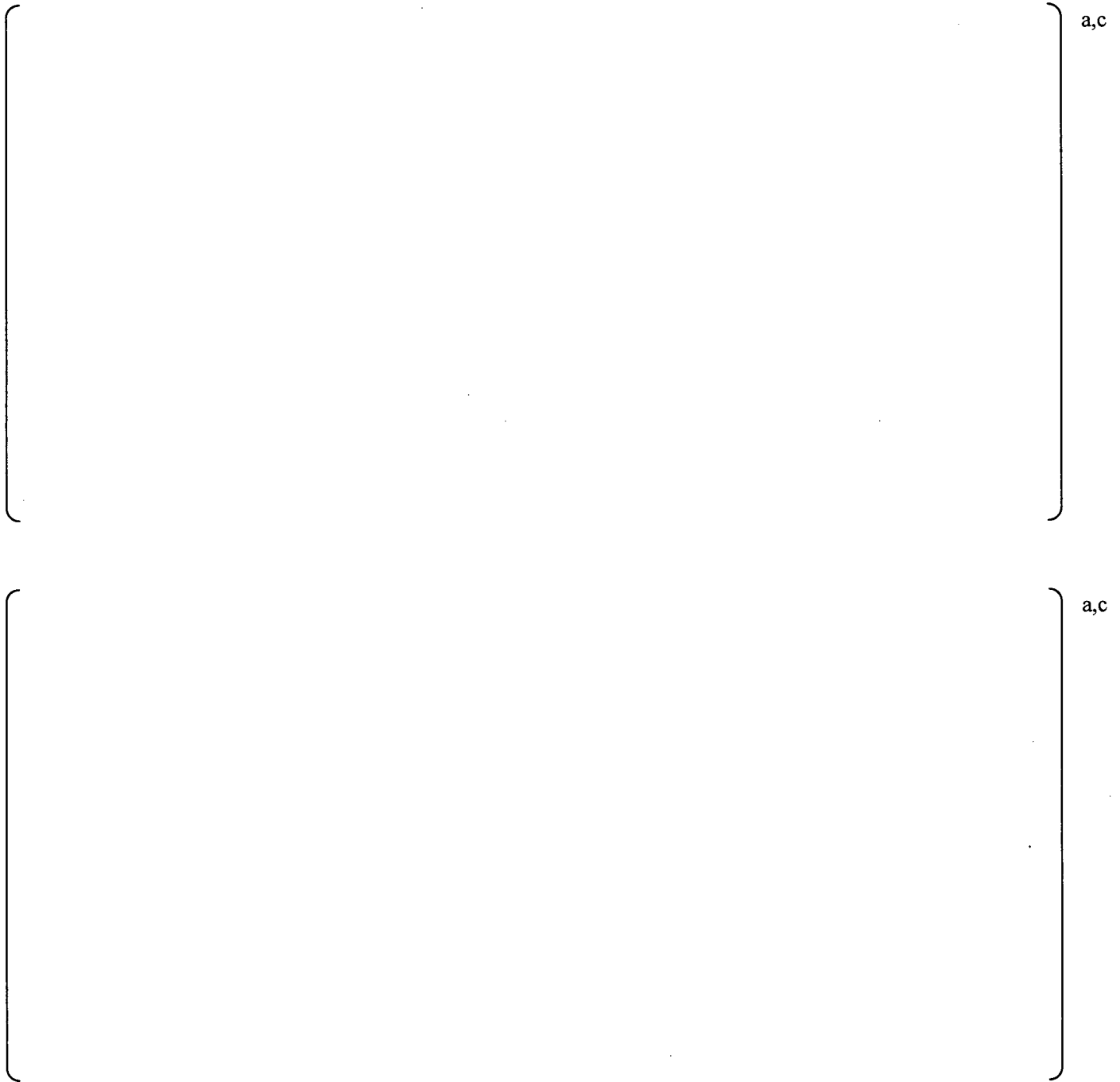


Figure 6-26: Comparison between measured and predicted peak pressures at the 27 pressure sensors in QC2 at 790 MWe, without (top) and with (bottom) corrected bias and uncertainty added to the predicted load. The lines are the one-to-one boundaries. [

] ^{a,c}

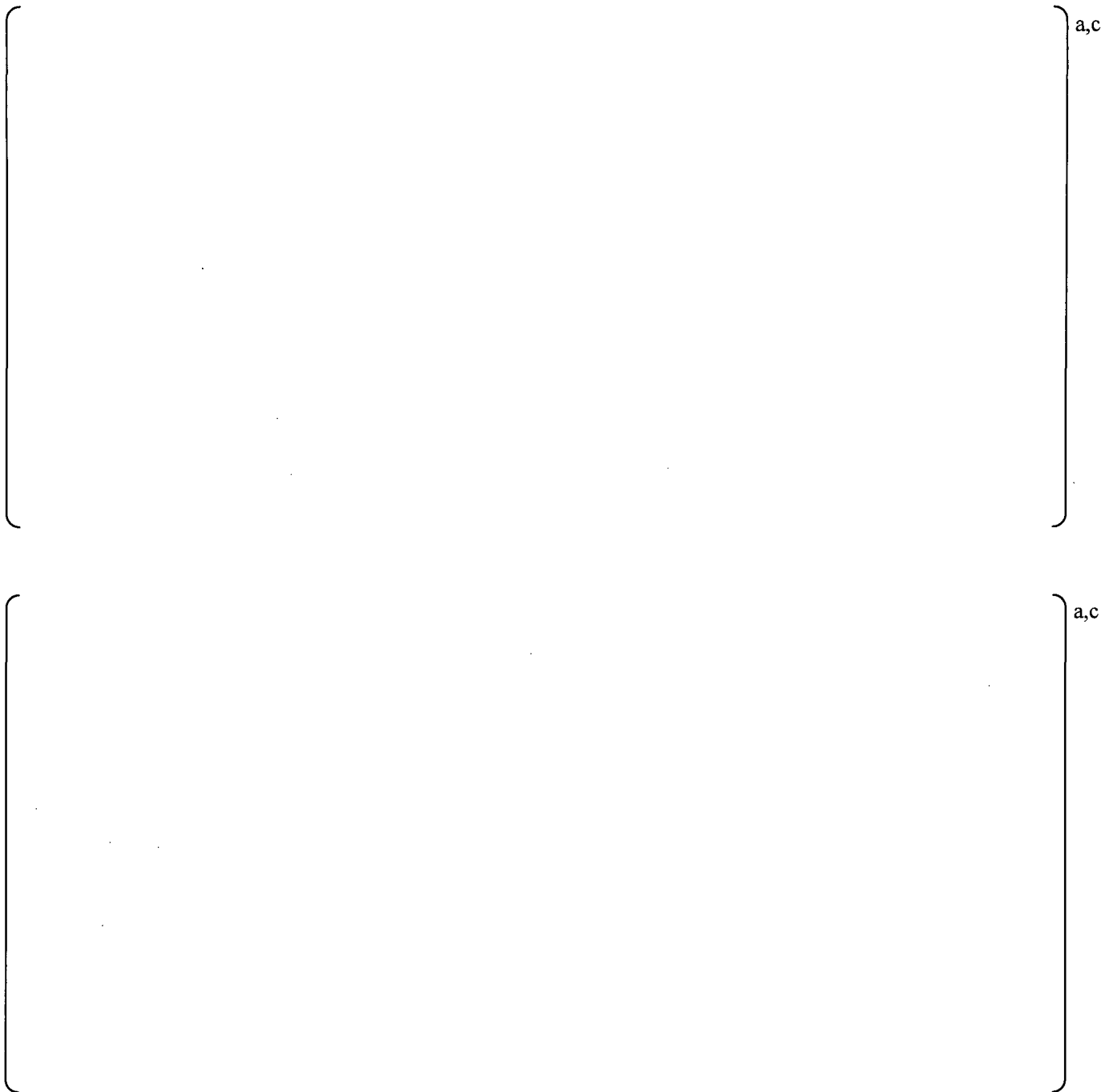


Figure 6-27: Comparison between measured and predicted peak pressures at the 27 pressure sensors in QC2 at 840 MWe (top) and at 930 MWe (bottom) with corrected bias and uncertainty added to the predicted loads. The lines are the one-to-one boundaries. [

]a,c

S. Section 6.7 Conclusions will be replaced in its entirety by the following:

6.7 Conclusions



An alternative evaluation approach, based on pressure transducer measurements on the steam dryer, is discussed in Appendix G.

T. Finally, in response to BWRVIP194-EMCB-RAI-01, Appendix C will contain the data and prediction comparisons at all 27 pressure sensors for 790 MWe, Appendix D will contain the comparisons for 840 MWe, and Appendix E will contain the comparisons for 930 MWe. Appendices A and B are unchanged, while the original Appendix E will be retitled Appendix F, and the original Appendix F will be retitled Appendix G. Appendices C, D, and E now follow, before addressing the second RAI.

Appendix C: ACM Rev. 4.1 Comparisons To Quad Cities Unit 2 790 MWe Test Data

This appendix provides the comparison of QC2 data collected at 790 MWe with ACM Rev. 4.1 model predictions.

Figure C-1 and Figure C-2 plot the main steam line data, while Figure C-3 to Figure C-16 plot the comparisons between model predictions and data at each of the 27 pressure transducer locations on the dryer.



Figure C-1: PSDs of pressure data at 790 MWe on main steam lines A (top) and B (bottom): upper strain gage locations (blue curves), lower strain gage locations (red curves). EMF and coherence filtering have been applied to these signals.

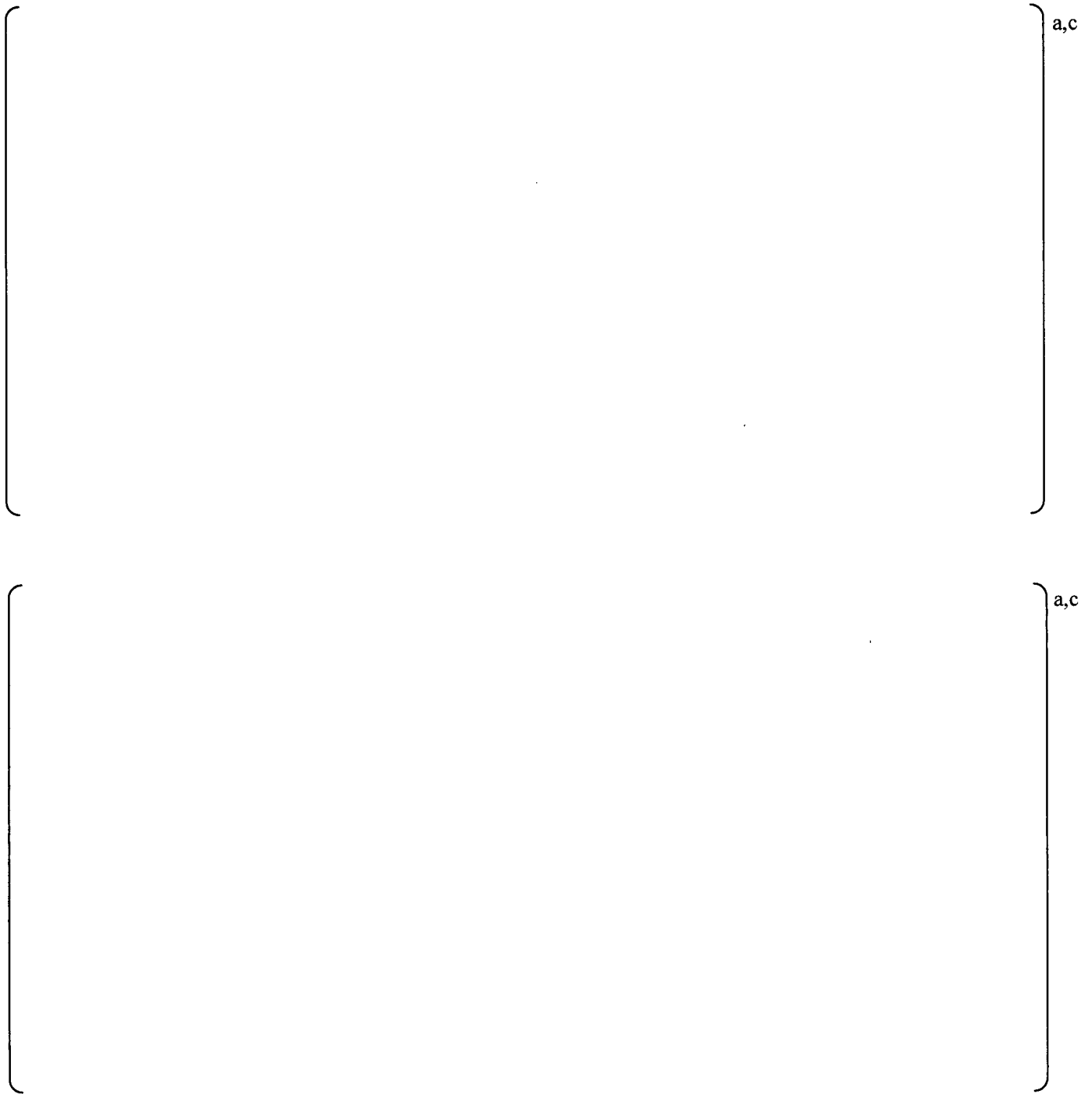


Figure C-2: PSDs of pressure data at 790 MWe on main steam lines C (top) and D (bottom): upper strain gage locations (blue curves), lower strain gage locations (red curves). EMF and coherence filtering have been applied to these signals.

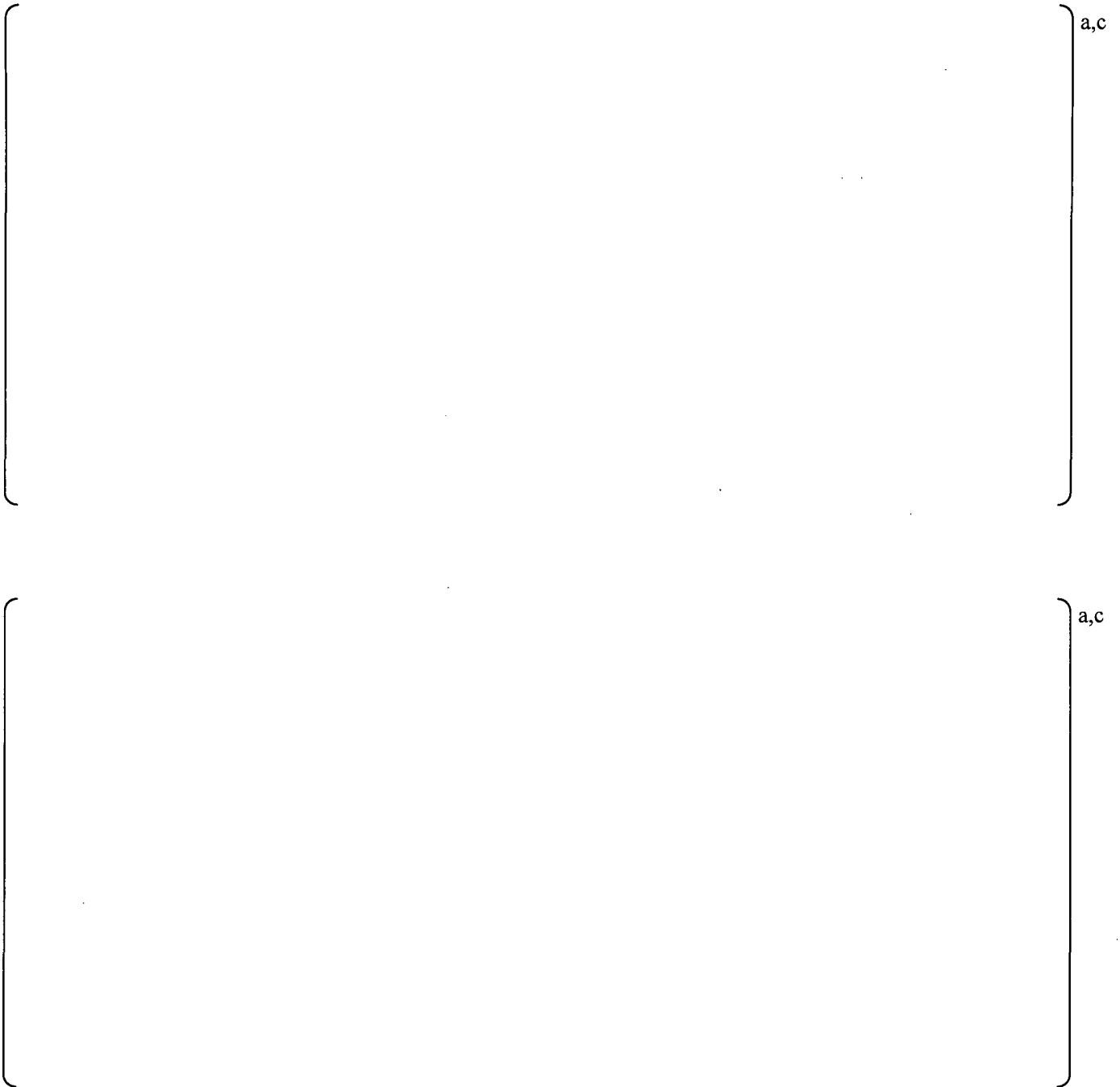


Figure C-3: PSD comparison at 790 MWe for pressure sensor data (black curves) and ACM Rev. 4.1 model predictions with corrected bias and uncertainty added (red curves), for P1 (top) and P2 (bottom).

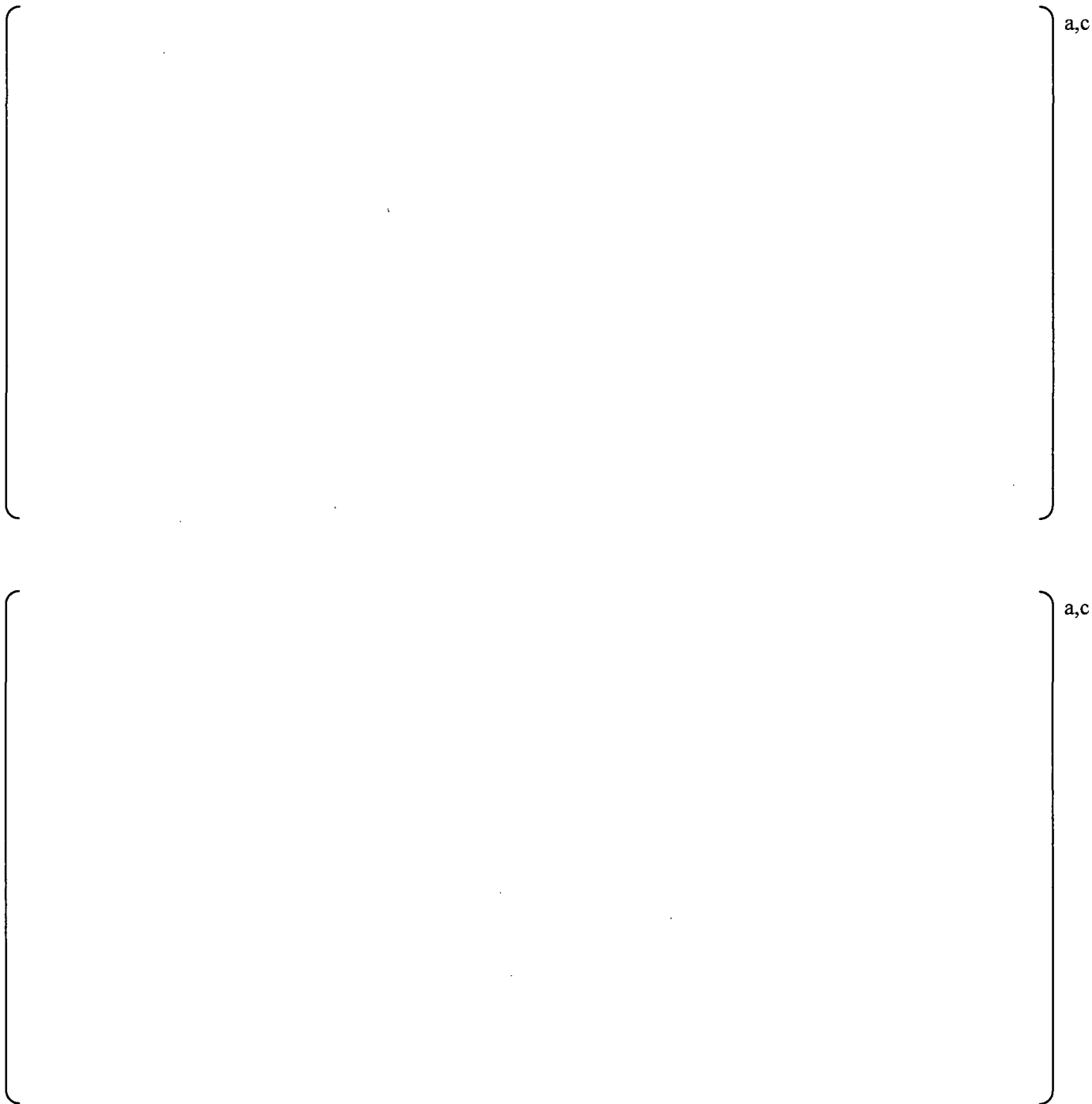


Figure C-4: PSD comparison at 790 MWe for pressure sensor data (black curves) and ACM Rev. 4.1 model predictions with corrected bias and uncertainty added (red curves), for P3 (top) and P4 (bottom).

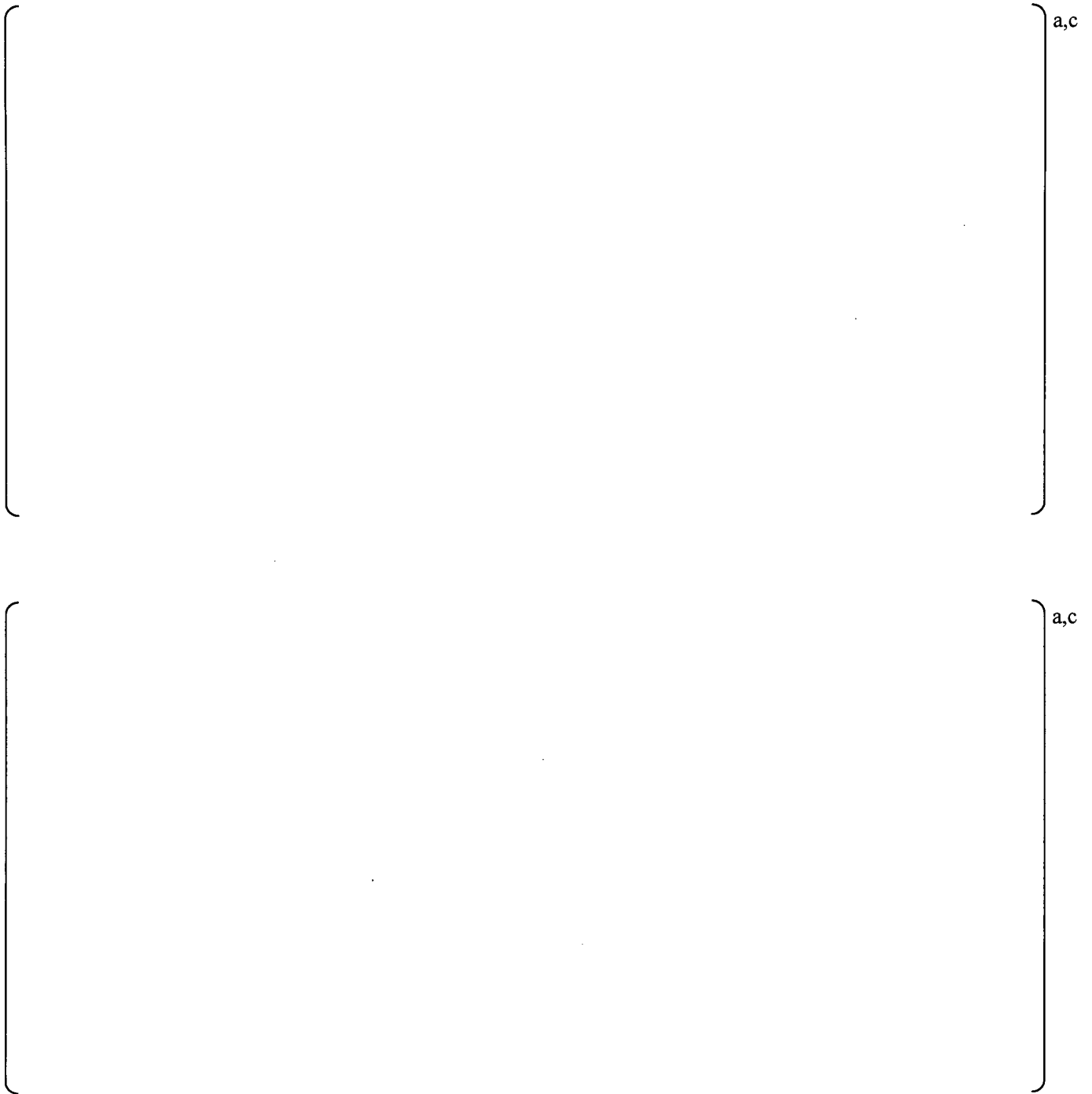


Figure C-5: PSD comparison at 790 MWe for pressure sensor data (black curves) and ACM Rev. 4.1 model predictions with corrected bias and uncertainty added (red curves), for P5 (top) and P6 (bottom).

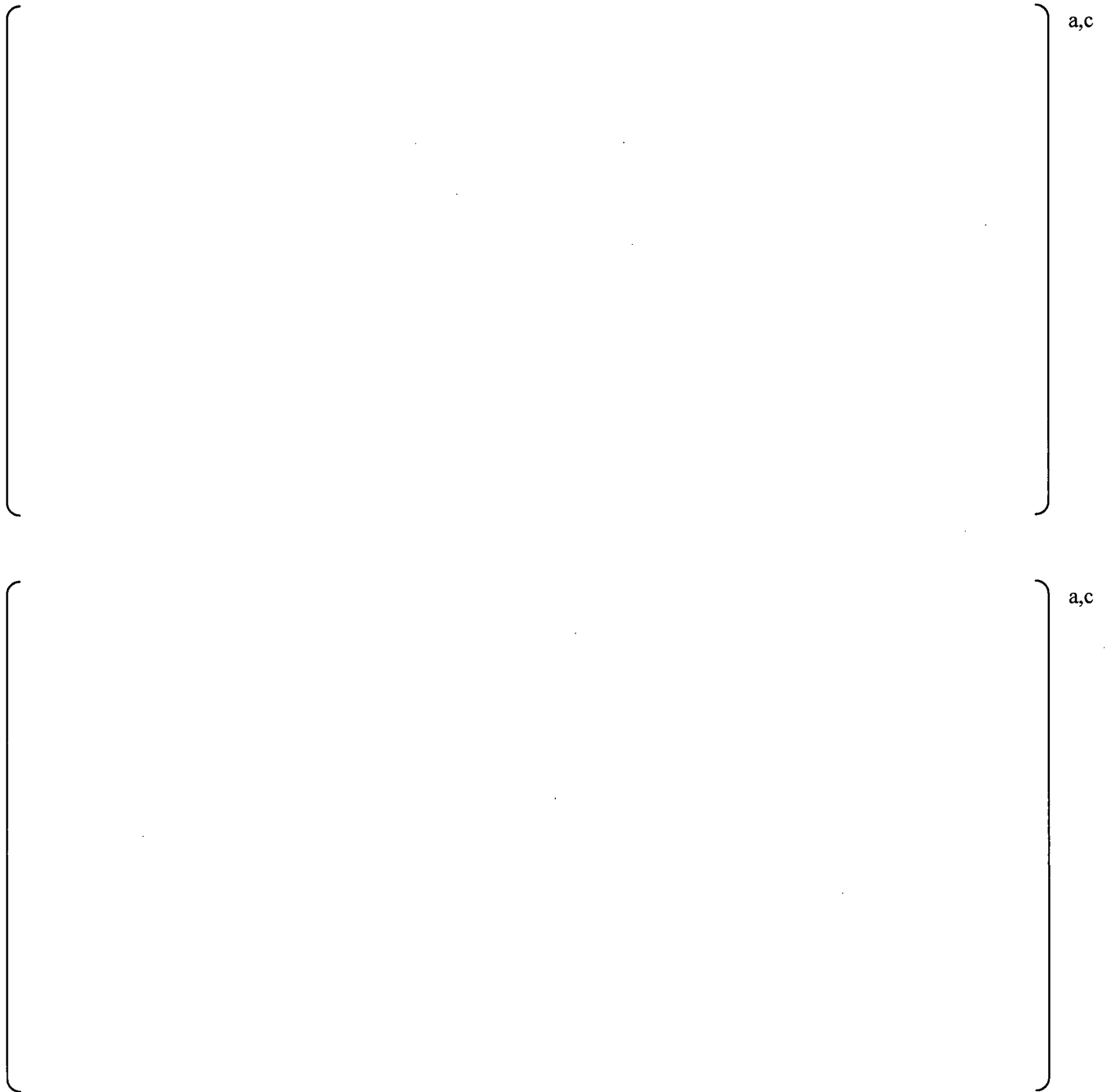


Figure C-6: PSD comparison at 790 MWe for pressure sensor data (black curves) and ACM Rev. 4.1 model predictions with corrected bias and uncertainty added (red curves), for P7 (top) and P8 (bottom).

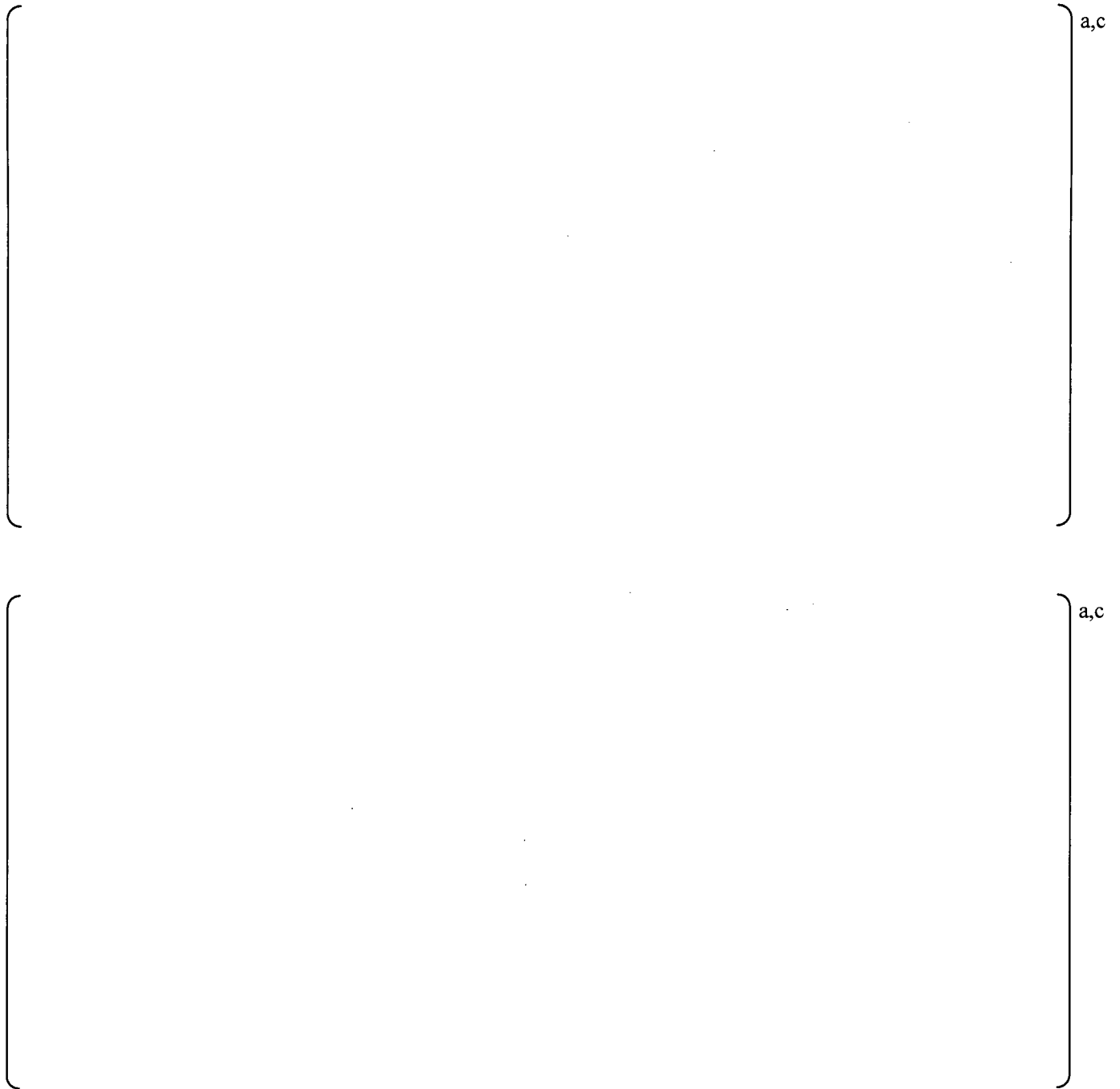


Figure C-7: PSD comparison at 790 MWe for pressure sensor data (black curves) and ACM Rev. 4.1 model predictions with corrected bias and uncertainty added (red curves), for P9 (top) and P10 (bottom).

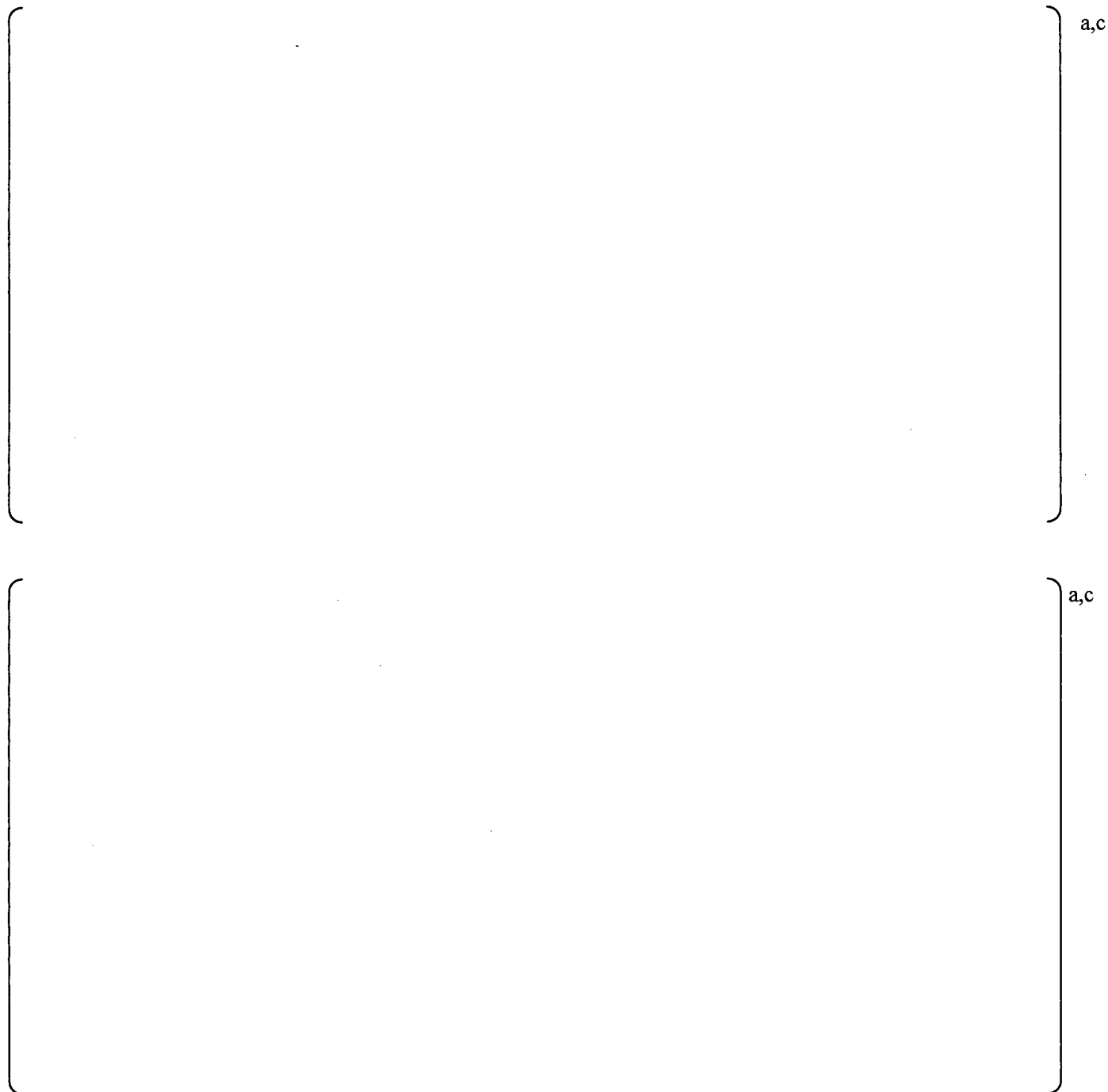


Figure C-8: PSD comparison at 790 MWe for pressure sensor data (black curves) and ACM Rev. 4.1 model predictions with corrected bias and uncertainty added (red curves), for P11 (top) and P12 (bottom).

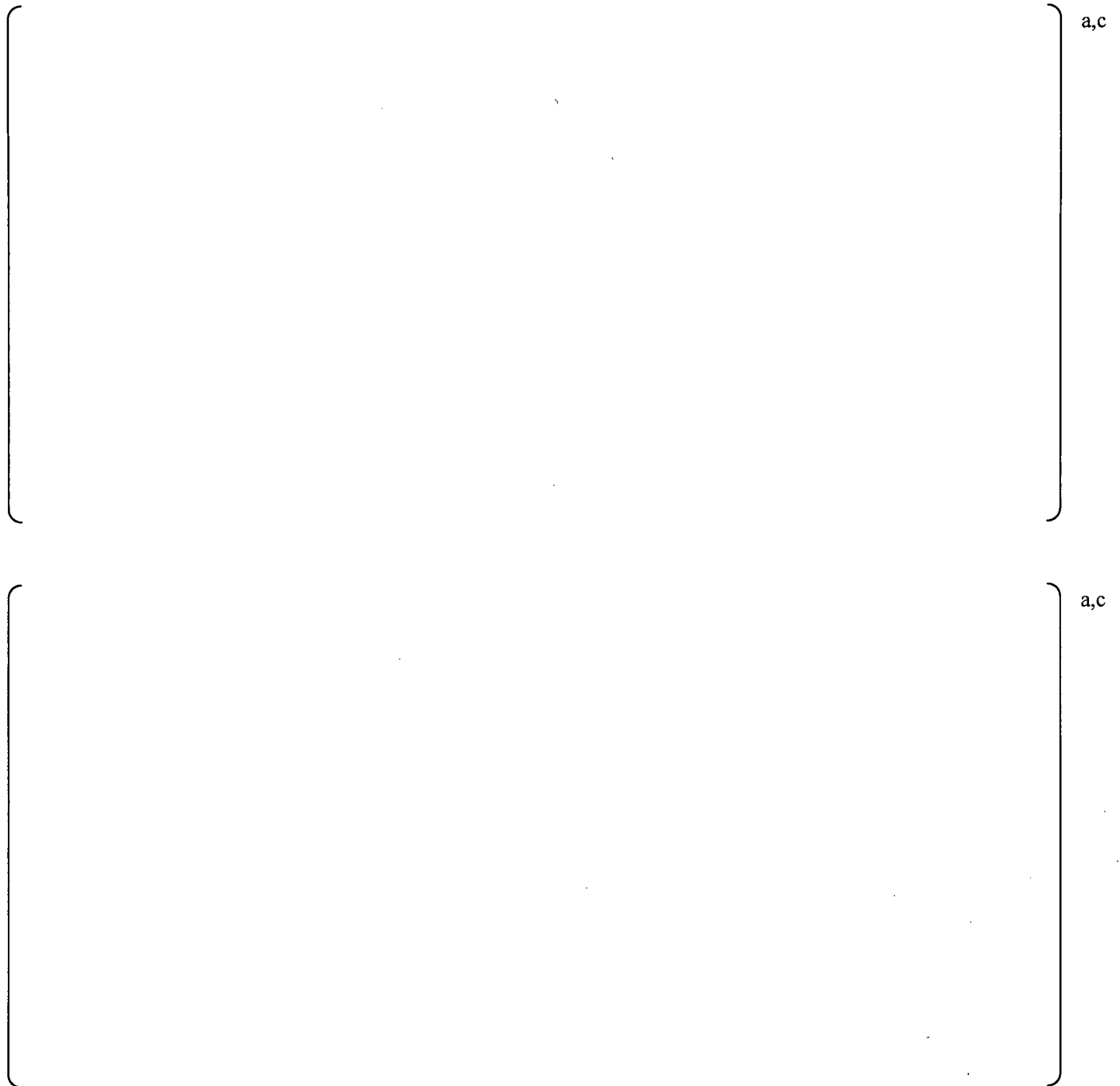


Figure C-9: PSD comparison at 790 MWe for pressure sensor data (black curves) and ACM Rev. 4.1 model predictions with corrected bias and uncertainty added (red curves), for P13 (top) and P14 (bottom).

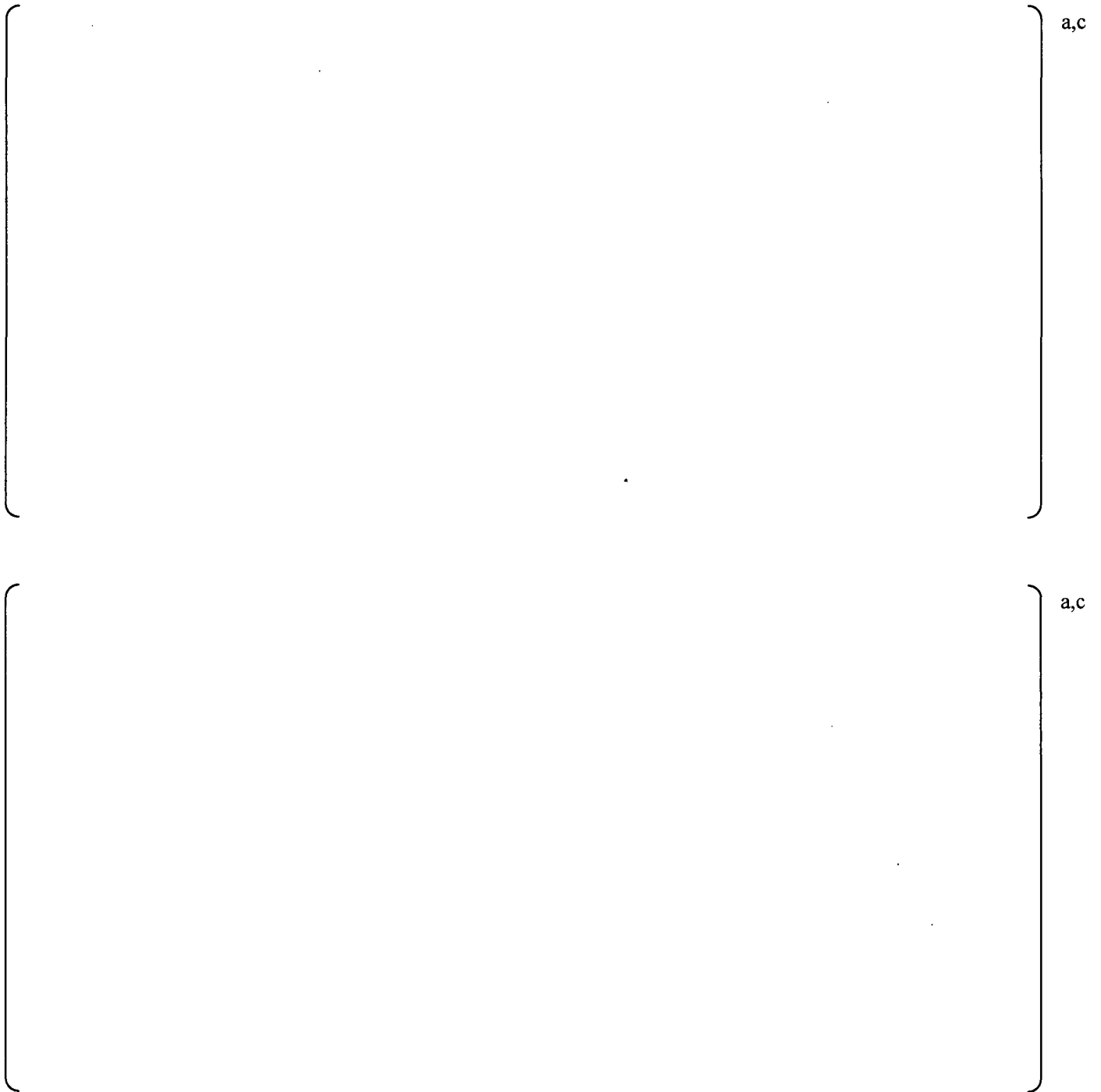


Figure C-10: PSD comparison at 790 MWe for pressure sensor data (black curves) and ACM Rev. 4.1 model predictions with corrected bias and uncertainty added (red curves), for P15 (top) and P16 (bottom).

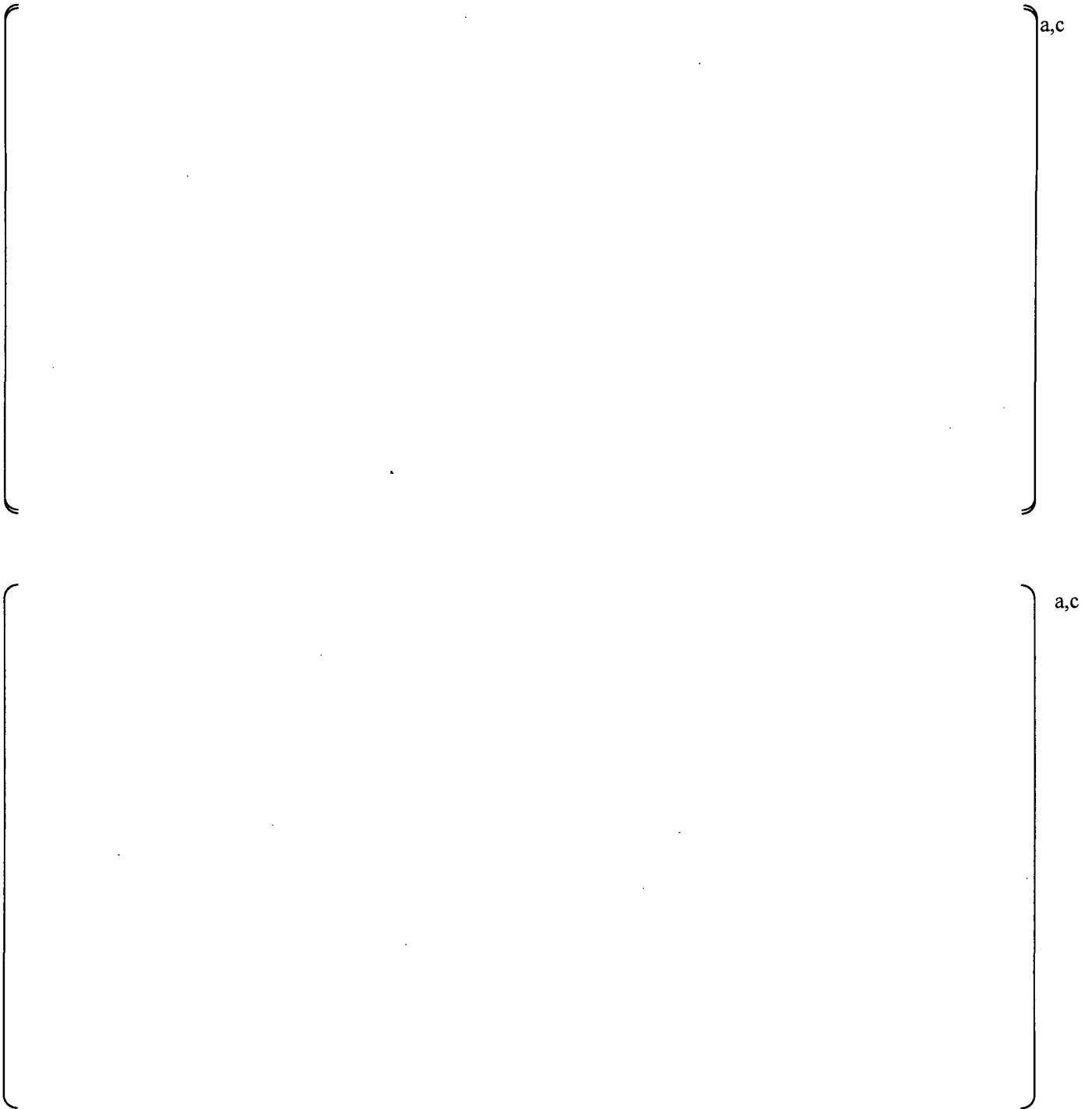


Figure C-11: PSD comparison at 790 MWe for pressure sensor data (black curves) and ACM Rev. 4.1 model predictions with corrected bias and uncertainty added (red curves), for P17 (top) and P18 (bottom).

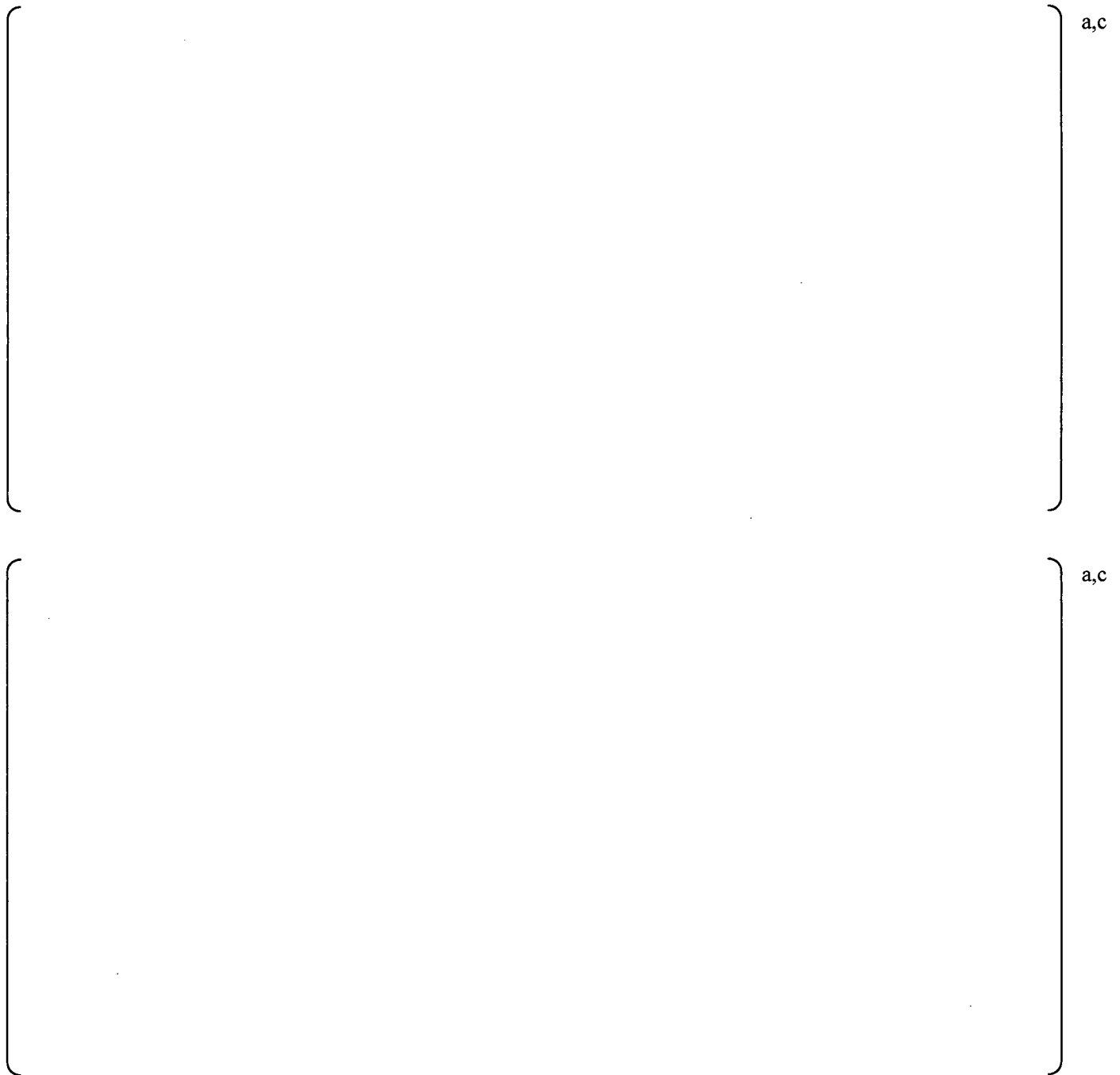


Figure C-12: PSD comparison at 790 MWe for pressure sensor data (black curves) and ACM Rev. 4.1 model predictions with corrected bias and uncertainty added (red curves), for P19 (top) and P20 (bottom).



Figure C-13: PSD comparison at 790 MWe for pressure sensor data (black curves) and ACM Rev. 4.1 model predictions with corrected bias and uncertainty added (red curves), for P21 (top) and P22 (bottom).

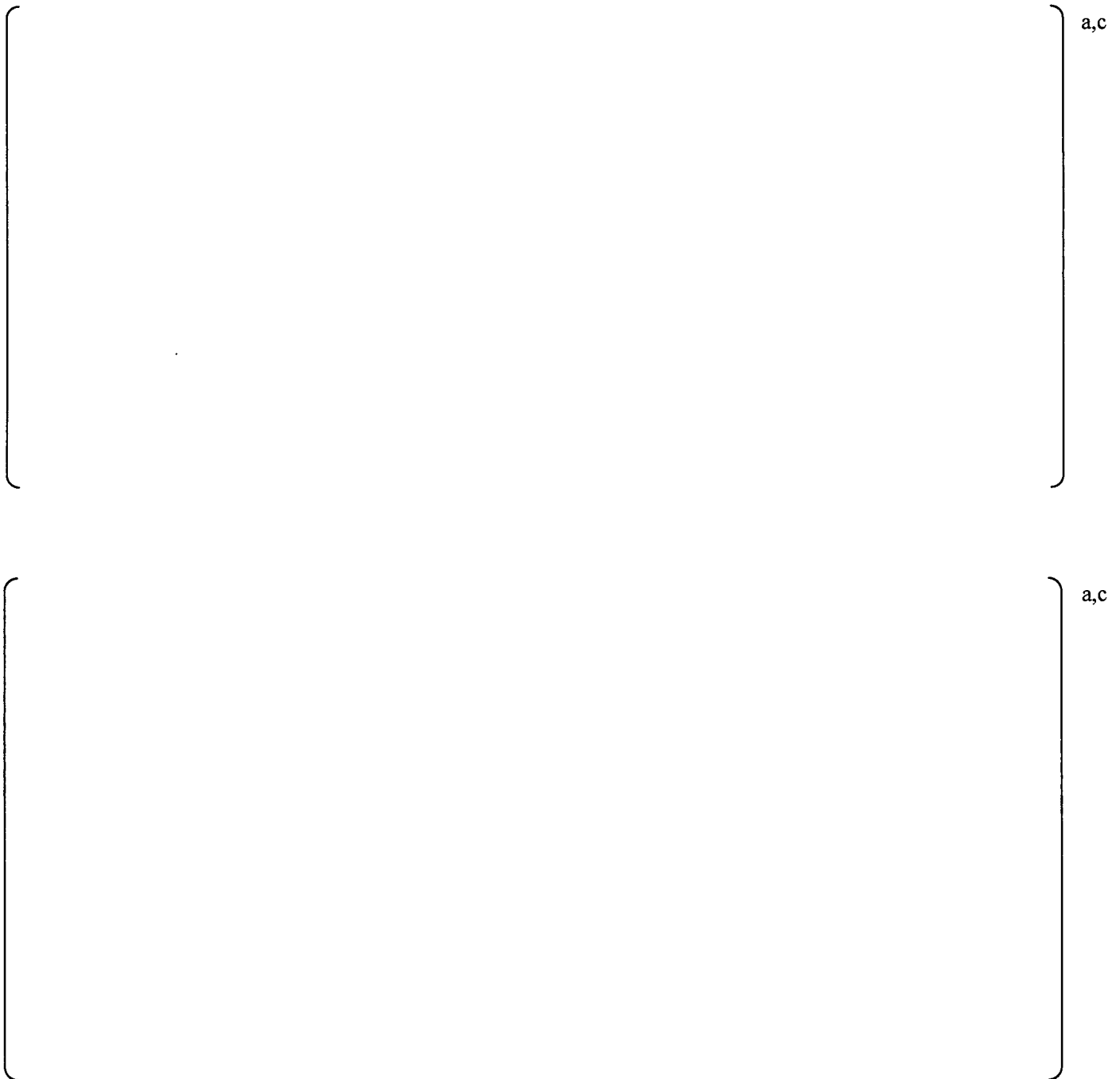


Figure C-14: PSD comparison at 790 MWe for pressure sensor data (black curves) and ACM Rev. 4.1 model predictions with corrected bias and uncertainty added (red curves), for P23 (top) and P24 (bottom).

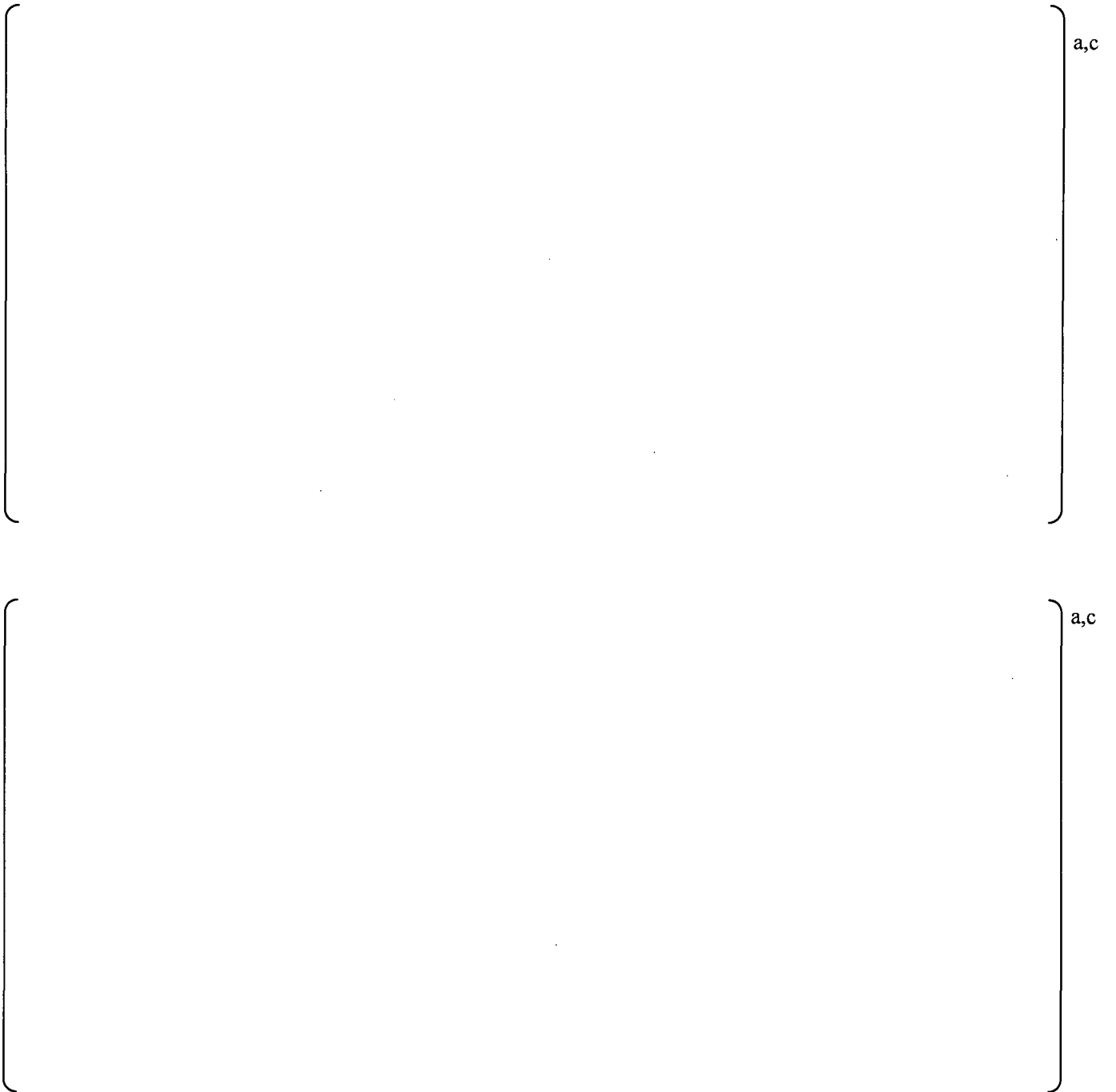


Figure C-15: PSD comparison at 790 MWe for pressure sensor data (black curves) and ACM Rev. 4.1 model predictions with corrected bias and uncertainty added (red curves), for P25 (top) and P26 (bottom).



Figure C-16: PSD comparison at 790 MWe for pressure sensor data (black curve) and ACM Rev. 4.1 model prediction with corrected bias and uncertainty added (red curve), for P27.

Appendix D: ACM Rev. 4.1 Comparisons To Quad Cities Unit 2 840 MWe Test Data

This appendix provides the comparison of QC2 data collected at 840 MWe with ACM Rev. 4.1 model predictions.

Figure D-1 and Figure D-2 plot the main steam line data, while Figure D-3 to Figure D-16 plot the comparisons between model predictions and data at each of the 27 pressure transducer locations on the dryer.



Figure D-1: PSDs of pressure data at 840 MWe on main steam lines A (top) and B (bottom): upper strain gage locations (blue curves), lower strain gage locations (red curves). EMF and coherence filtering have been applied to these signals.



Figure D-2: PSDs of pressure data at 840 MWe on main steam lines C (top) and D (bottom): upper strain gage locations (blue curves), lower strain gage locations (red curves). EMF and coherence filtering have been applied to these signals.

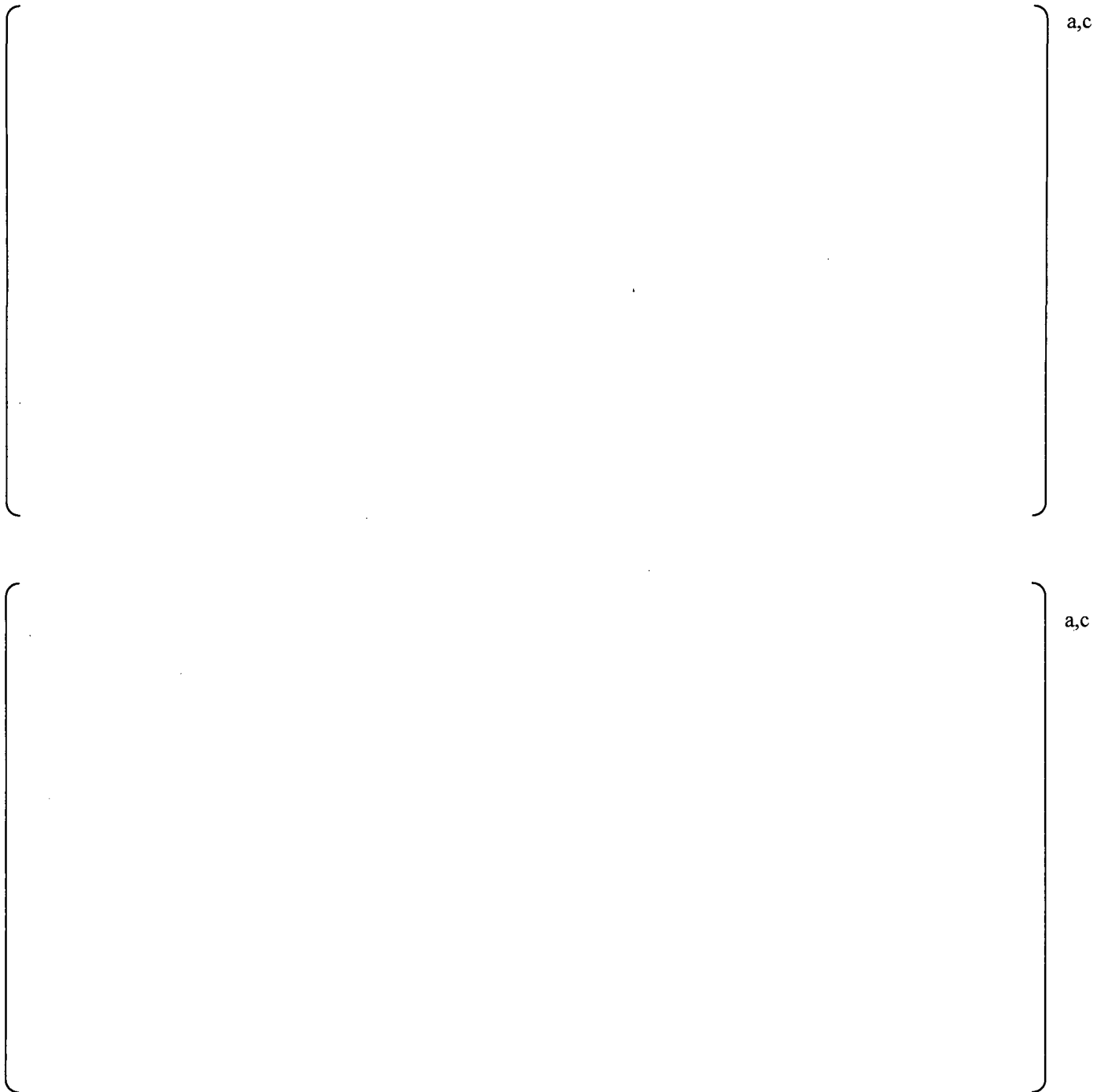


Figure D-3: PSD comparison at 840 MWe for pressure sensor data (black curves) and ACM Rev. 4.1 model predictions with corrected bias and uncertainty added (red curves), for P1 (top) and P2 (bottom).

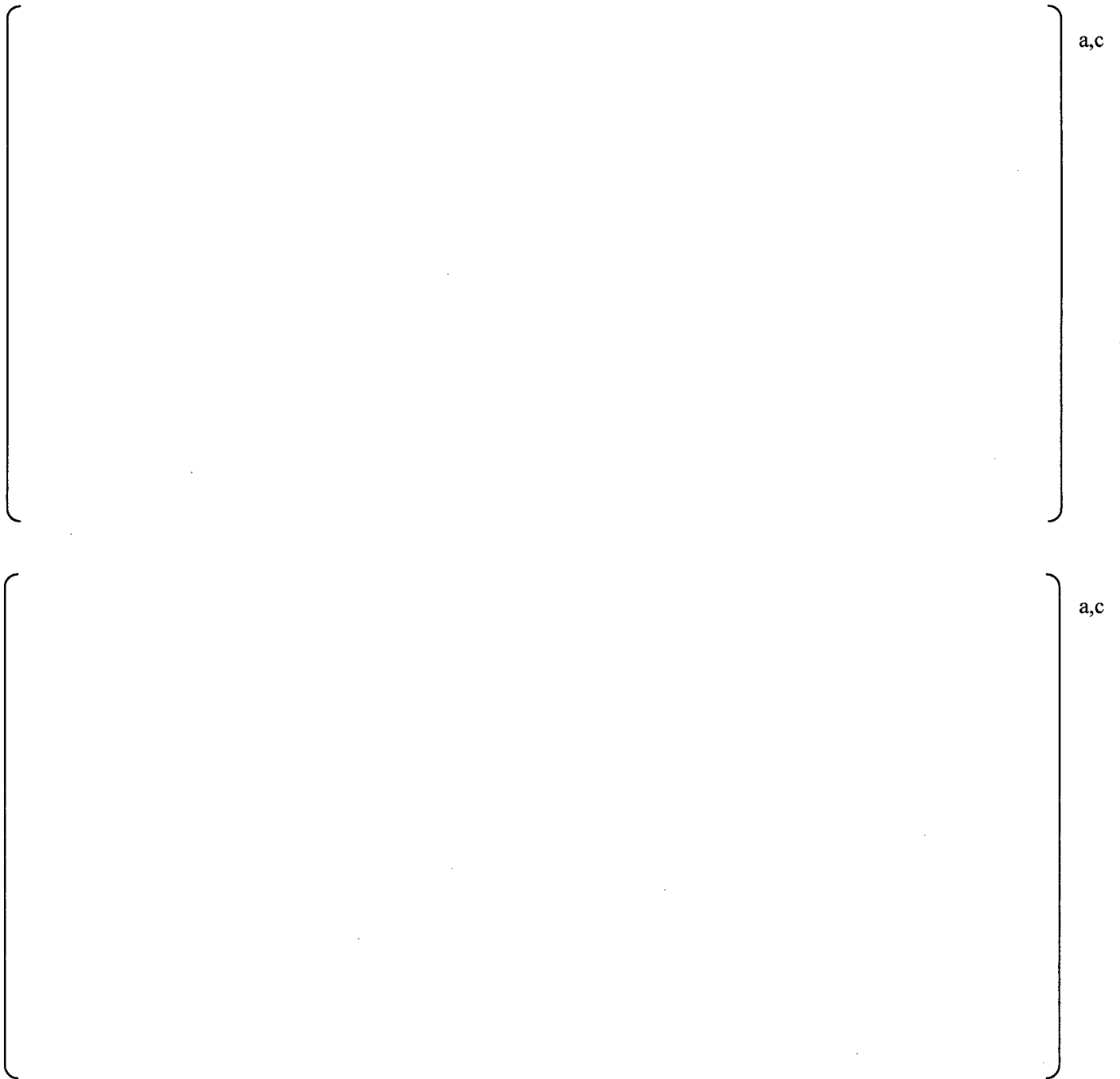


Figure D-4: PSD comparison at 840 MWe for pressure sensor data (black curves) and ACM Rev. 4.1 model predictions with corrected bias and uncertainty added (red curves), for P3 (top) and P4 (bottom).

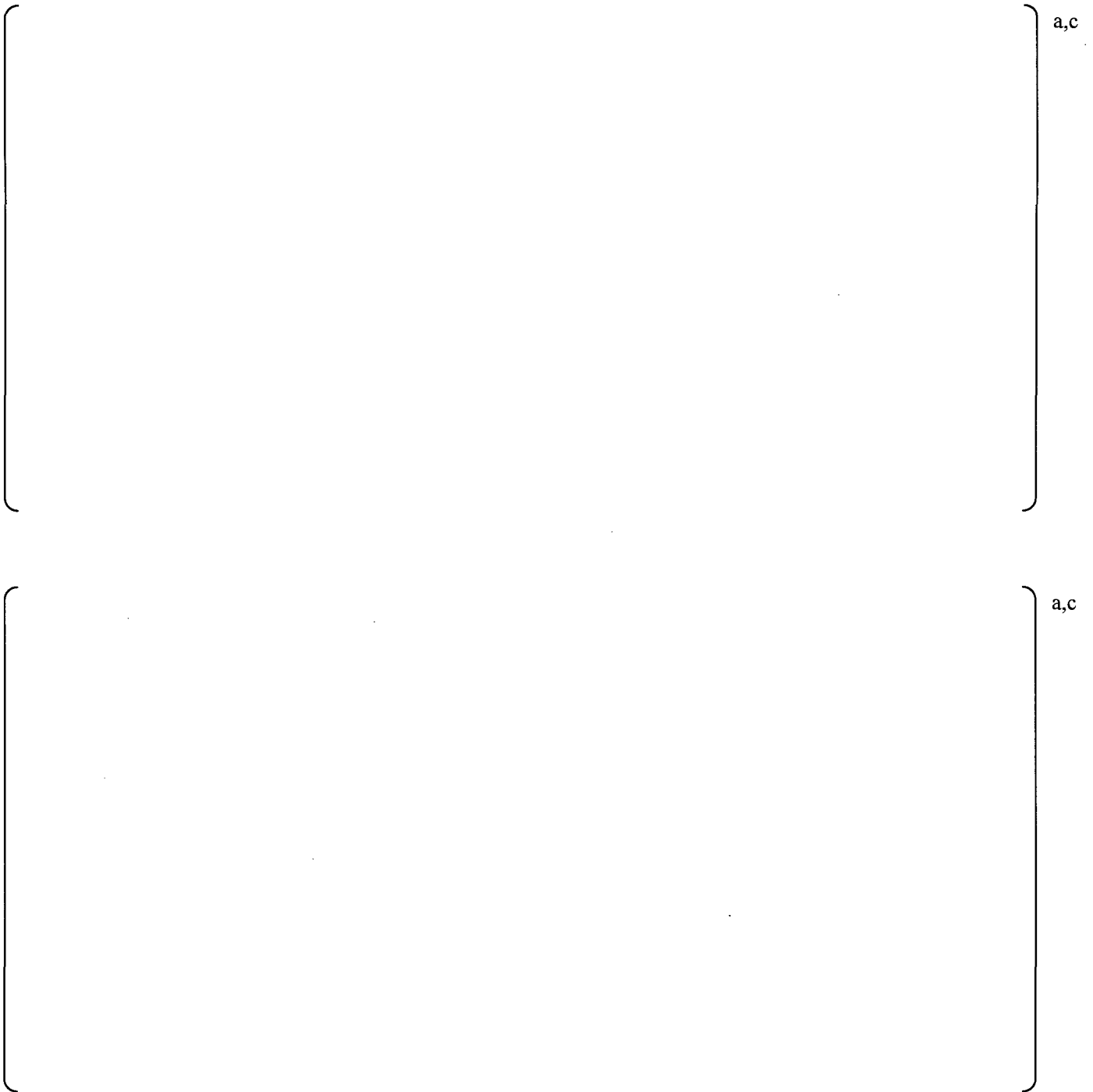


Figure D-5: PSD comparison at 840 MWe for pressure sensor data (black curves) and ACM Rev. 4.1 model predictions with corrected bias and uncertainty added (red curves), for P5 (top) and P6 (bottom).

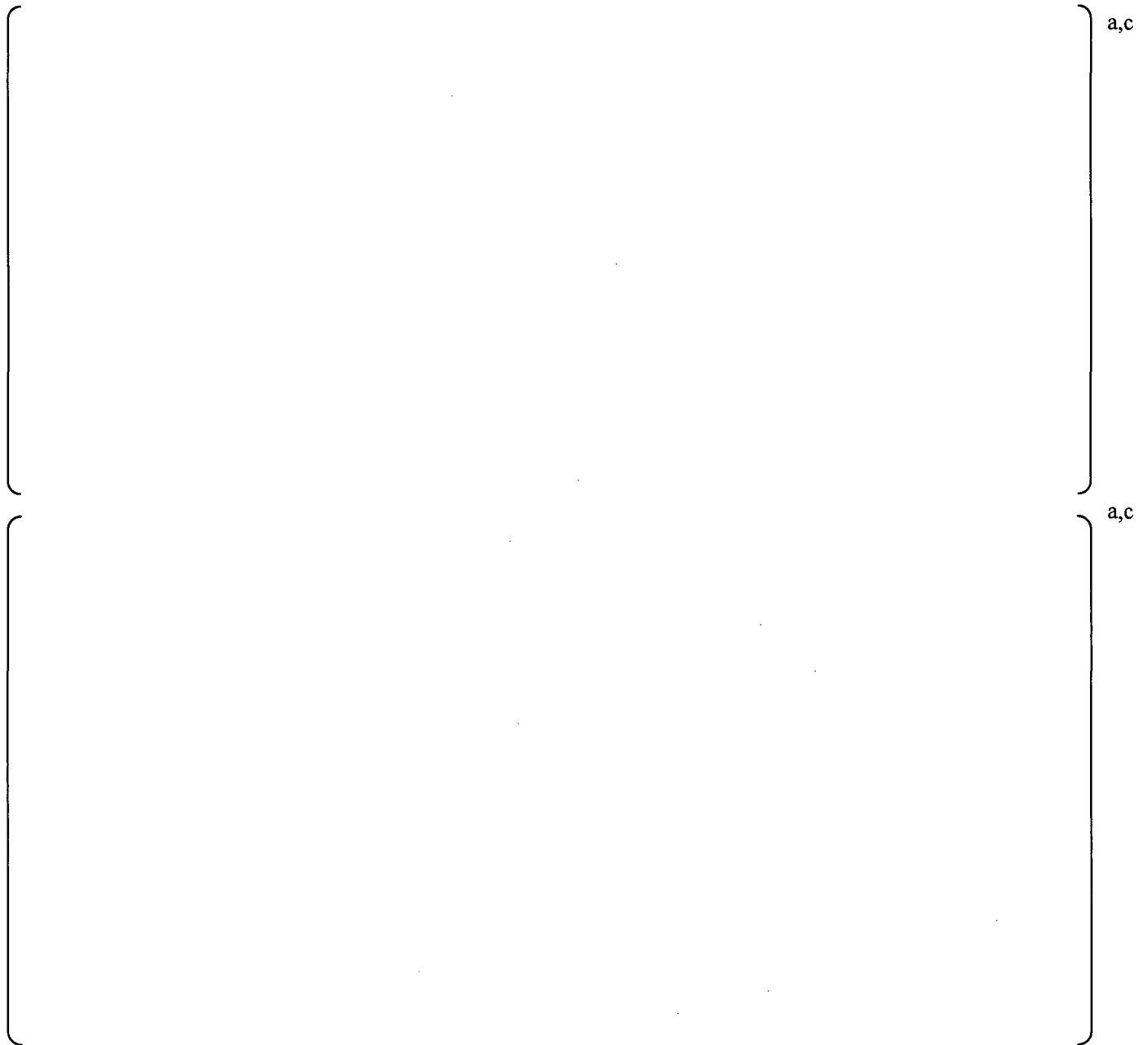


Figure D-6: PSD comparison at 840 MWe for pressure sensor data (black curves) and ACM Rev. 4.1 model predictions with corrected bias and uncertainty added (red curves), for P7 (top) and P8 (bottom).

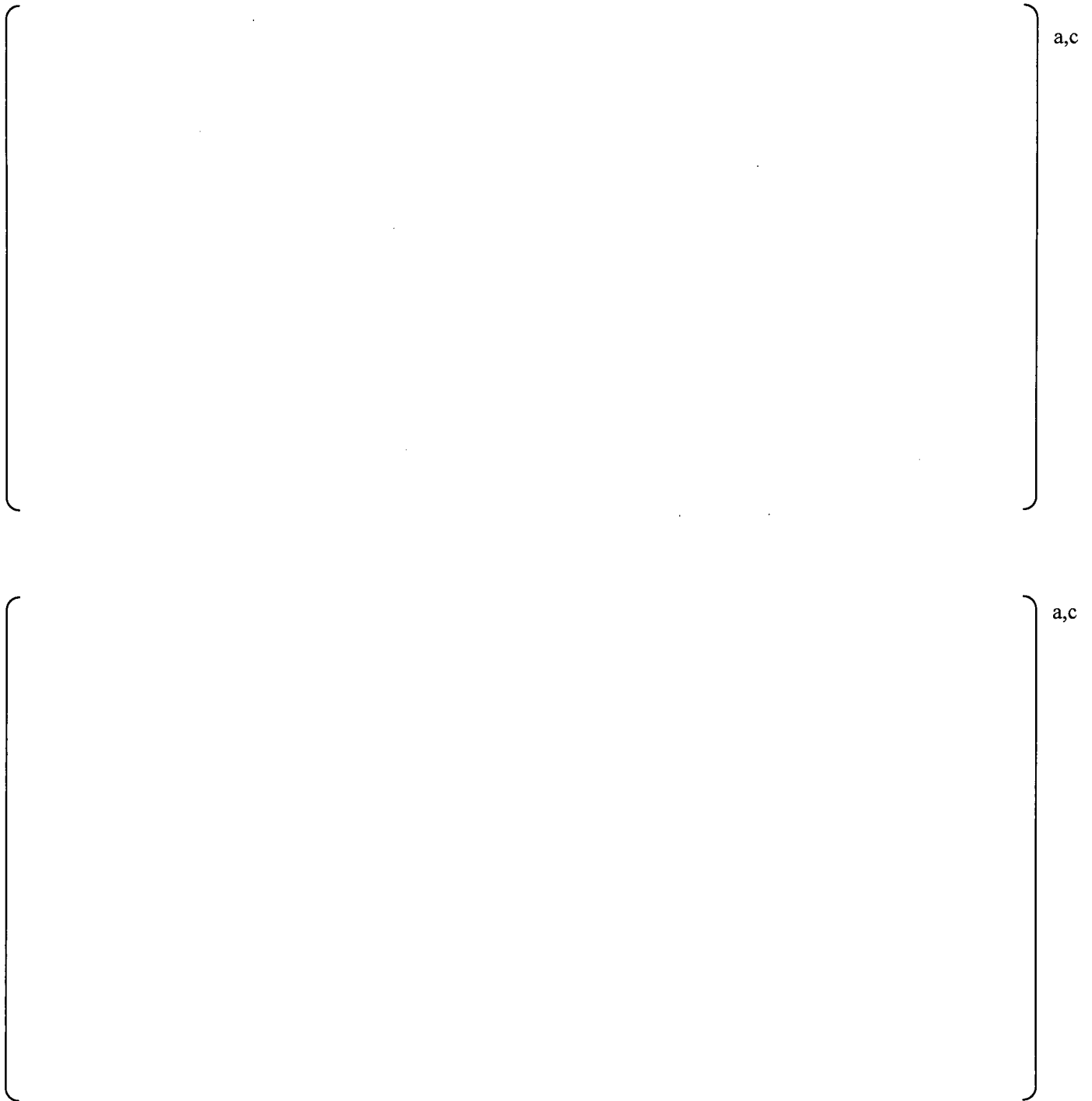


Figure D-7: PSD comparison at 840 MWe for pressure sensor data (black curves) and ACM Rev. 4.1 model predictions with corrected bias and uncertainty added (red curves), for P9 (top) and P10 (bottom).

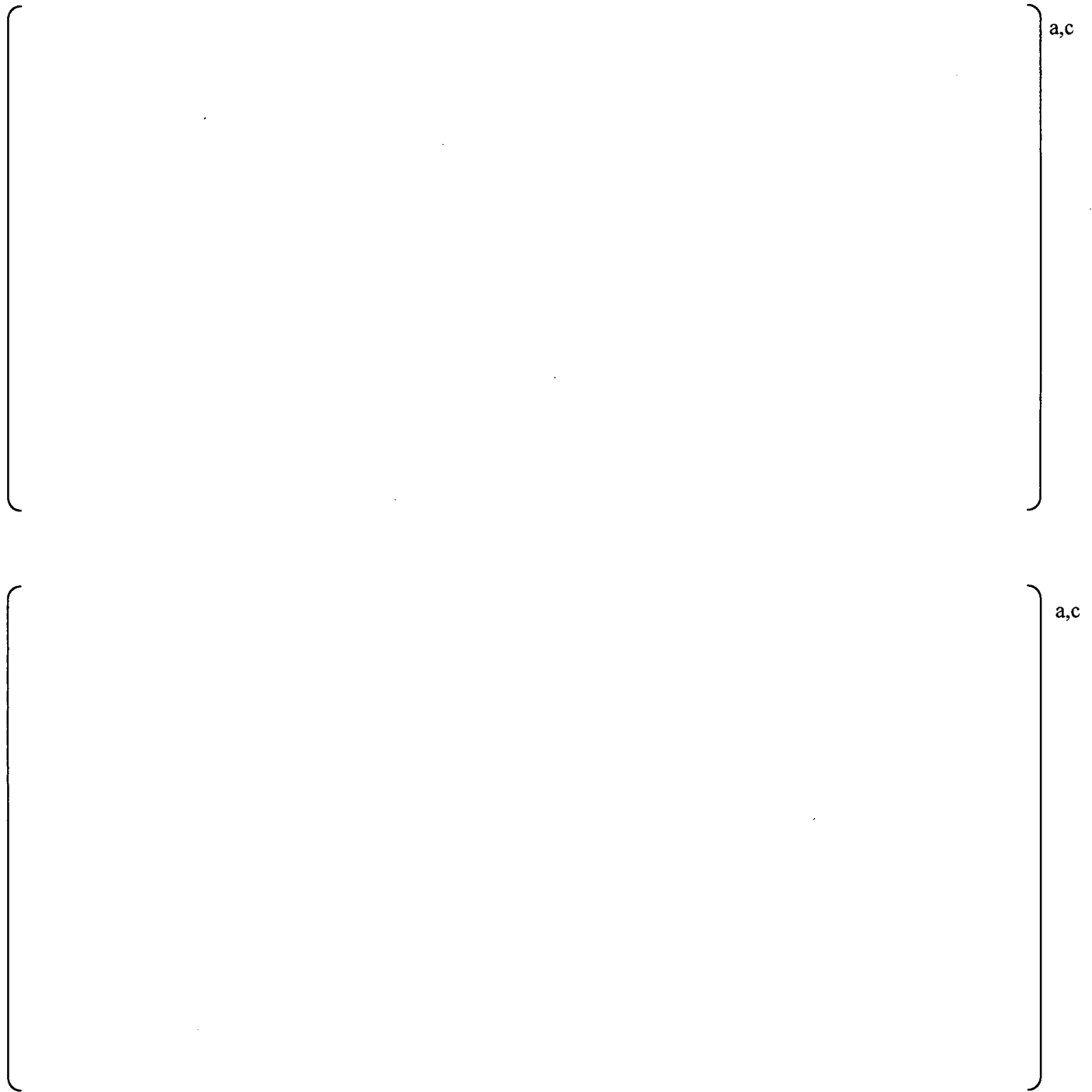


Figure D-8: PSD comparison at 840 MWe for pressure sensor data (black curves) and ACM Rev. 4.1 model predictions with corrected bias and uncertainty added (red curves), for P11 (top) and P12 (bottom).

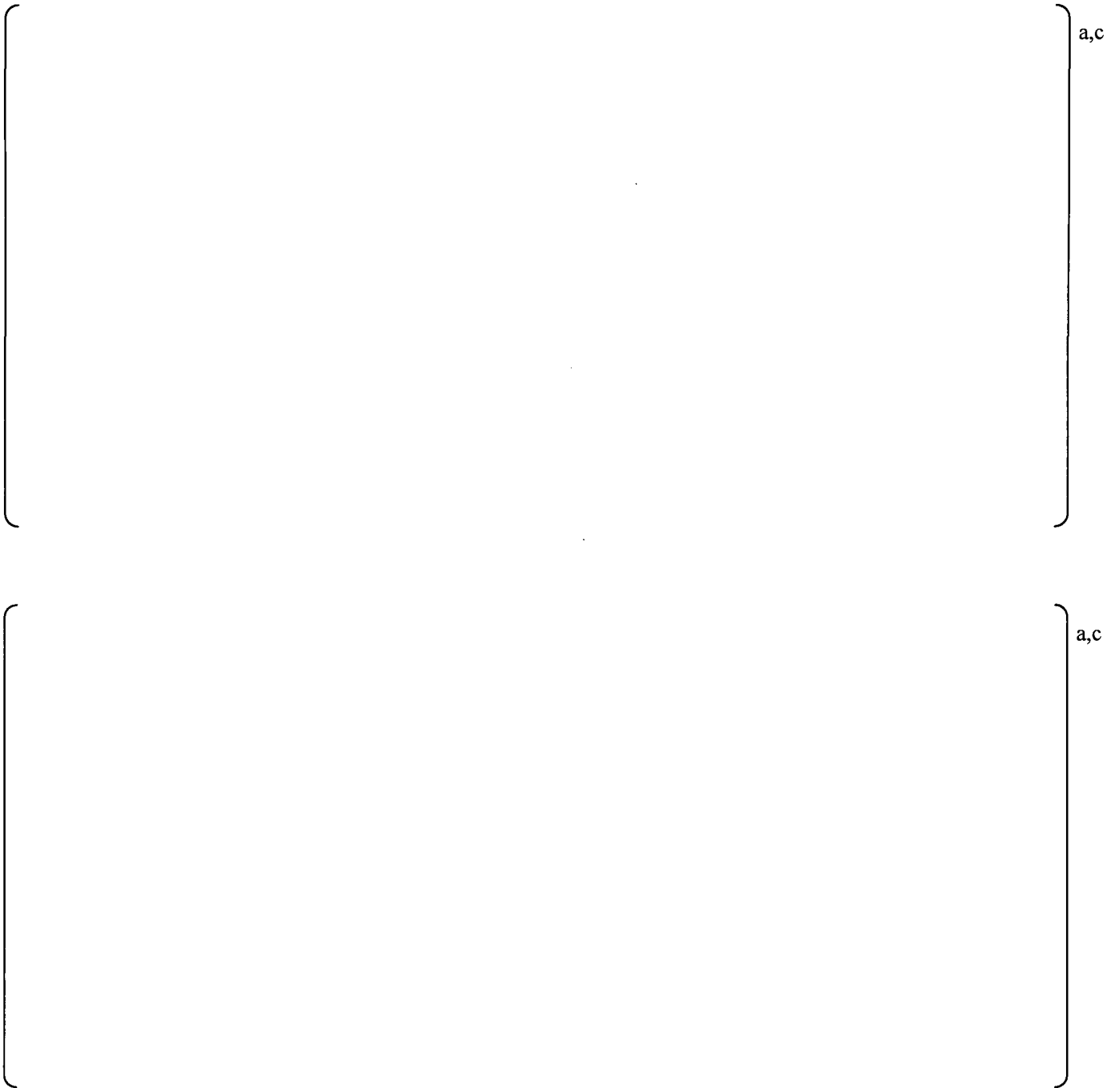


Figure D-9: PSD comparison at 840 MWe for pressure sensor data (black curves) and ACM Rev. 4.1 model predictions with corrected bias and uncertainty added (red curves), for P13 (top) and P14 (bottom).

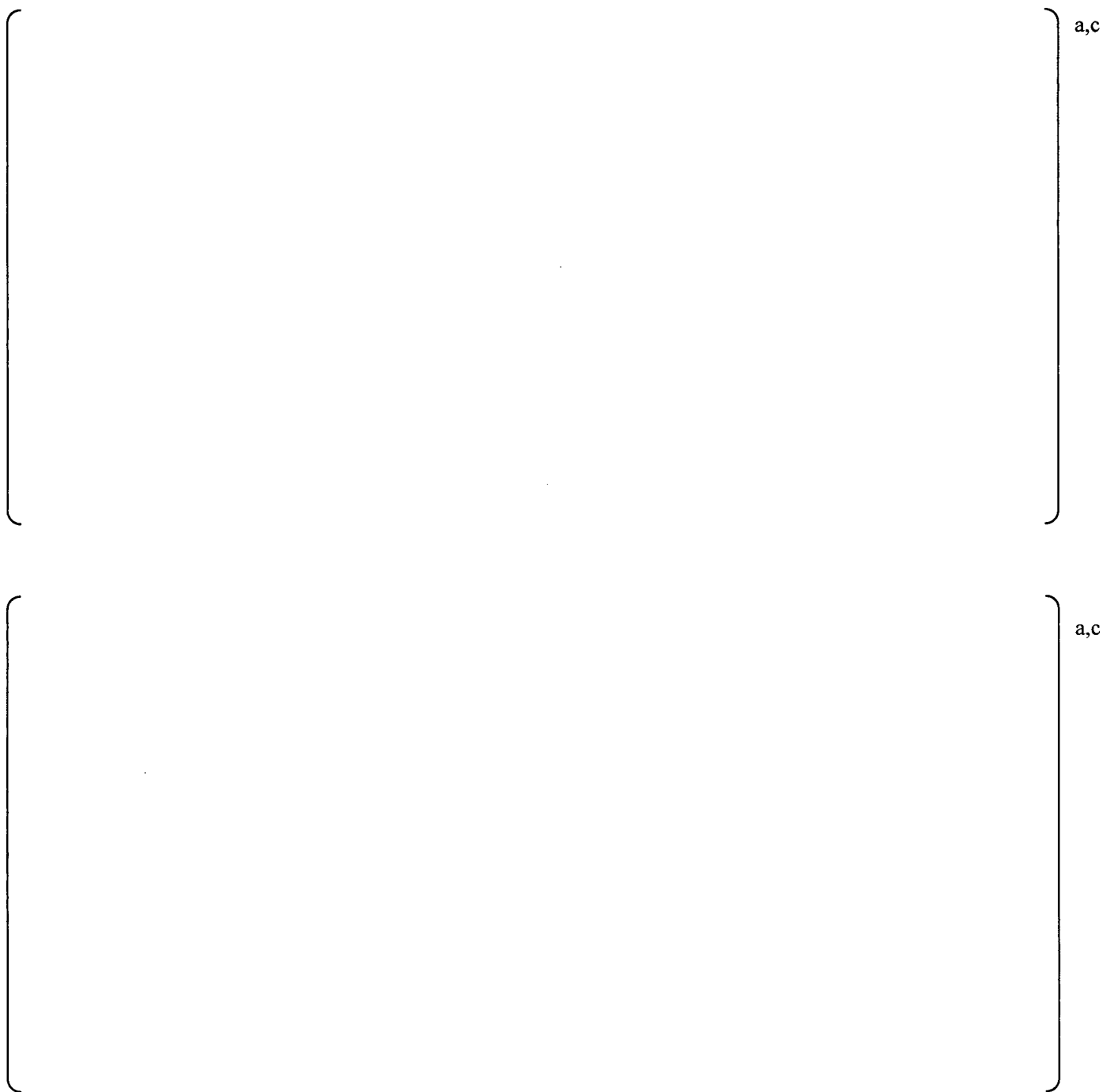


Figure D-10: PSD comparison at 840 MWe for pressure sensor data (black curves) and ACM Rev. 4.1 model predictions with corrected bias and uncertainty added (red curves), for P15 (top) and P16 (bottom).

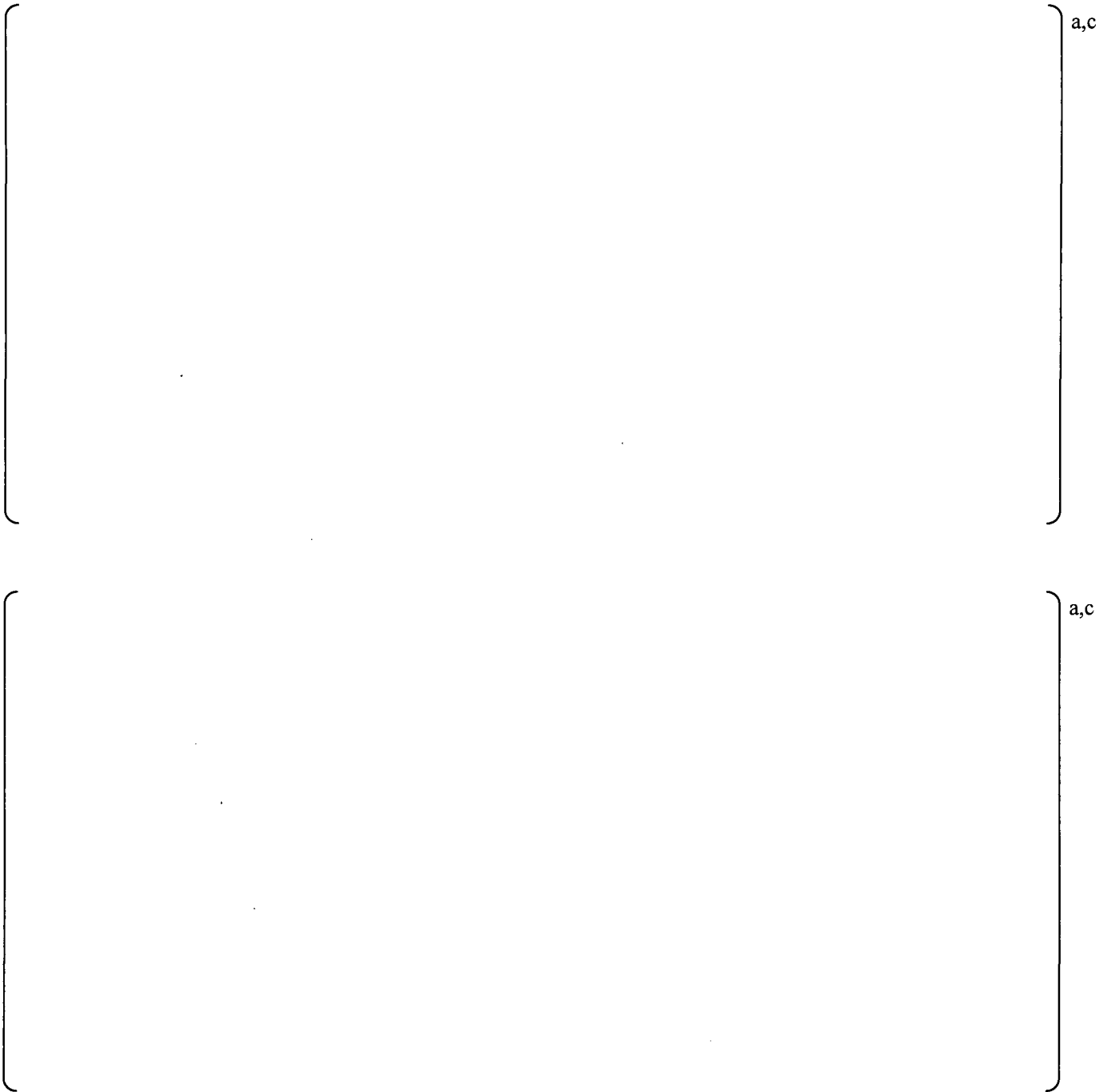


Figure D-11: PSD comparison at 840 MWe for pressure sensor data (black curves) and ACM Rev. 4.1 model predictions with corrected bias and uncertainty added (red curves), for P17 (top) and P18 (bottom).

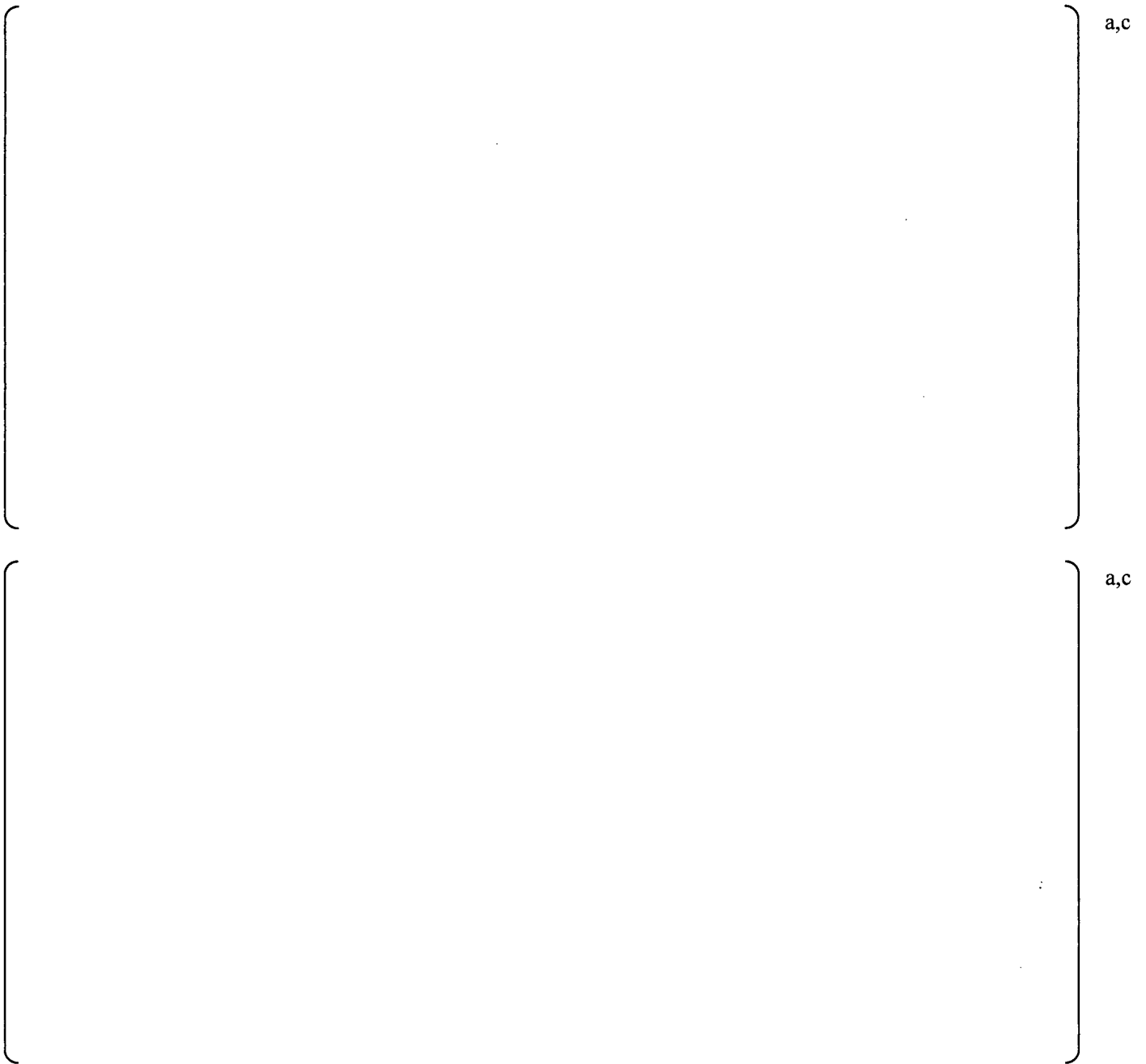


Figure D-12: PSD comparison at 840 MWe for pressure sensor data (black curves) and ACM Rev. 4.1 model predictions with corrected bias and uncertainty added (red curves), for P19 (top) and P20 (bottom).

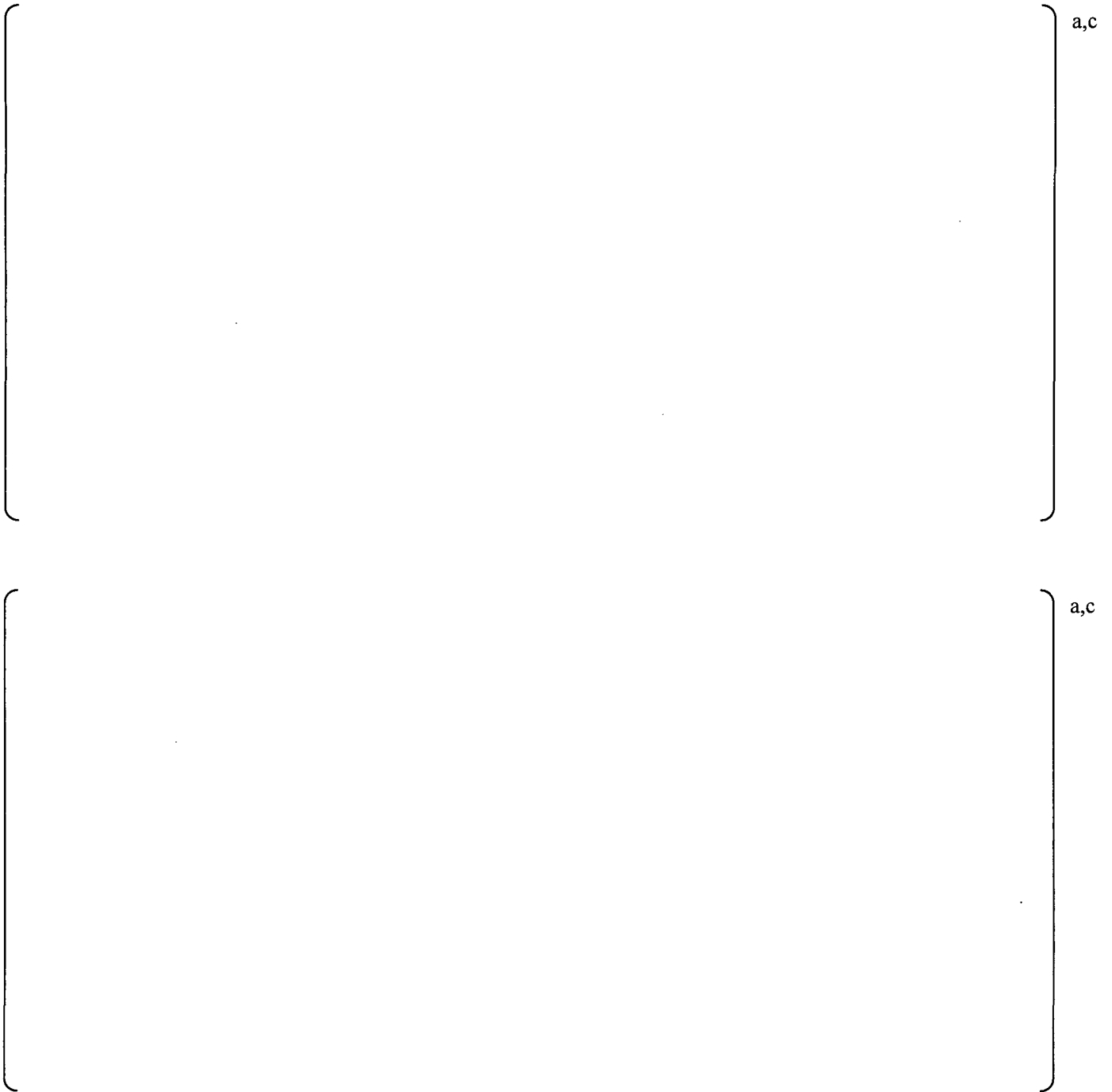


Figure D-13: PSD comparison at 840 MWe for pressure sensor data (black curves) and ACM Rev. 4.1 model predictions with corrected bias and uncertainty added (red curves), for P21 (top) and P22 (bottom).

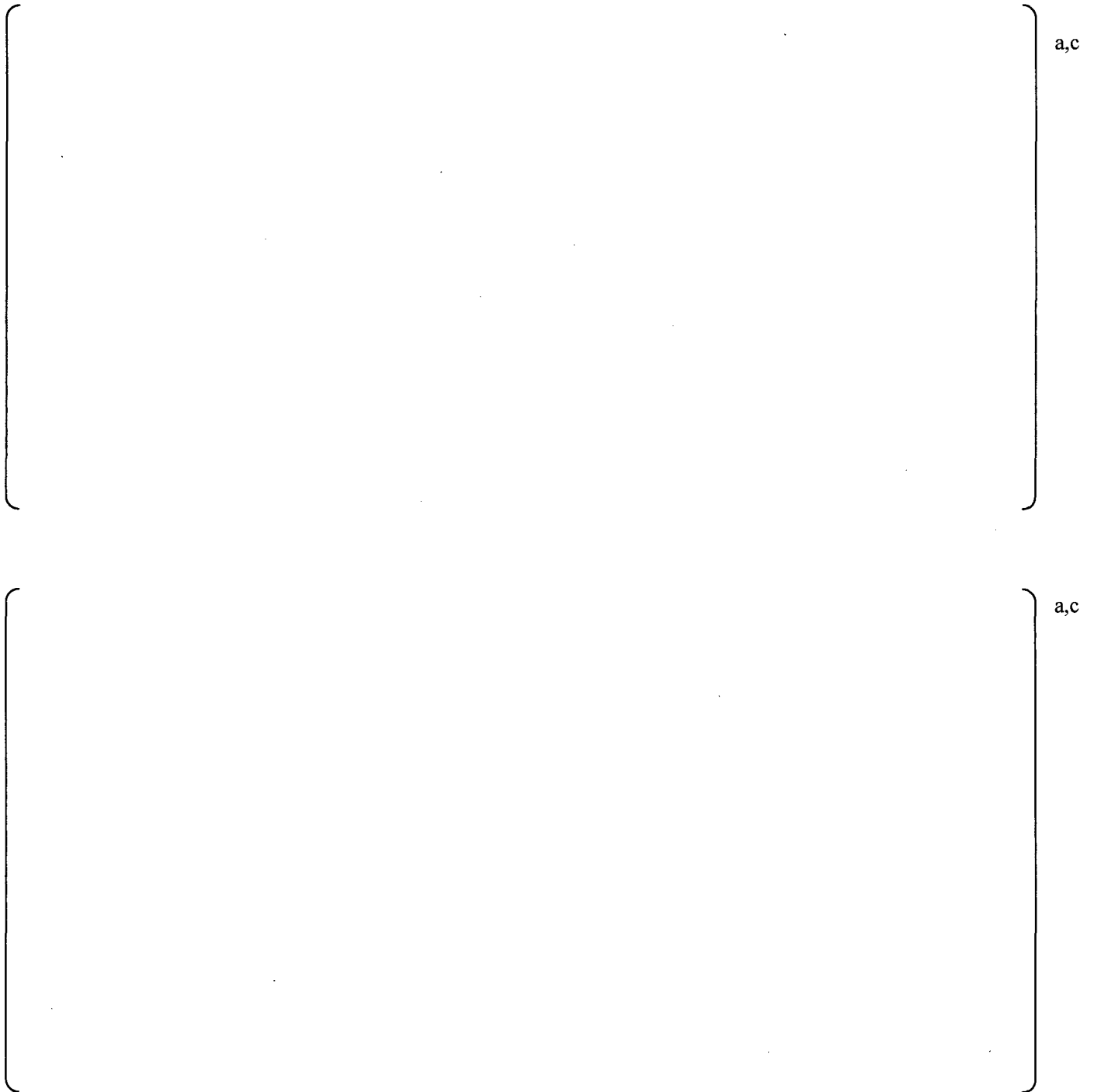


Figure D-14: PSD comparison at 840 MWe for pressure sensor data (black curves) and ACM Rev. 4.1 model predictions with corrected bias and uncertainty added (red curves), for P23 (top) and P24 (bottom).

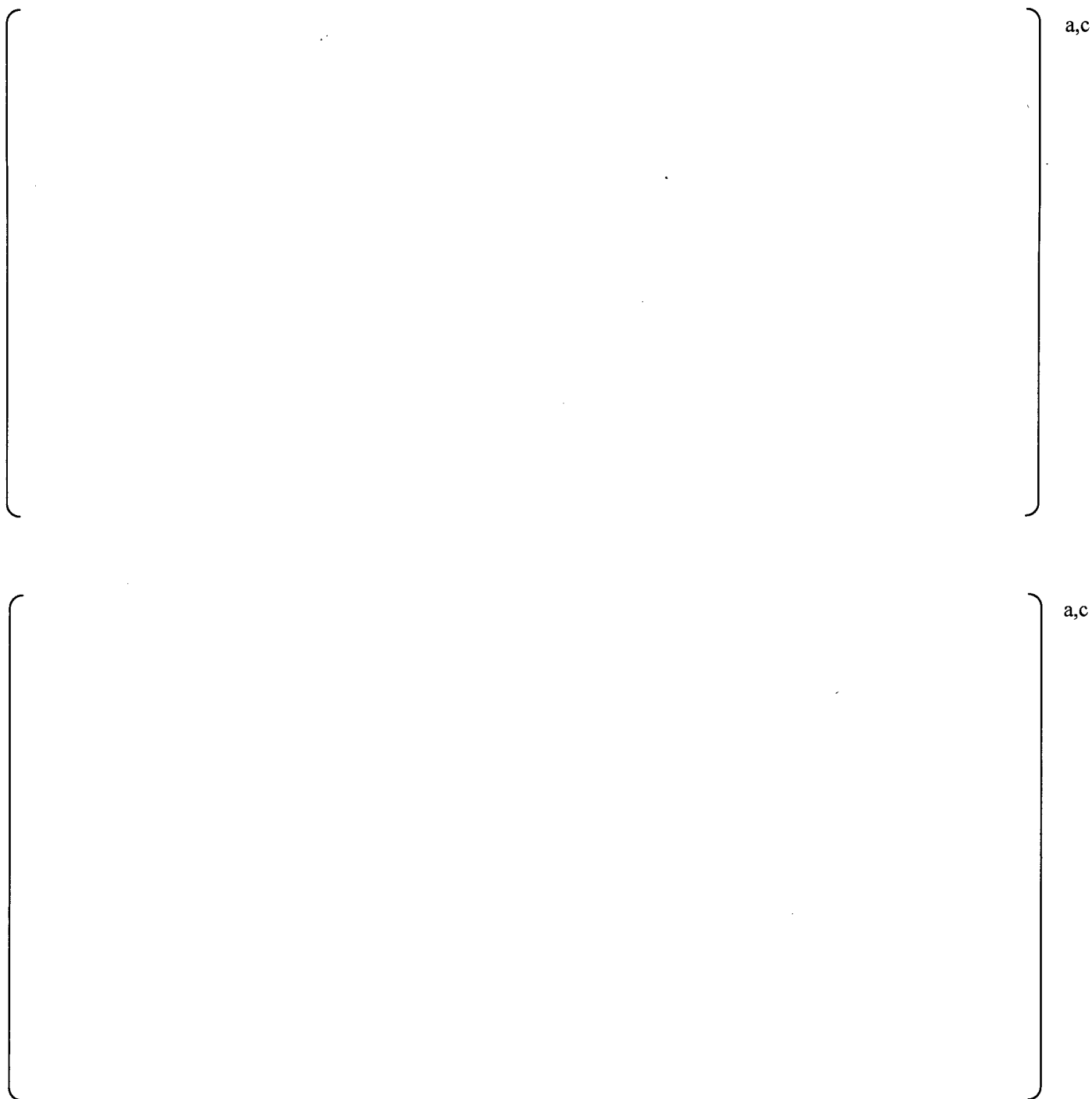


Figure D-15: PSD comparison at 840 MWe for pressure sensor data (black curves) and ACM Rev. 4.1 model predictions with corrected bias and uncertainty added (red curves), for P25 (top) and P26 (bottom).



Figure D-16: PSD comparison at 840 MWe for pressure sensor data (black curve) and ACM Rev. 4.1 model prediction with corrected bias and uncertainty added (red curve), for P27.

Appendix E: ACM Rev. 4.1 Comparisons To Quad Cities Unit 2 930 MWe Test Data

This appendix provides the comparison of QC2 data collected at 930 MWe with ACM Rev. 4.1 model predictions.

Figure E-1 and Figure E-2 plot the main steam line data, while Figure E-3 to Figure E-16 plot the comparisons between model predictions and data at each of the 27 pressure transducer locations on the dryer.

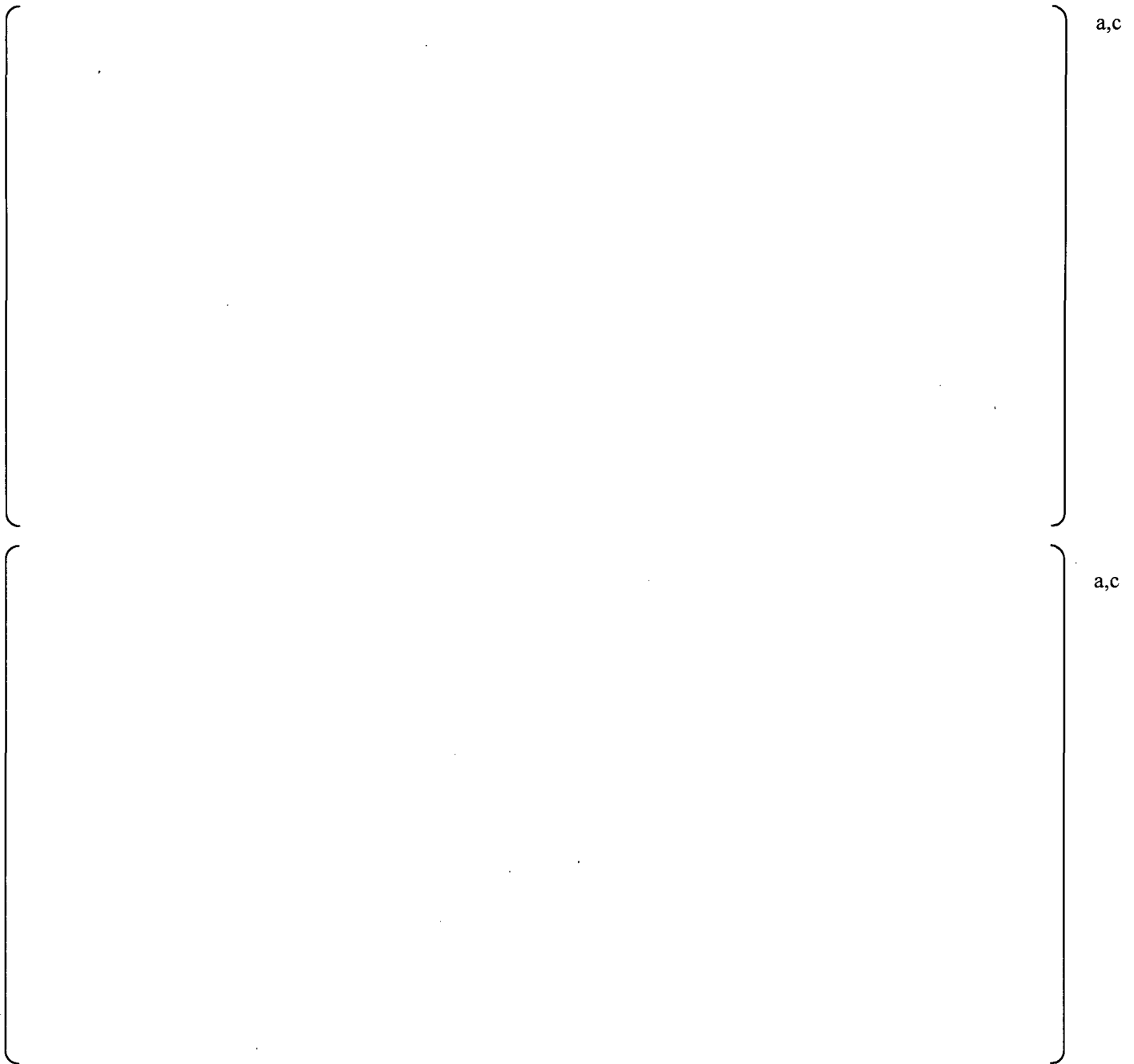


Figure E-1: PSDs of pressure data at 930 MWe on main steam lines A (top) and B (bottom): upper strain gage locations (blue curves), lower strain gage locations (red curves). EMF and coherence filtering have been applied to these signals.

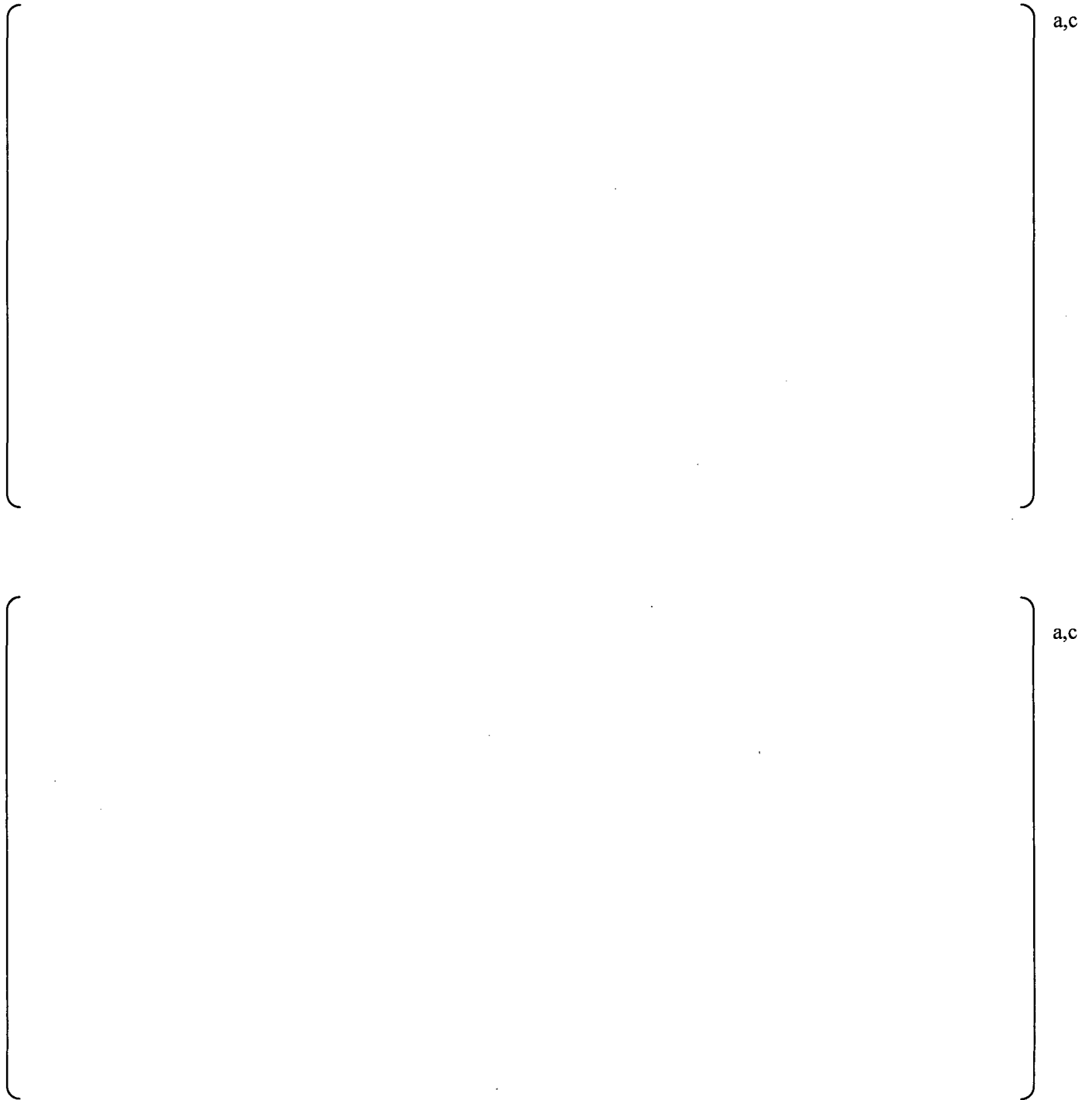


Figure E-2: PSDs of pressure data at 930 MWe on main steam lines C (top) and D (bottom): upper strain gage locations (blue curves), lower strain gage locations (red curves). EMF and coherence filtering have been applied to these signals.

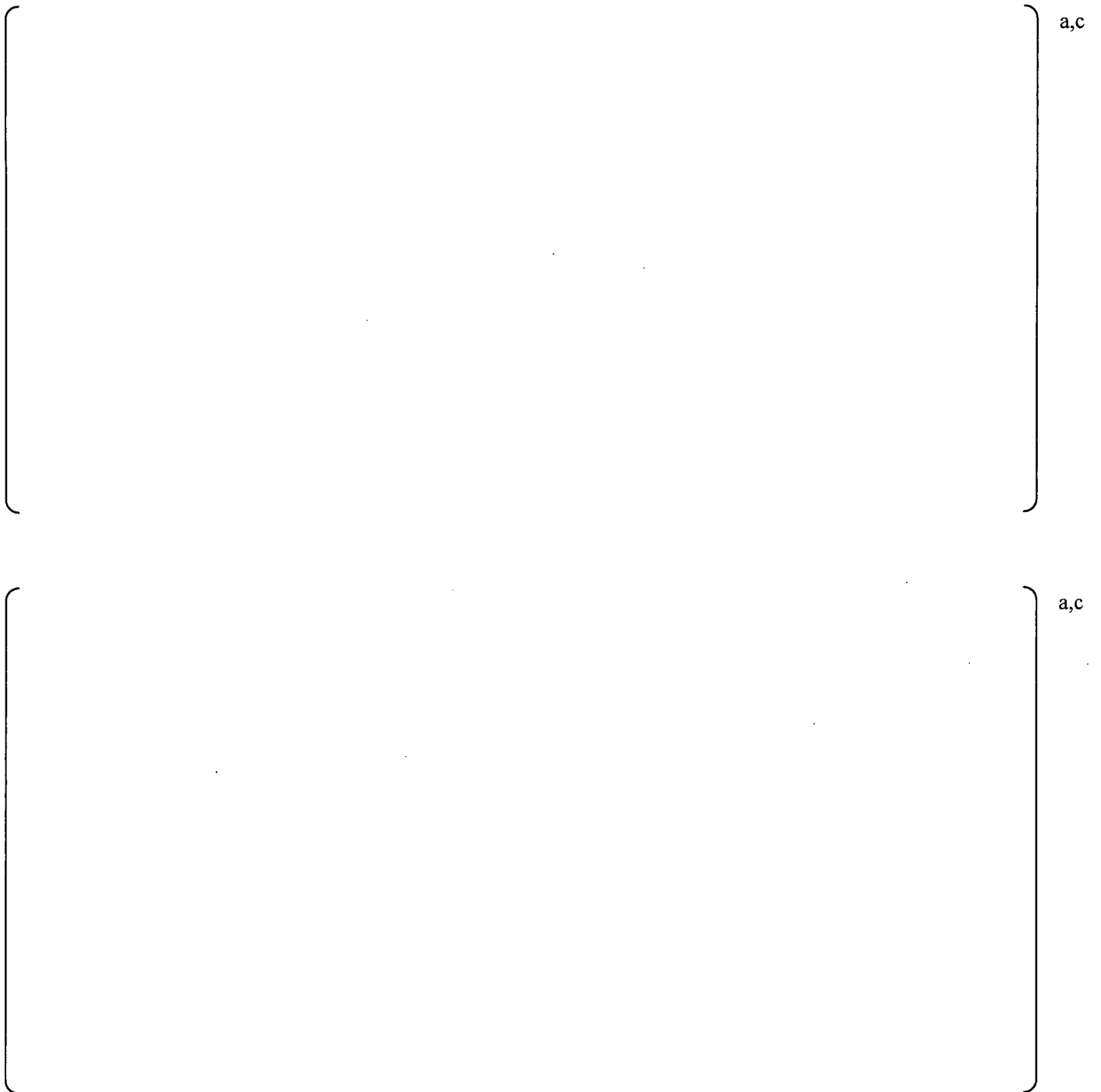


Figure E-3: PSD comparison at 930 MWe for pressure sensor data (black curves) and ACM Rev. 4.1 model predictions with corrected bias and uncertainty added (red curves), for P1 (top) and P2 (bottom).

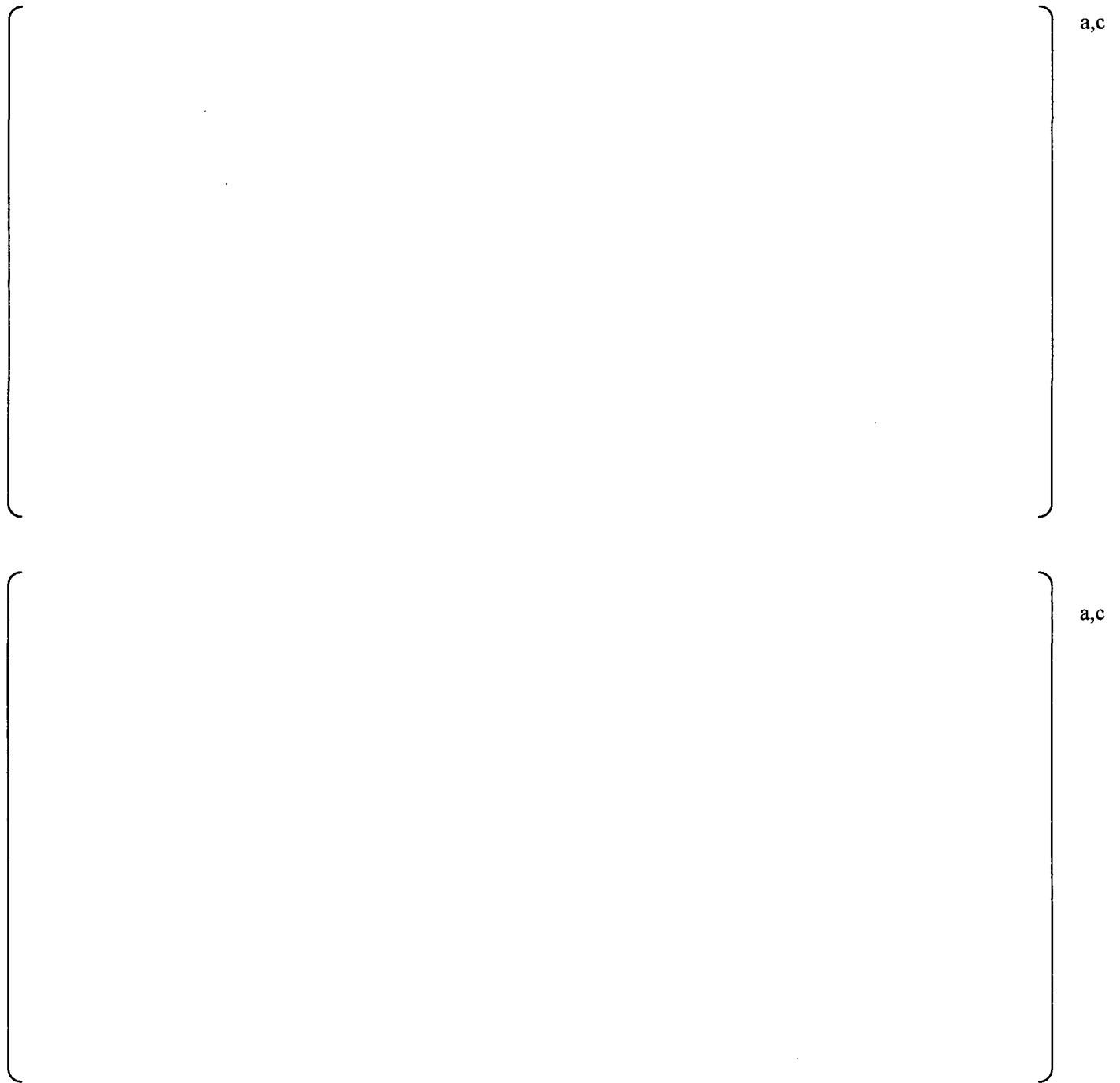


Figure E-4: PSD comparison at 930 MWe for pressure sensor data (black curves) and ACM Rev. 4.1 model predictions with corrected bias and uncertainty added (red curves), for P3 (top) and P4 (bottom).

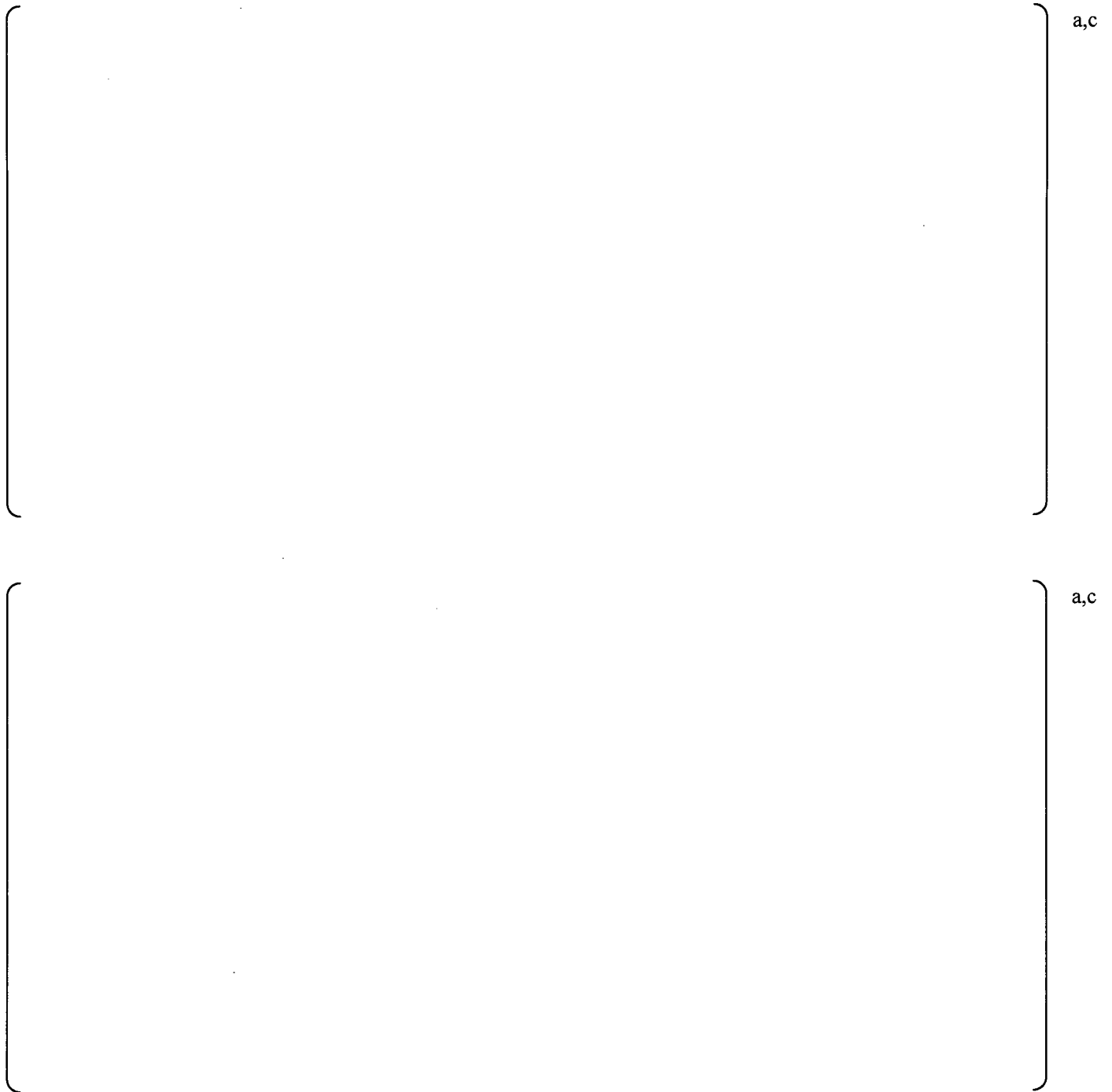


Figure E-5: PSD comparison at 930 MWe for pressure sensor data (black curves) and ACM Rev. 4.1 model predictions with corrected bias and uncertainty added (red curves), for P5 (top) and P6 (bottom).

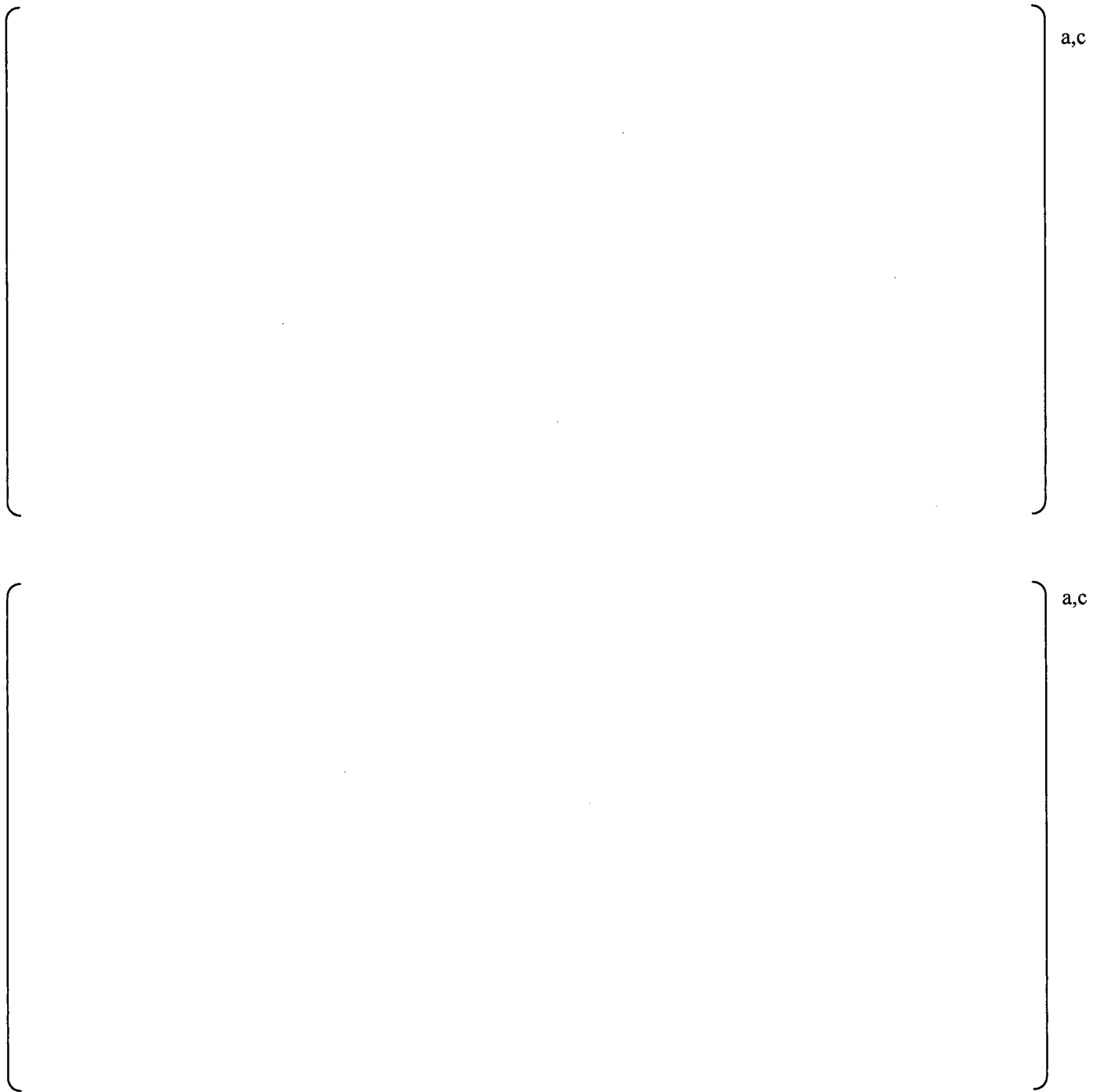


Figure E-6: PSD comparison at 930 MWe for pressure sensor data (black curves) and ACM Rev. 4.1 model predictions with corrected bias and uncertainty added (red curves), for P7 (top) and P8 (bottom).

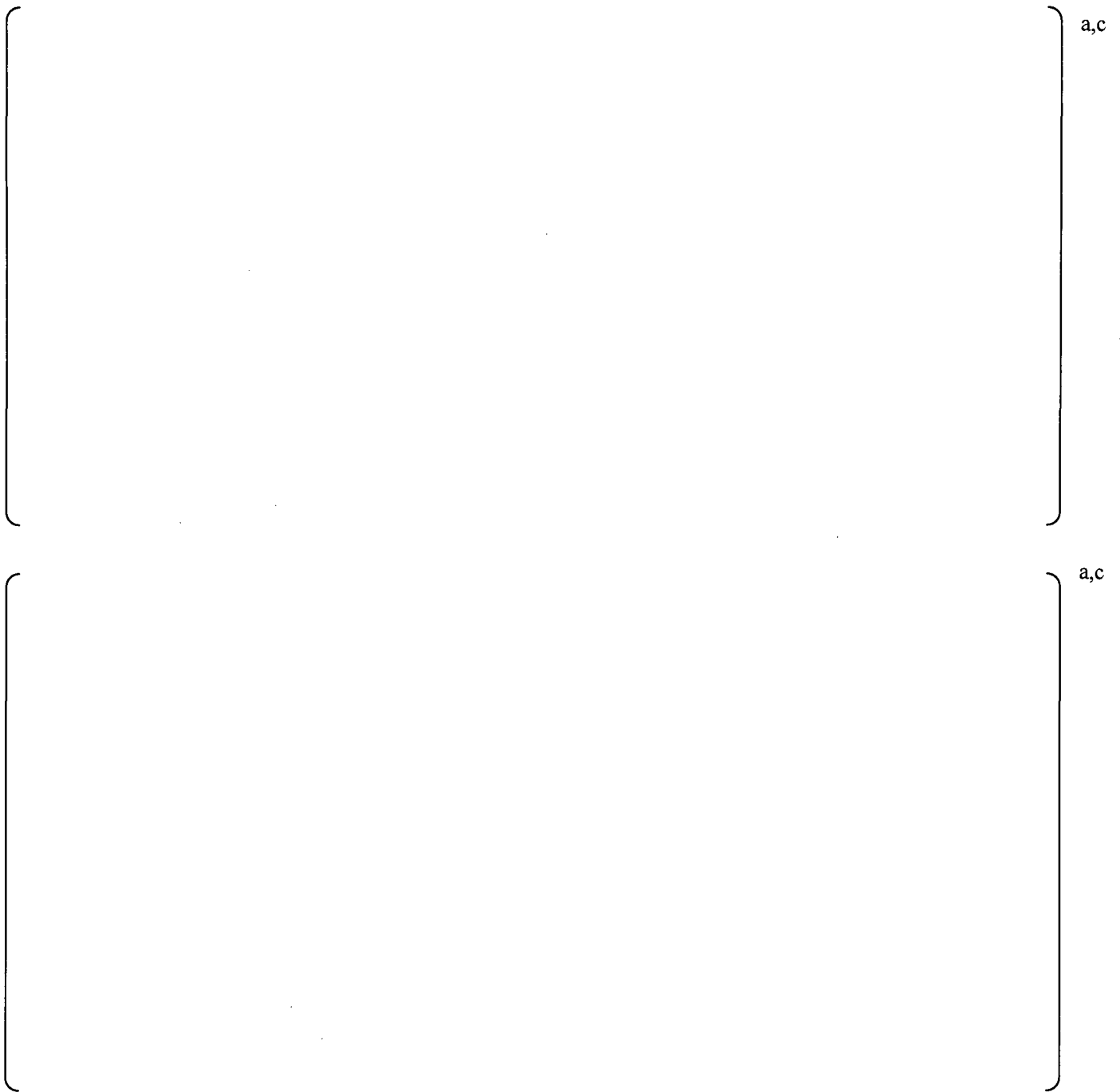


Figure E-7: PSD comparison at 930 MWe for pressure sensor data (black curves) and ACM Rev. 4.1 model predictions with corrected bias and uncertainty added (red curves), for P9 (top) and P10 (bottom).

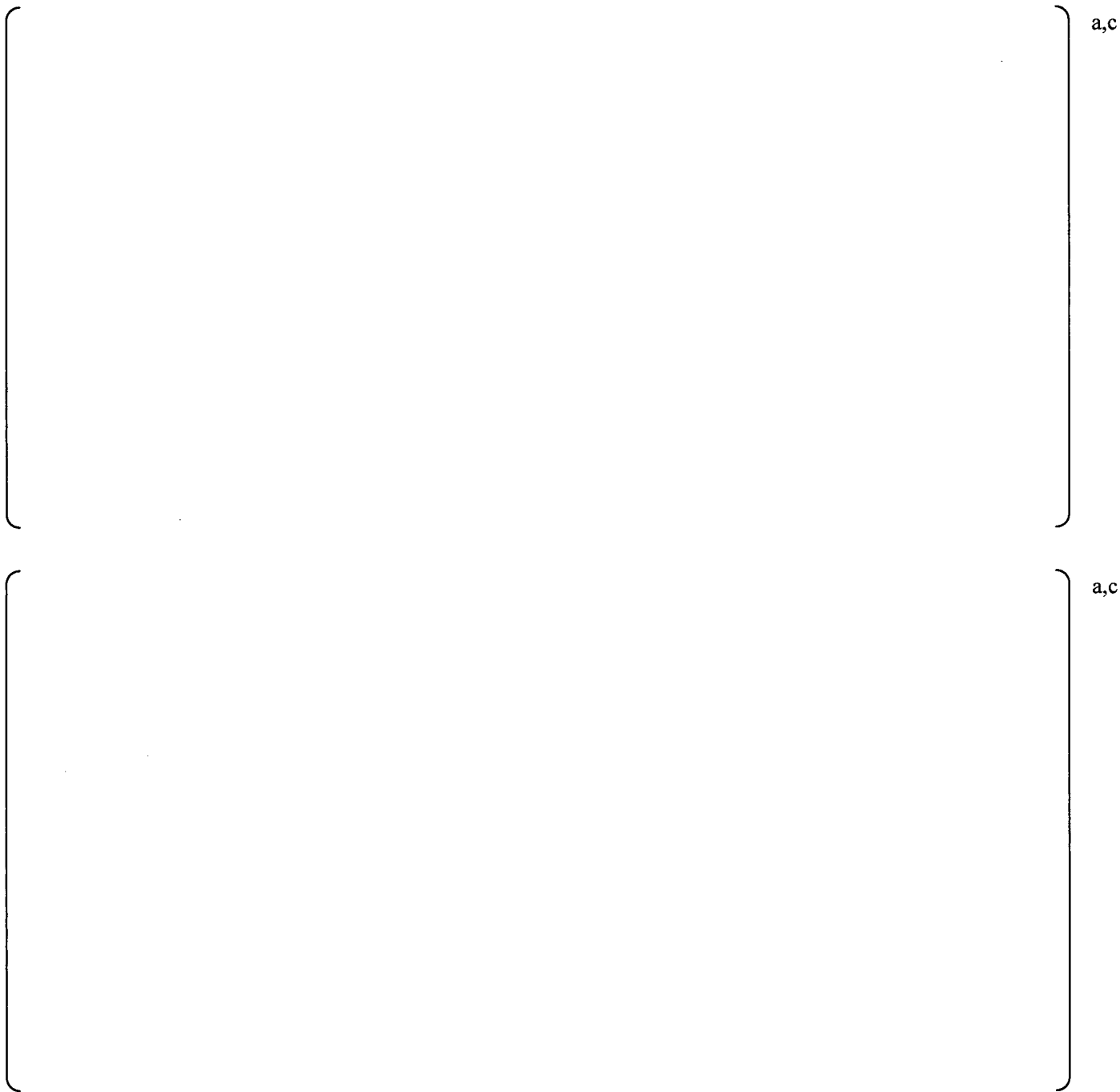


Figure E-8: PSD comparison at 930 MWe for pressure sensor data (black curves) and ACM Rev. 4.1 model predictions with corrected bias and uncertainty added (red curves), for P11 (top) and P12 (bottom).

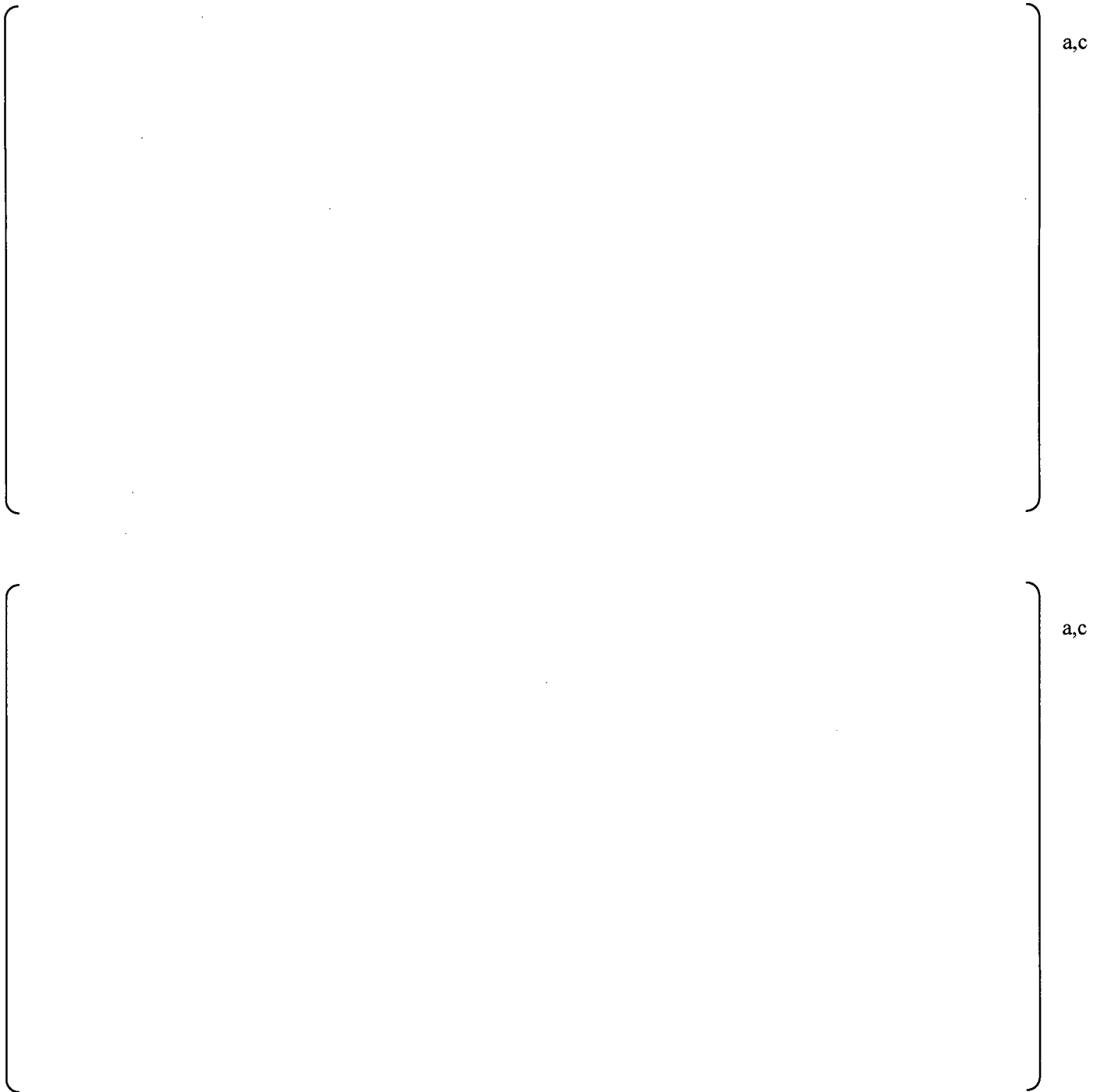


Figure E-9: PSD comparison at 930 MWe for pressure sensor data (black curves) and ACM Rev. 4.1 model predictions with corrected bias and uncertainty added (red curves), for P13 (top) and P14 (bottom).

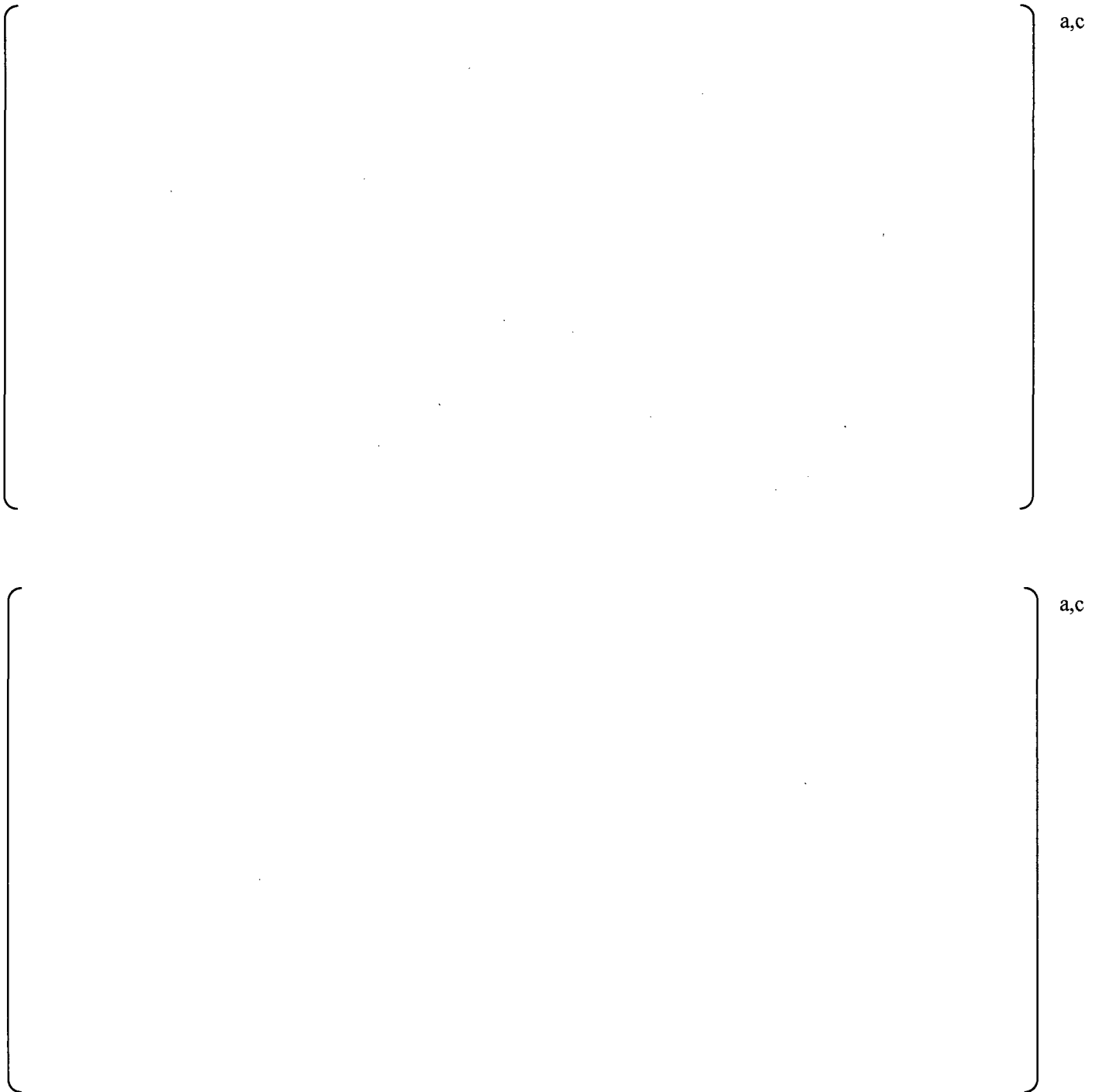


Figure E-10: PSD comparison at 930 MWe for pressure sensor data (black curves) and ACM Rev. 4.1 model predictions with corrected bias and uncertainty added (red curves), for P15 (top) and P16 (bottom).

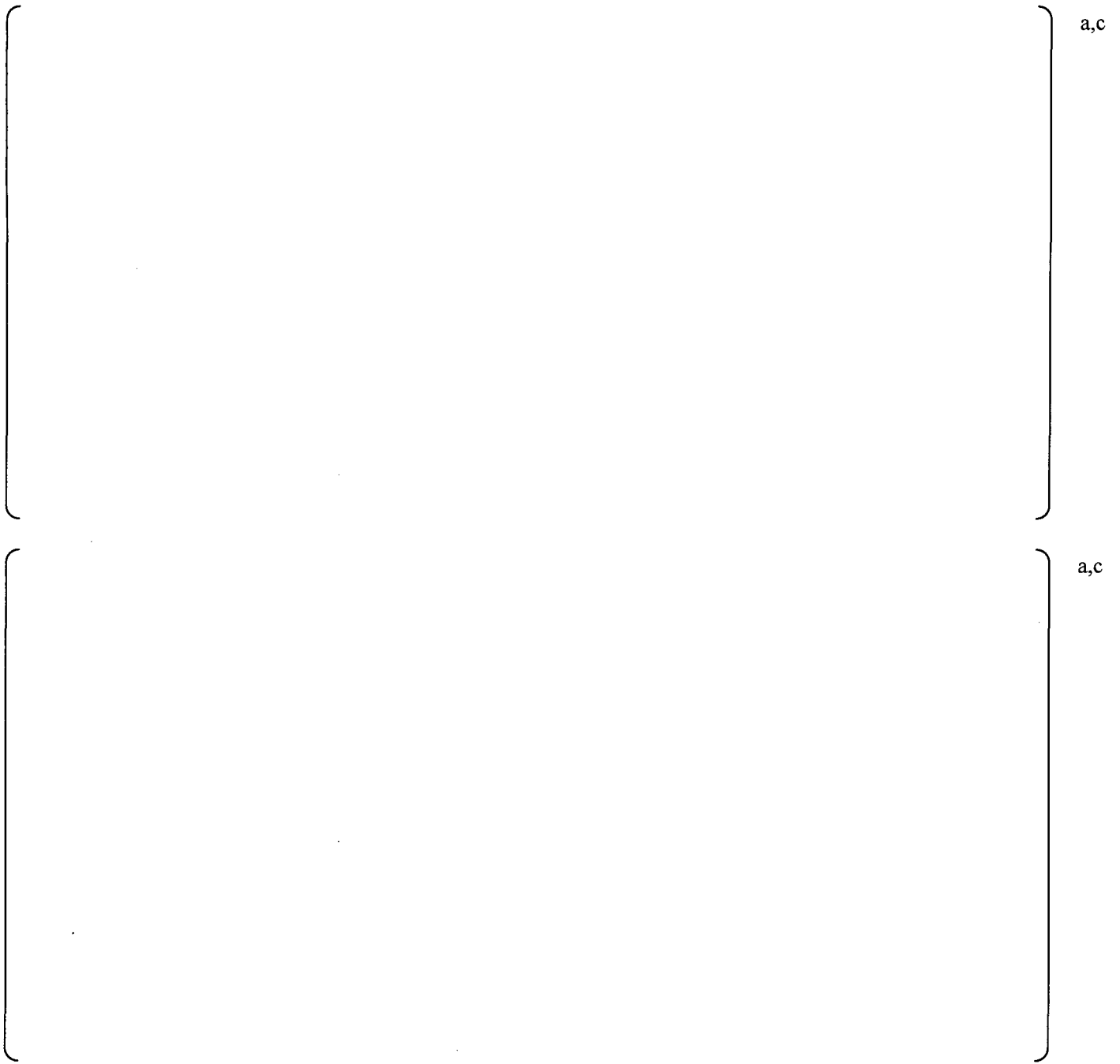


Figure E-11: PSD comparison at 930 MWe for pressure sensor data (black curves) and ACM Rev. 4.1 model predictions with corrected bias and uncertainty added (red curves), for P17 (top) and P18 (bottom).

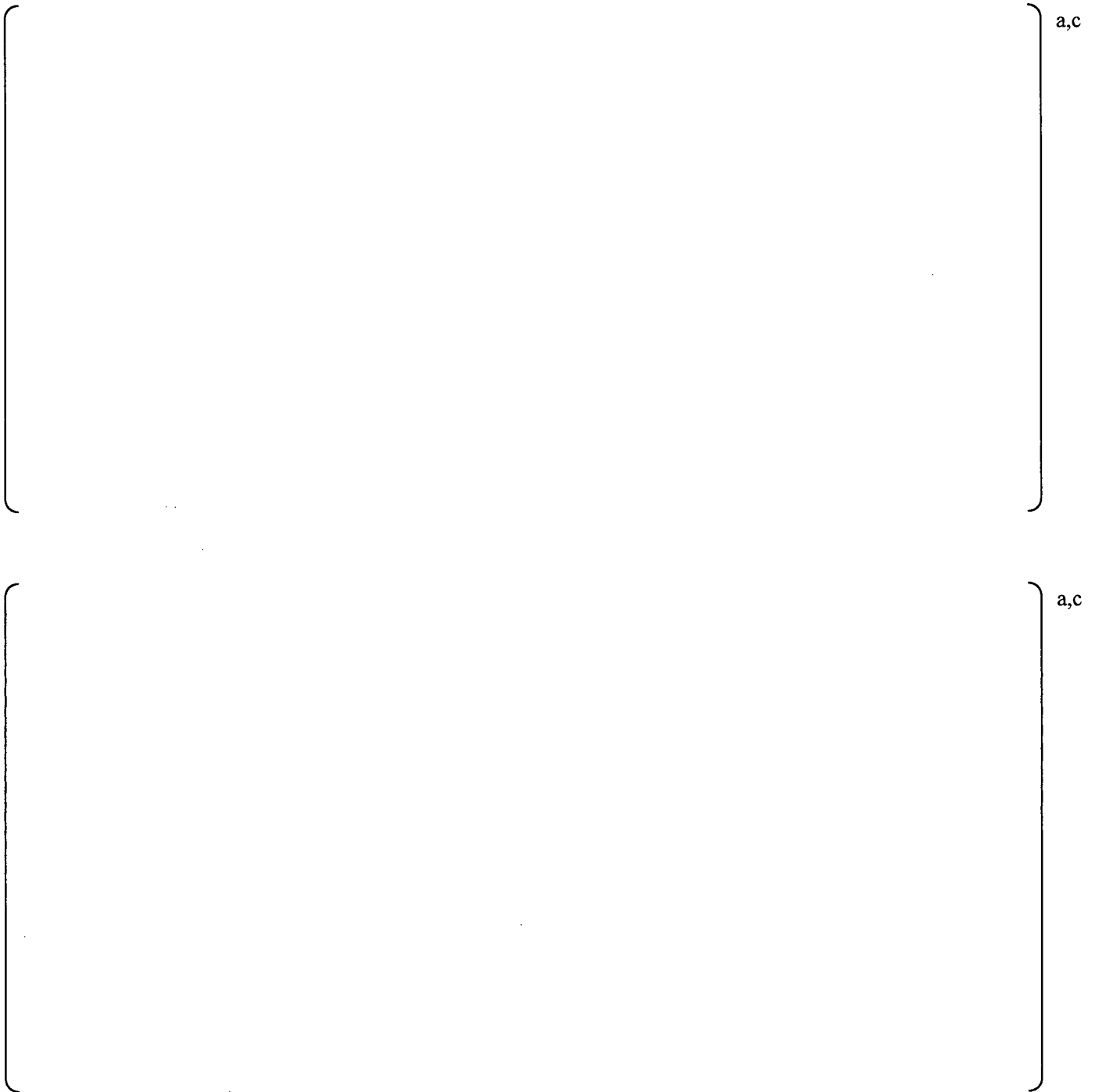


Figure E-12: PSD comparison at 930 MWe for pressure sensor data (black curves) and ACM Rev. 4.1 model predictions with corrected bias and uncertainty added (red curves), for P19 (top) and P20 (bottom).

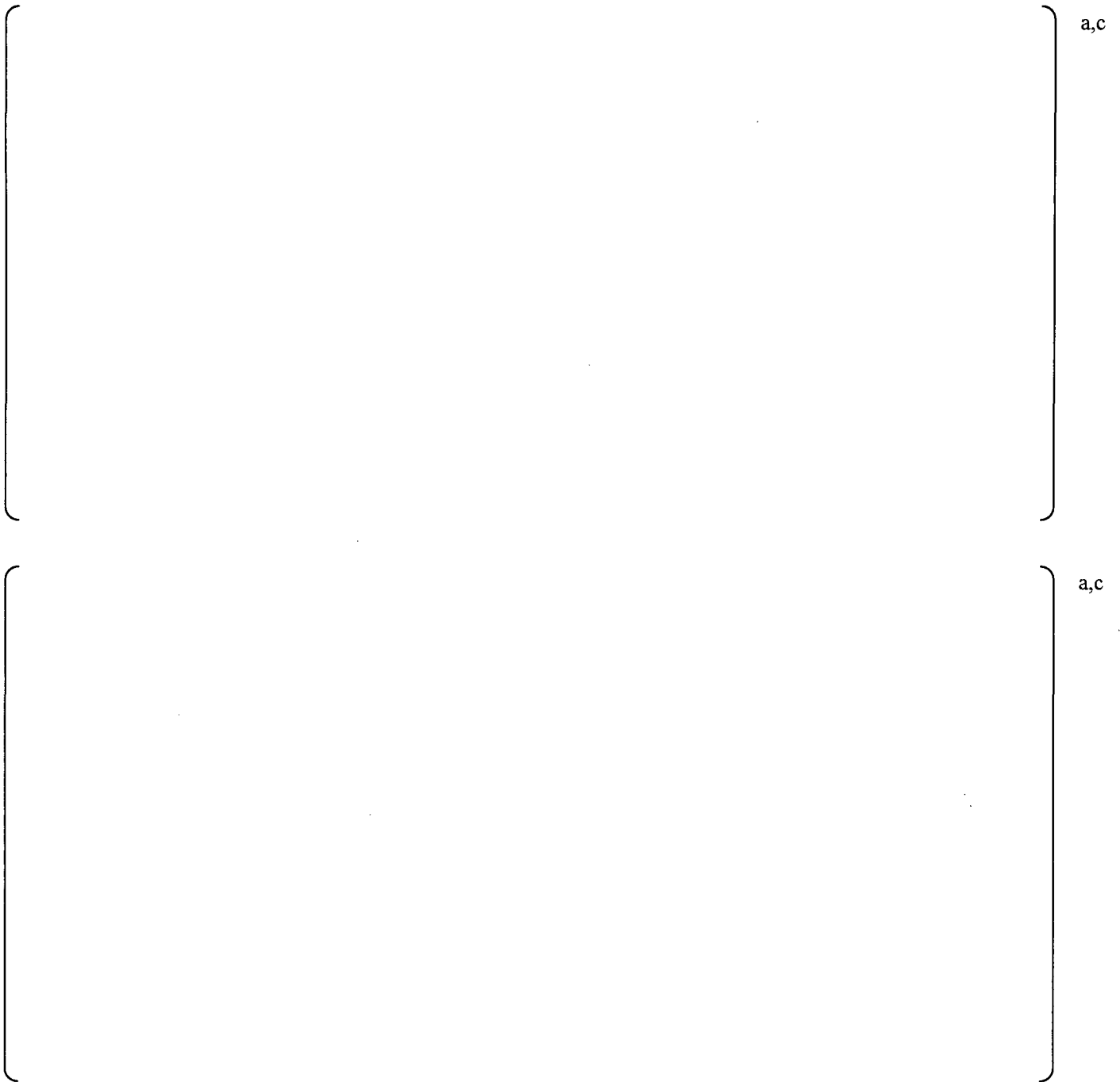


Figure E-13: PSD comparison at 930 MWe for pressure sensor data (black curves) and ACM Rev. 4.1 model predictions with corrected bias and uncertainty added (red curves), for P21 (top) and P22 (bottom).

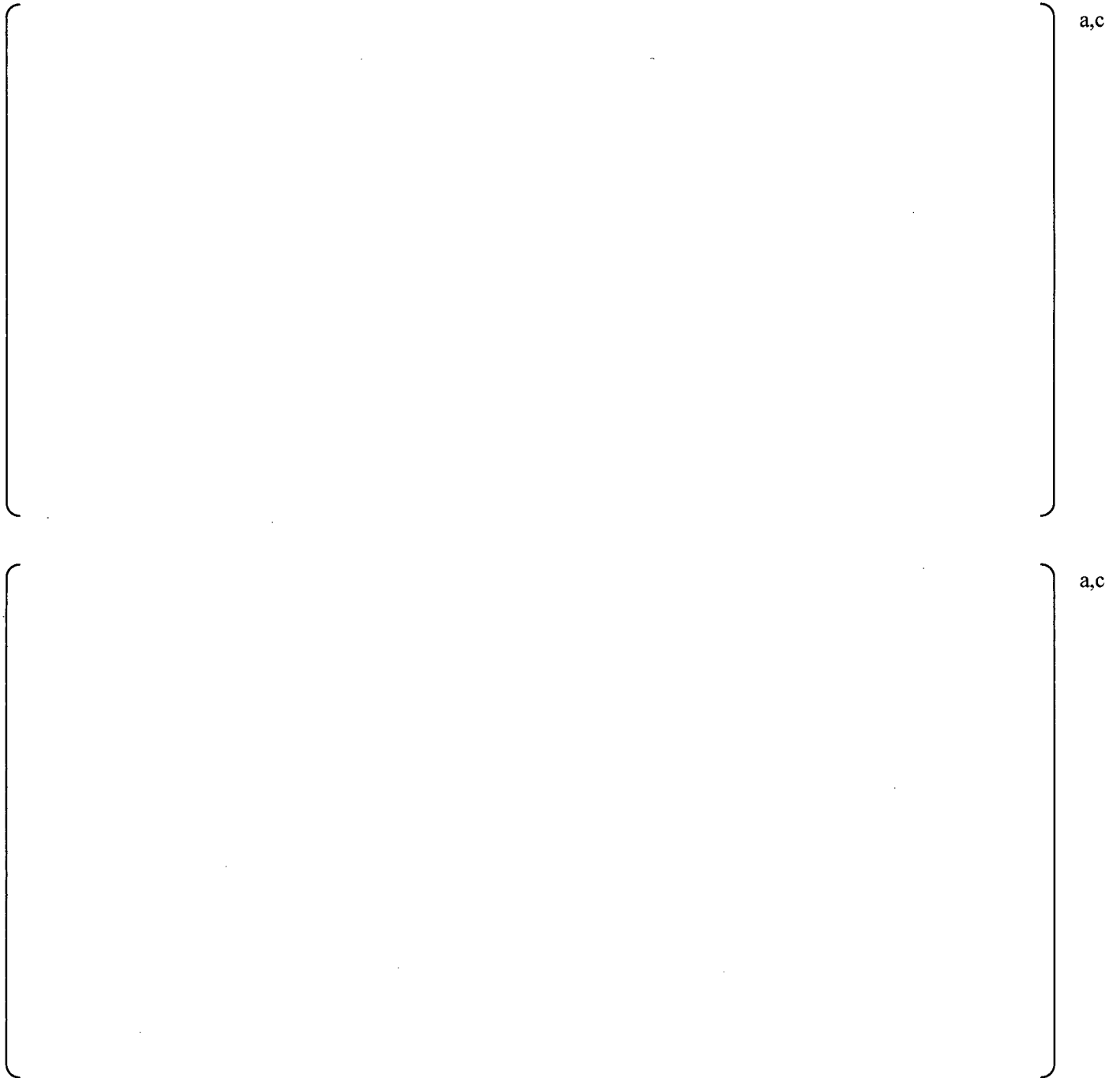


Figure E-14: PSD comparison at 930 MWe for pressure sensor data (black curves) and ACM Rev. 4.1 model predictions with corrected bias and uncertainty added (red curves), for P23 (top) and P24 (bottom).

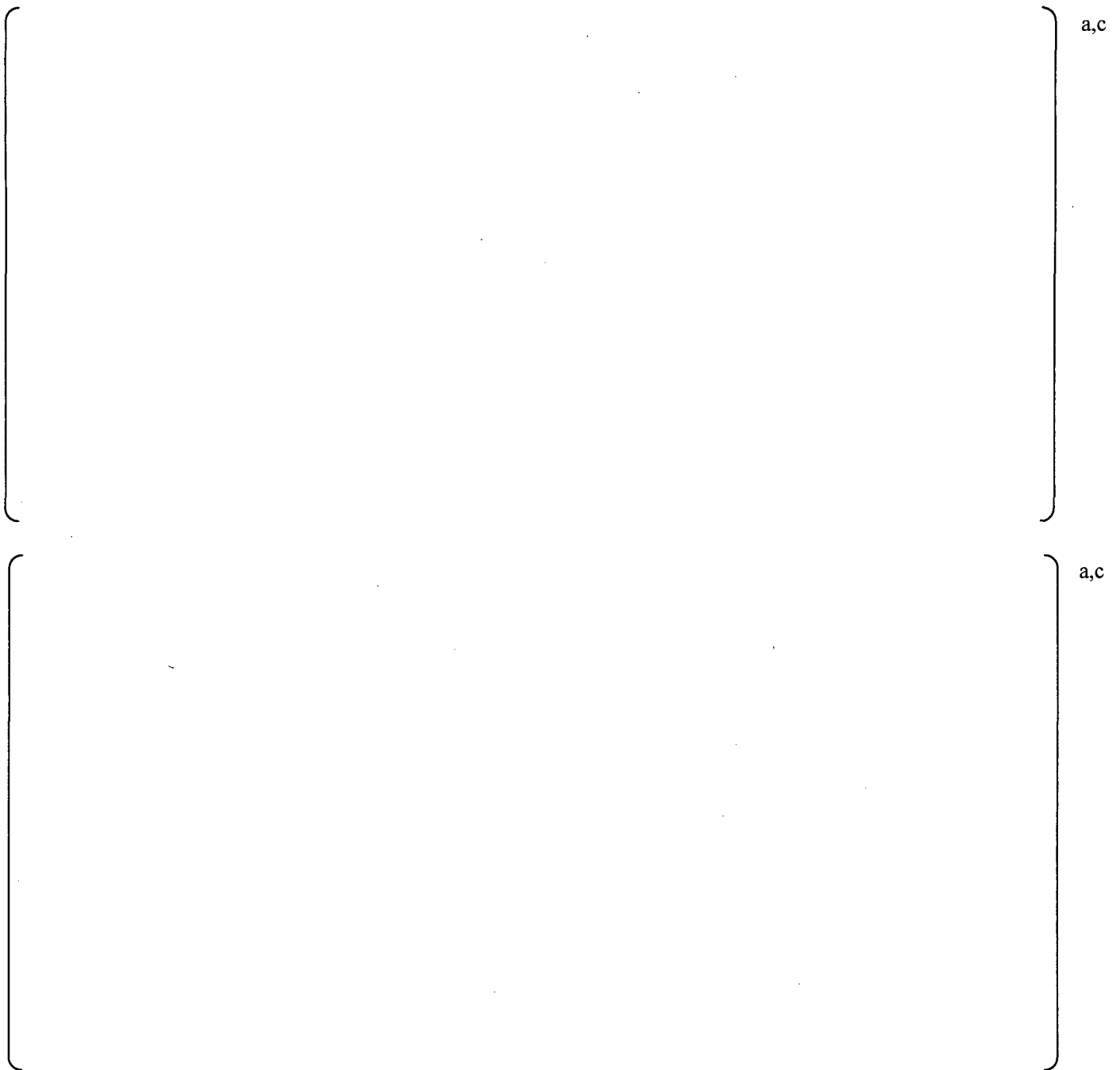


Figure E-15: PSD comparison at 930 MWe for pressure sensor data (black curves) and ACM Rev. 4.1 model predictions with corrected bias and uncertainty added (red curves), for P25 (top) and P26 (bottom).



Figure E-16: PSD comparison at 930 MWe for pressure sensor data (black curve) and ACM Rev. 4.1 model prediction with corrected bias and uncertainty added (red curve), for P27.

BWRVIP194-EMCB-RAI-02

Section 6.5.3, Evaluation of ACM Revision 4 Bias and Uncertainty: BWRVIP utilized ACM Rev. 4 for steam dryer analyses. Figures 6-19, 6-20, and 6-21, as well as Figures C-1 to C-16 of Appendix C, and Figures D-1 to D-16 of Appendix D of the topical report show PSD plots comparing data from the instrumented QC2 steam dryer with ACM Rev. 4 predictions. The topical report also provided tables of bias and uncertainty values for specified frequency intervals as shown in Table 6-4 (page 6-29) and Table 10-1 (page 10-2). [

]a,c

BWRVIP Response to NRC RAI BWRVIP194-EMCB-RAI-02

[

]^{a,c} The revised tables were shown in the response to BWRVIP194-EMCB-RAI-01, Tables 6-4, 6-8 and 6-9. In addition, the following changes will be made to Section 10:

- A. Section 10.1 Sources of Bias and Uncertainty will replace “Revision 4” with “Rev. 4.1”.
- B. Table 10-1 will be replaced with the following table:

Table 10-1: Frequency-dependent corrected bias and uncertainty for the ACM Rev. 4.1, combining Table 6-4 with Table 6-8. A negative bias indicates that the ACM overpredicts the QC2 data in that interval.



a,c

C. Section 10.2 Example will be replaced in its entirety by the following:

10.2 Example

[] a,c

BWRVIP194-EMCB-RAI-03

Section 3, Overview of Steam Dryer Evaluation Approach (Page 3-4), and Section 9.4.3.2, Comparison to Allowable Range of Alternating Stress Intensity (Page 9-32): Considering all known end-to-end bias errors and uncertainties in approved EPU license amendment requests, such as Hope Creek, as well as the applicable stress concentration factors, a minimum stress margin of 100% on alternating stress, or a minimum alternating stress ratio of 2.0, shall be maintained in steam dryer components at EPU power levels when the fluctuating pressure loads prediction on the dryer relies on main steam line (MSL) measurements. The minimum alternating stress ratio is defined as the endurance limit of the material divided by the maximum alternating stress. The topical report should be revised to state that the minimum required stress margin is 100% at EPU conditions, or the minimum required alternating stress ratio in Sections 3 and 9.4.3.2 at EPU conditions is 2.0. Specifically, the Alternating Stress Ratio at EPU shall be ≥ 2.0 , or the Stress Margin on Alternating Stress at EPU $\geq 100\%$.

BWRVIP Response to NRC RAI BWRVIP194-EMCB-RAI-03

In BWRVIP-182-A, BWRVIP acknowledges that an interim minimum alternating stress ratio of 2.0 for EPU conditions shall be maintained until additional validation is conducted demonstrating improved prediction accuracy for un-instrumented steam dryers relying on MSL strain gage measurements for steam dryer analysis. Accordingly, Section 3 will be modified as discussed in the response to BWRVIP194-EMCB-RAI-05, and the following paragraph will be inserted into Section 9.4.3.2:

For un-instrumented steam dryers relying on MSL strain gage measurements for steam dryer analysis, an interim minimum alternating stress ratio of 2.0 for EPU conditions will be applied until additional validation of ACM Rev. 4.1 is conducted demonstrating improved prediction accuracy.

BWRVIP194-EMCB-RAI-04

Section 9.3.2.2 (Table 9-5, Load Combinations for Mark II and Mark III Plants, Page 9-27): Table 9-5 of BWRVIP-194 is incomplete, as faulted load combinations D-5 and D-6 for MSL break occurring under critical initial conditions are missing. The load combination tables should be revised to provide the missing information.

BWRVIP Response to NRC RAI BWRVIP194-EMCB-RAI-04

Table 9-5 will be revised to include the faulted load combinations D-5 and D-6, as shown below, which were inadvertently omitted.

Table 9-5: Load Combinations for Mark II and Mark III Plants

Load Case	Service Conditions	Operating Condition	Load Combination ^(1,2,3,4,5,6)
A	Normal	Normal Operation	$DW + DP_N + FIV$
B-1	Upset	SRV Opening	$DW + DP_N + SRV$
B-2	Upset	Single SRV Opening	$DW + DP_N + (SRV_1^2 + FIV^2)^{1/2}$
B-3 ⁽⁷⁾	Upset	Operating Basis Earthquake	$DW + DP_N + OBE + FIV$
B-4	Upset	Upset DP	$DW + DP_U + FIV$
B-5	Upset	Turbine Stop Valve Closure (Acoustic Load)	$DW + DP_N + (TSV_A^2 + FIV^2)^{1/2}$
B-6	Upset	Turbine Stop Valve Closure (Flow Reversal Load)	$DW + DP_N + TSV_F$
C-1	Emergency	Emergency Depressurization	$DW + DP_N + SRV_{ADS}$
C-2	Emergency	Emergency DP	$DW + DP_E + FIV$
D-1	Faulted	SSE plus SRV Valves Actuate	$DW + DP_N + (SSE^2 + SRV^2)$
D-2	Faulted	Single SRV opening with SSE	$DW + DP_N + FIV + (SSE^2 + SRV_1^2)^{1/2}$
D-3	Faulted	Main Steam Line Break plus SSE Under Rated Power Conditions	$DW + DP_N + (MSLB_{A1}^2 + SSE^2 + FIV^2)^{1/2}$
D-4	Faulted	Main Steam Line Break plus SSE Under Rated Power Conditions	$DW + MSLB_{DP1} + SSE$
D-5	Faulted	Main Steam Line Break plus SSE Under Critical Initial Conditions	$DW + DP_N + (MSLB_{A2}^2 + SSE^2 + FIV^2)^{1/2}$
D-6	Faulted	Main Steam Line Break plus SSE Under Critical Initial Conditions	$DW + MSLB_{DP2} + SSE$

Notes:

1. The intention of considering a number of load combinations is to help determine the most conservative load condition. Owners may eliminate load combinations that can be technically justified to be bounded by other load combinations.
2. For definitions of terms see Table 9-6.
3. FIV loads are for the normal operating condition. FIV loads could be higher at some particular steam line velocities other than the normal steam line velocity. Accordingly, dwelling for extended periods of time at such flow velocities is to be avoided.
4. For plants that do not combine MSLB (limiting DBA) with SSE, MSLB may be considered separately from an SSE.
5. These load combinations are based on MSLB bounding other pipe break loads for the Steam Dryer. If other pipe break loads are bounding, they should be used in-place of the MSLB loads.

6. Thermal, pressure and seismic anchor displacements can result in localized loads on the dryer. If these loads are not determined to be negligible (BWRVIP-181-A Sections 7.1.6 and 7.1.9) they must be addressed in addition to the load combinations listed here.
7. SRSS can be used to combine OBE and FIV provided with plant specific justification.

BWRVIP194-EMCB-RAI-05

Section 3, Overview of Steam Dryer Evaluation Approach (Page 3-4), Figure 3-1, “BWRVIP Steam Dryer Integrity Demonstration Flowchart”: The flow chart is incomplete and several steps need to be included to fully address significant evolution considerations not present in the proposed guidance. The topical report should be revised to address the following items:

- a. Rectangular Box, right hand side, third row: This block – Conduct in-plant test at Current Licensed Thermal Power – should refer to Note 1. Note 1 should be added to the flowchart to reflect the following: If analytical screening indicates a potential for acoustic excitation, subscale tests or in-plant MSIV closure tests, when feasible, may be conducted.
- b. Rectangular Box, right hand side, sixth row: This block – Increase in-plant CLTP MSL pressure at each frequency by ratio of subscale results (power uprate / CLTP) – should refer to Note 2. Note 2 should be added to the flowchart to reflect the following: At any frequency, the factor used to increase the in-plant CLTP pressures to power uprate pressures shall not be less than the ratio of flow velocity squared. At acoustic resonance frequencies, larger bump-up factors, typically much higher than the ratio of flow velocity squared, determined from subscale tests, shall be used.
- c. Diamond Box, left hand side, ninth row: This block – Stress Margin – should refer to Note 3. Note 3 should be added to the flowchart to reflect the following: For un-instrumented steam dryers relying on MSL strain gage measurements for steam dryer analysis, an interim minimum alternating stress ratio of 2.0 for EPU conditions will be applied until additional validation of ACM Rev. 4.1 is conducted demonstrating improved prediction accuracy.
- d. Rectangular Box, right hand side, seventh row: This block – Modify/Replace Dryer – should refer to Note 4. Note 4 should be added to the flowchart to reflect the following: If steam dryers are replaced by new steam dryers, the topical report should state that the new replacement dryers shall be instrumented instead of simply relying on measurements from the MSL strain gage data to establish the structural integrity of the steam dryer for power uprate conditions.

BWRVIP Response to NRC RAI BWRVIP194-EMCB-RAI-05

The revised flowchart is shown below. The four Notes are summarized below. A Note 5 has been added consistent with the identical figure in BWRVIP-182-A.

The Notes appended to Figure 3-1 will become the following:

Notes:

1. If analytical screening indicates a potential for acoustic excitation, subscale tests or, when feasible, in-plant main steam isolation valve (MSIV) closure tests may be conducted.
2. At any frequency, the factor used to increase the in-plant CLTP pressures shall not be less than the ratio of flow velocities squared. At acoustic resonance frequencies, bump-up factors determined from subscale tests or an alternative validated methodology, such as acoustic finite element modeling or MSIV closure testing, shall be used. Bump-up factors near acoustic resonance frequencies can in some cases be much higher than the ratio of velocities squared.
3. For un-instrumented steam dryers relying on MSL strain gage measurements for steam dryer analysis, an interim minimum alternating stress ratio of 2.0 for EPU conditions will be applied until additional validation of ACM Rev. 4.1 is conducted demonstrating improved prediction accuracy.
4. If existing steam dryers are replaced by new steam dryers, consideration shall be given to instrument the new dryers instead of simply relying on measurements from MSL strain gage data to establish the structural integrity of the steam dryer for power uprate conditions.
5. If the decision to pursue acoustic mitigation is made after completing the in-plant testing and load definition process, then the Power Uprate pressure loading previously obtained shall be revised to reflect the elimination of acoustic excitation removed by the mitigation devices and confirmed by subscale testing. Once stress margin is confirmed, an application for power uprate is submitted. Acoustic mitigation is installed prior to power ascension. Final confirmation of the effectiveness of the mitigation devices and the increased stress margin is made based on power uprate pressure loading revised to reflect the results of power ascension testing.

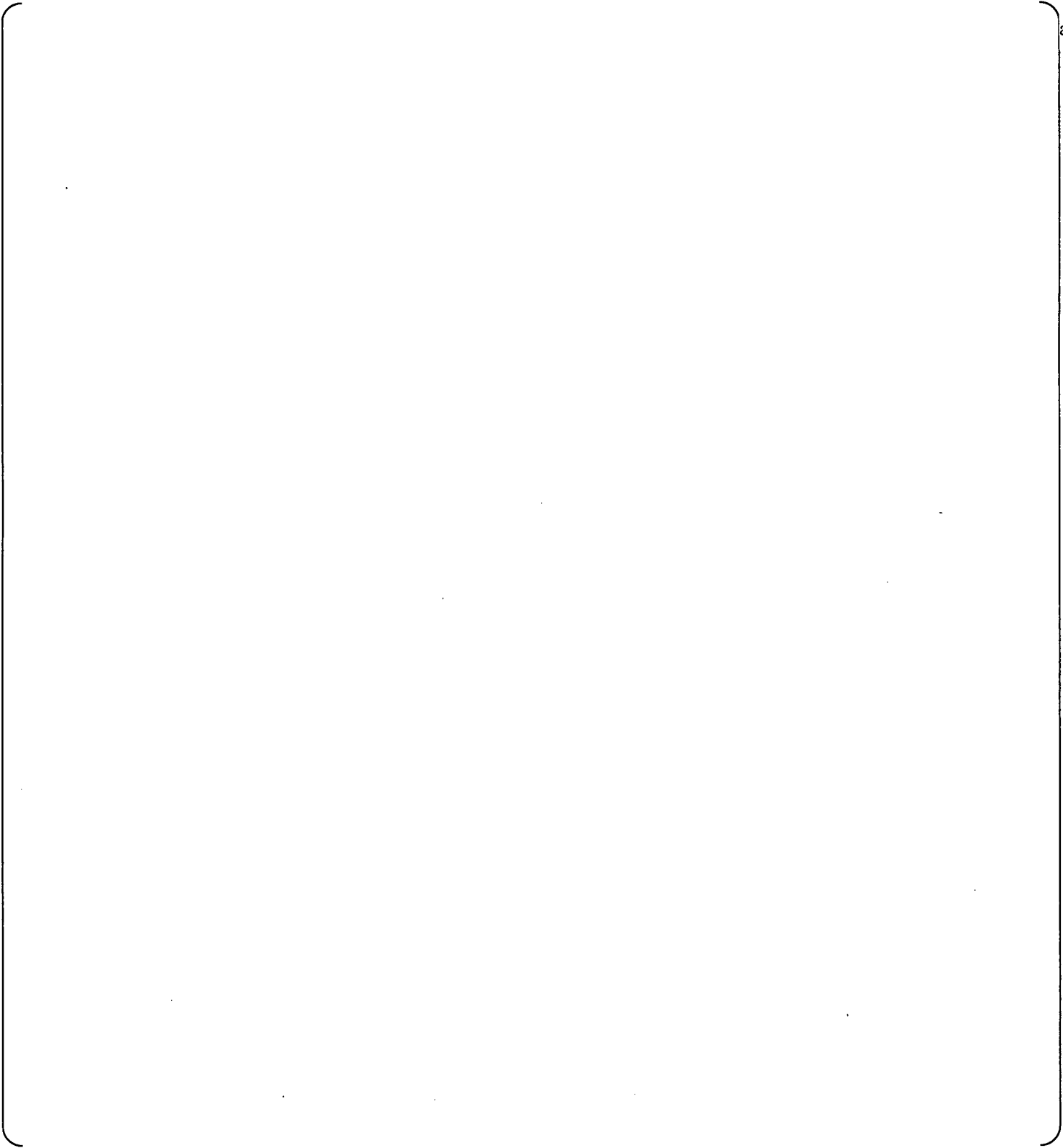


Figure 3-1: BWRVIP steam dryer integrity demonstration flowchart.

BWRVIP194-EMCB-RAI-06

Section 11.2.2, Limit Curve Generation (Page 11-3): The topical report states that in-plant CLTP strain gage data are filtered across the frequency range of interest to remove noise and extraneous signal content. The resulting PSD curve for each of the eight strain gage locations is then used to develop limit curves, as shown in Figures 11-1 to 11-4. Level 1 limit curves are found by multiplying the main steam line pressure PSD traces by the square of the minimum alternating stress ratio.

This procedure is non-conservative because the CLTP strain gage signals would be reduced by filtering the corresponding LF signals prior to stress analysis. Therefore, the staff requests revision of the limit curve generation methodology to address this non-conservatism.

BWRVIP Response to NRC RAI BWRVIP194-EMCB-RAI-06

The replacement of ACM Rev. 4 with ACM Rev. 4.1 eliminates []^{a,c}, as discussed in response to NRC RAI BWRVIP194-EMCB-RAI-01. The following changes will be made to Section 11:

A. Section 11.2.1 CLTP Stress Analysis will be replaced in its entirety by the following:

11.2.1 CLTP Stress Analysis

A typical finite element analysis using the CLTP data from Plant A results in a lowest/minimum alternating stress ratio (fatigue allowable stress divided by maximum predicted stress) of []^{a,c}, as summarized in Table 11-1. The minimum stress ratio includes the ACM Rev. 4.1 model bias and uncertainties for specific frequency ranges for the QC2 790 MWe power level as defined in Table 6-4 and reproduced in Table 11-2. []^{a,c}. The additional bias and uncertainty, as identified in Section 10, are shown in Table 11-3. SRSS of all uncertainties, added to the ACM bias and the other identified bias, results in the total uncertainties shown in Table 11-4. These uncertainties are applied to the finite element analysis, resulting in the minimum alternating stress ratio of []^{a,c}.

Table 11-1: Alternating stress limit summary for Plant A.

	a,c
--	-----

Table 11-2: Bias and uncertainty for ACM Rev. 4.1.

	a,c
--	-----

Table 11-3: Additional bias and uncertainty for Plant A.



a,c

Table 11-4: Total uncertainty for Plant A.



a,c

B. The figures in Section 11.2.2 Limit Curve Generation will be replaced in their entirety with the following:

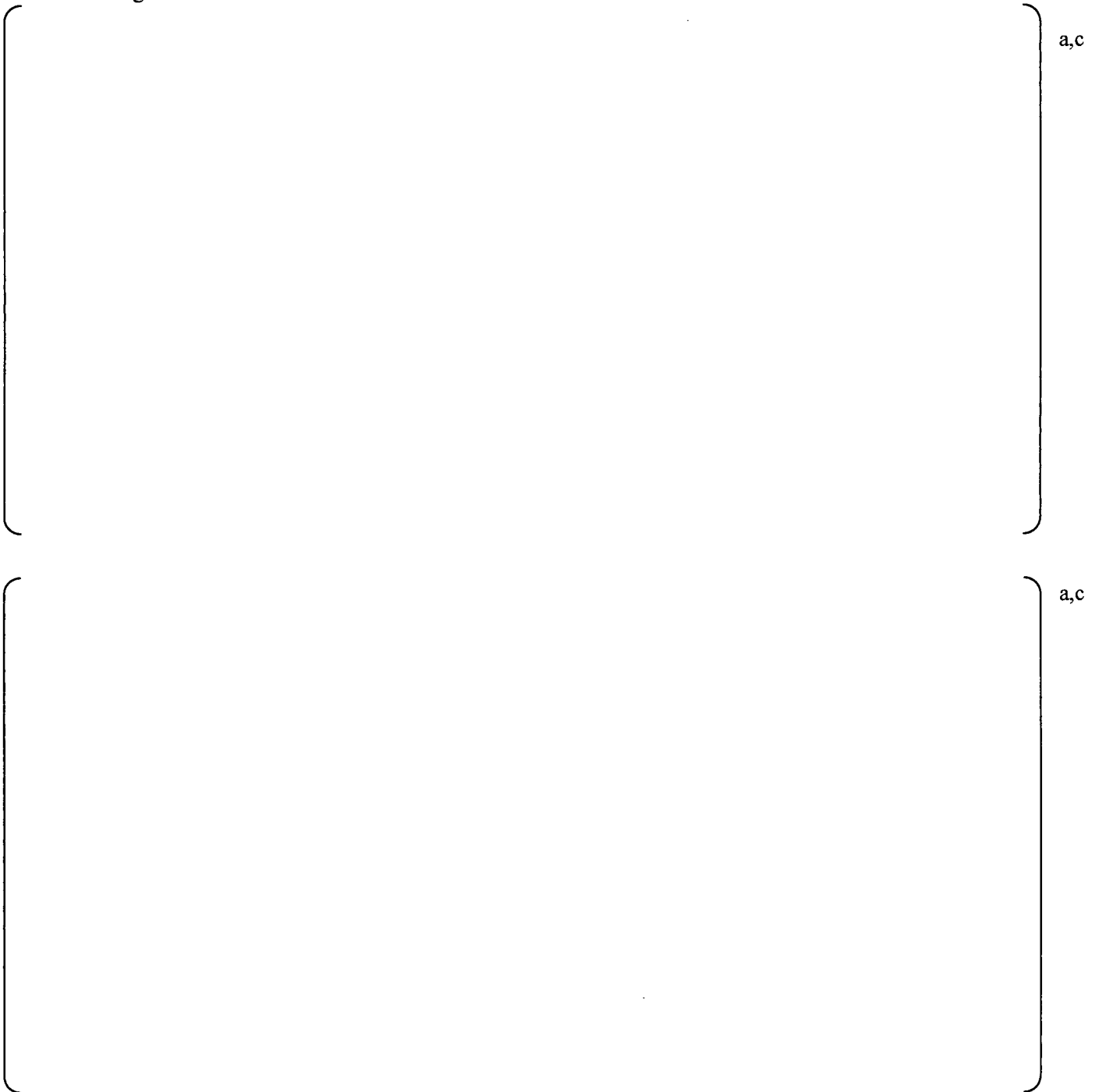


Figure 11-1: Level 1 (black) and Level 2 (red) limit curves for MSL A, compared against the base curves (blue) over the frequency range of interest: A upper strain gage location (top); A lower strain gage location (bottom).

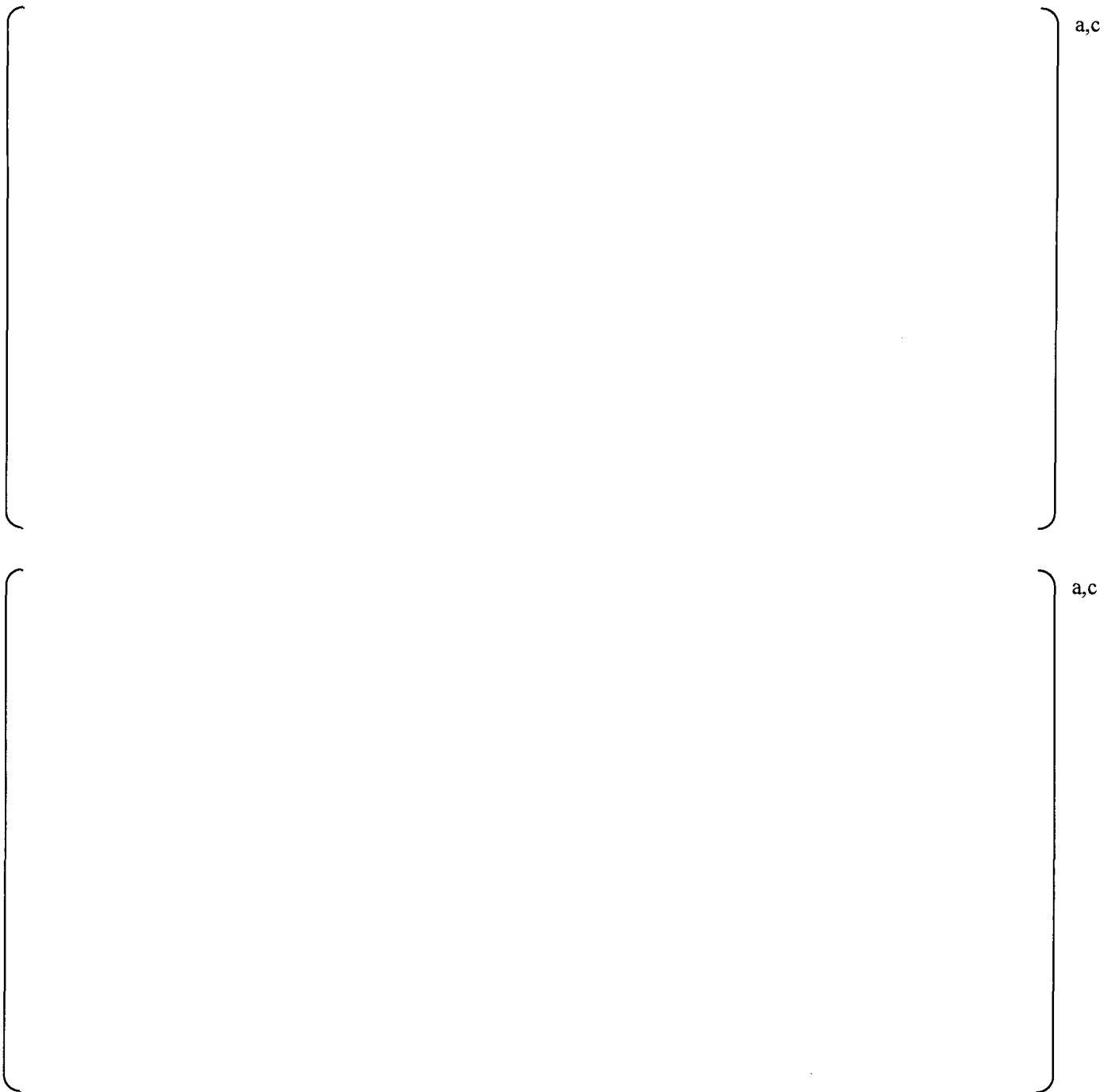


Figure 11-2: Level 1 (black) and Level 2 (red) limit curves for MSL B, compared against the base curves (blue) over the frequency range of interest: B upper strain gage location (top); B lower strain gage location (bottom).

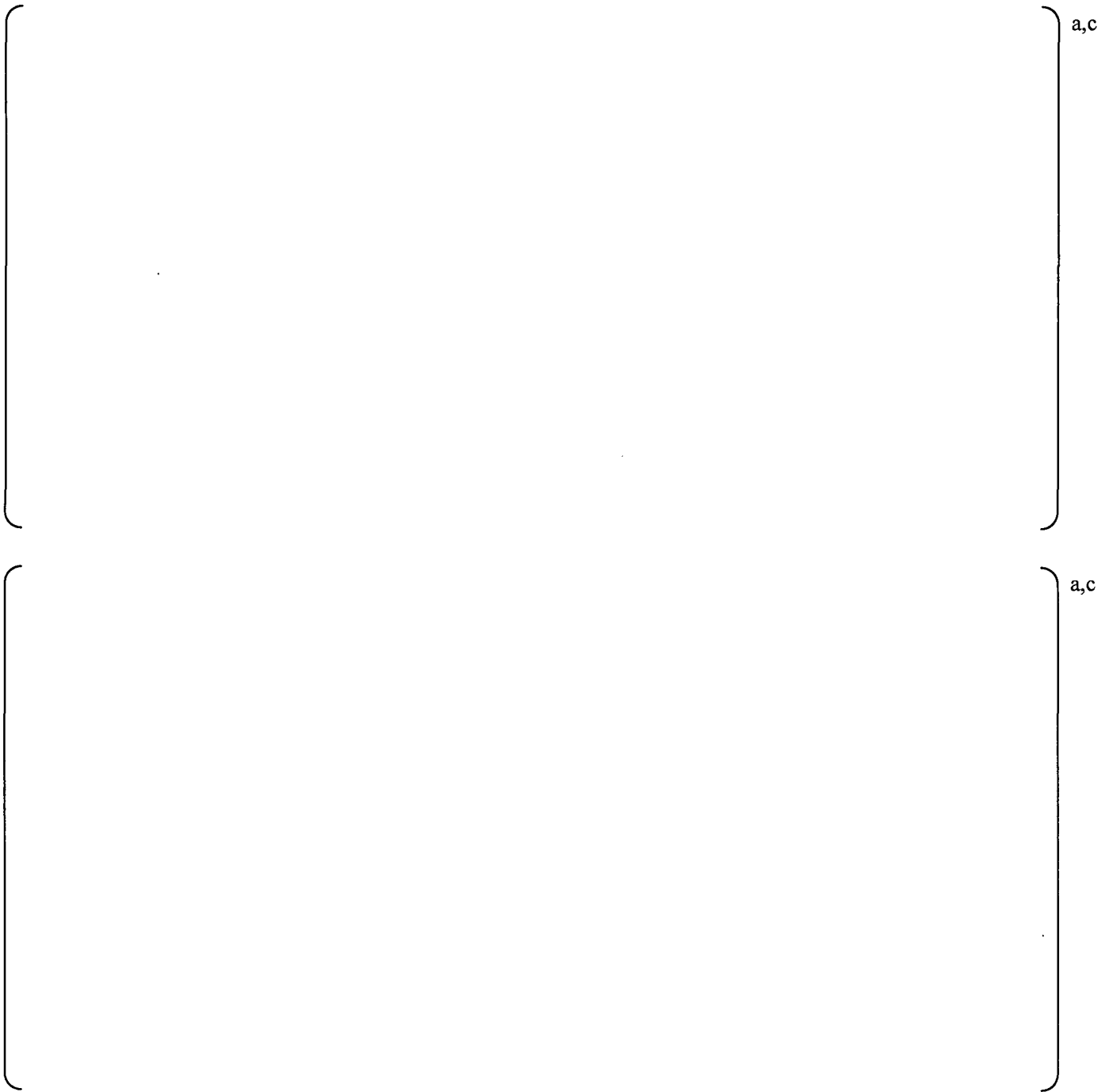


Figure 11-3: Level 1 (black) and Level 2 (red) limit curves for MSL C, compared against the base curves (blue) over the frequency range of interest: C upper strain gage location (top); C lower strain gage location (bottom).

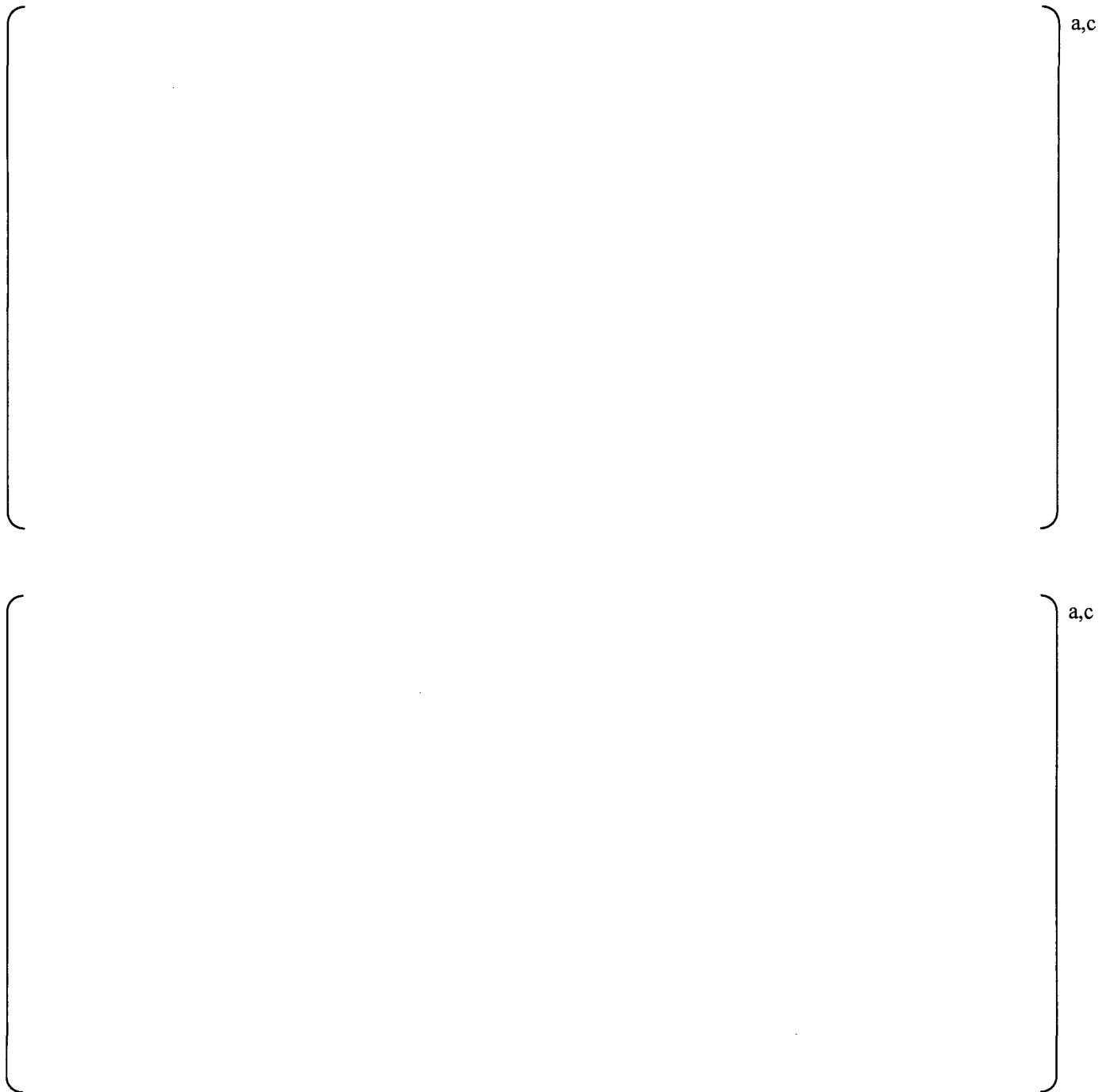


Figure 11-4: Level 1 (black) and Level 2 (red) limit curves for MSL D, compared against the base curves (blue) over the frequency range of interest: D upper strain gage location (top); D lower strain gage location (bottom).

BWRVIP194-EMCB-RAI-07

Sections 8.3 and 8.4, One-Eighth Scale Test: Figures 8-10, 8-23, and 8-24 show plots of bump-up factors []^{a,c}. The bump-up factors that are higher than the square of the flow velocity, determined from subscale tests, [

] ^{a,c}. Some of the values of bump-up factors are less than the ratio of flow velocity squared. BWRVIP is requested that the topical report include a cautionary note stating that the bump-up factor used for MSL data prediction for CLTP to EPU shall not be less than the ratio of flow velocity squared.

BWRVIP Response to NRC RAI BWRVIP194-EMCB-RAI-07

As discussed previously in the response to BWRVIP194-EMCB-RAI-05, the factor used to increase the in-plant CLTP pressures to EPU []^{a,c}

Changes that will be made to Section 8 are the following:

- A. Figures 8-10, 8-23 and 8-24 will be replaced with frequency scales to 250 Hz, as shown below.
- B. The last paragraph in Section 8.4 Validation of One-Eighth Scale Test System will be replaced by the following paragraphs:

[]^{a,c}

It is straightforward to multiply through the OLTP pressure data on the main steam lines to estimate the EPU pressure data, and to run ACM Rev. 4.1, following the same procedure as if the estimated signals were measured at EPU. Corrected bias and uncertainty, based on the 16 pressure sensors at QC2, were shown previously in Table 6-4 and Table 6-8. Minimum and maximum peak pressure comparisons with the data are shown in Figure 8-25 and Figure 8-26. []^{a,c}, and exhibit a behavior somewhat different from that shown in Figure 6-25 and Figure 6-27 (bottom), respectively.

- C. Figures 8-25 and 8-26 will be replaced, as shown below, and Figures 8-27 and 8-28 will be removed, as will Section 8.5 Bias and Uncertainty Associated with Prediction of MSL Flow Rate Effects on MSL Pressure Amplitudes.



Figure 8-10: Bump-up factors generated from QC2 main steam line data between OLTP and EPU power levels. The separate curves identify the strain gage locations on the main steam lines. The standpipe excitation frequencies of 115 Hz (Target Rock), 135 Hz (Electromatic), and 155 Hz (Dresser 6x8) are clearly seen in the plot.



Figure 8-23: Bump-up factors generated from subscale data qc2-2 (OLTP) and qc2-8 (EPU). The separate curves identify the strain gage locations on the main steam lines.



Figure 8-24: Bump-up factors generated from subscale data qc2-2 (OLTP) and qc2-12 (EPU). The separate curves identify the strain gage locations on the main steam lines.

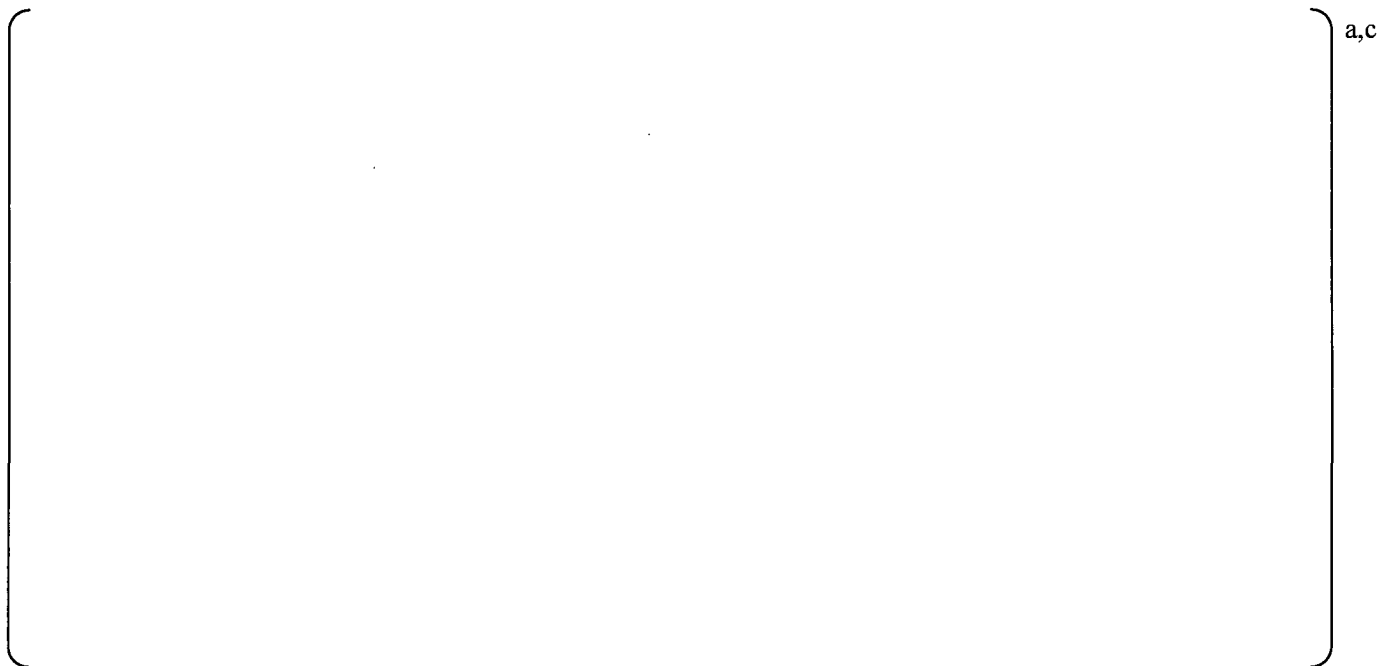


Figure 8-25: ACM Rev. 4.1 predictions at 930 MWe at the dryer pressure sensors: peak maximum (top) and peak minimum (bottom) pressure levels, with data (black) and predictions with corrected bias and uncertainty added for subscale data no. 1 (red) and subscale data no. 2 (blue).

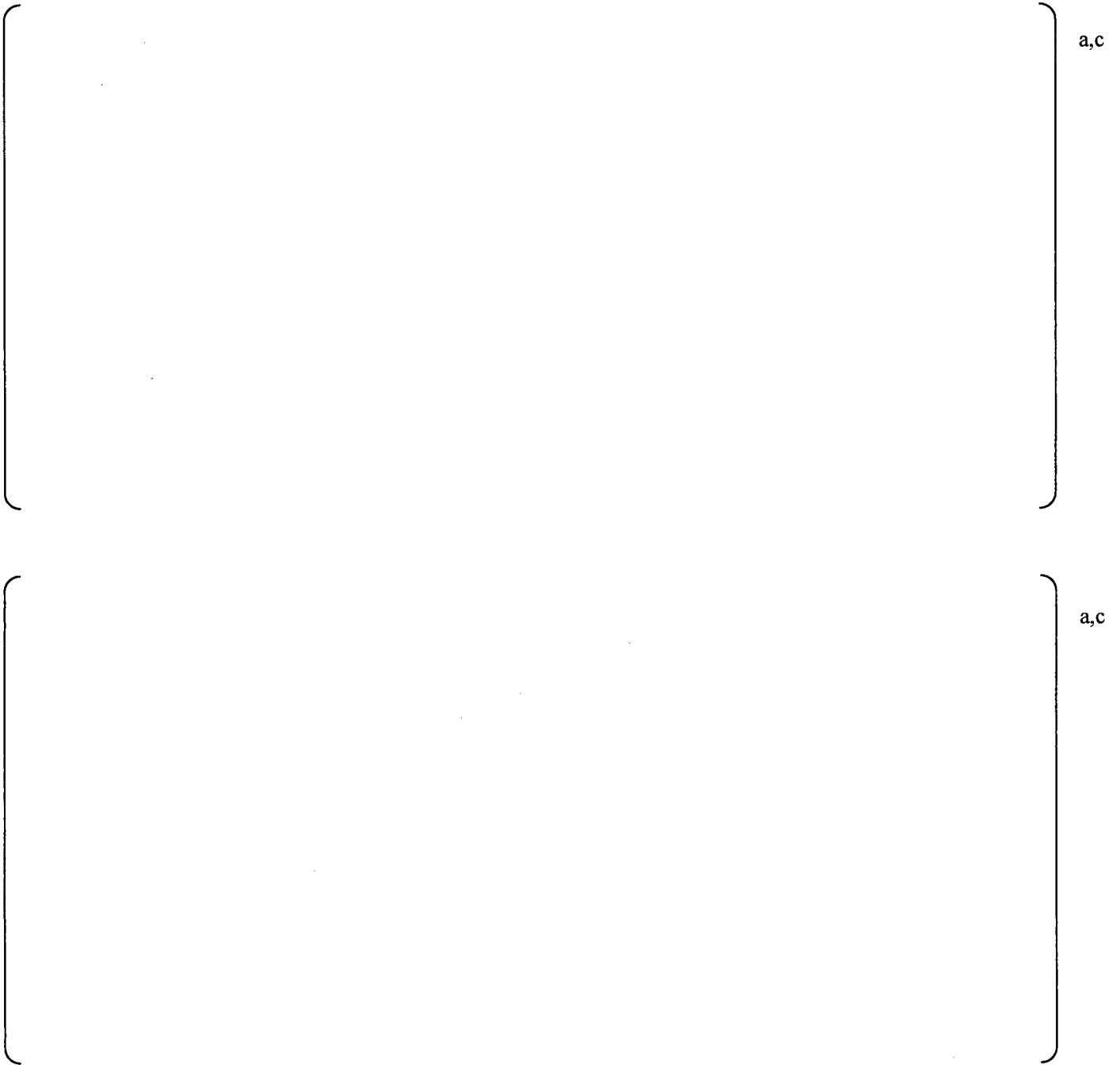


Figure 8-26: Comparison between measured and predicted peak pressures at the 27 pressure sensors in QC2 at 930 MWe for subscale data no. 1 (top) and subscale data no. 2 (bottom) with overall uncertainty added to the predicted load. The lines are the one-to-one boundaries. [

]a,c

BWRVIP194-EMCB-RAI-08

Section 9.4.3.3, Finite Element Analysis Sub-Modeling at Welds, Page 9-34: The topical report presents two approaches, one formal approach and an alternative procedure. While the formal approach is acceptable, the staff finds the alternative procedure to sub-modeling to be questionable. The staff does not endorse the alternative procedure for sub-modeling, where non-unique forces or displacements are applied to the sub-model to reproduce the stress. This unconventional, non-traditional, non-standard sub-modeling approach is not acceptable, because this method allows for a different analyst to select a different set of forces or displacement loadings and locations to reproduce the stress in the region of interest. This application of arbitrary input loadings or displacements at arbitrary locations is non-unique. The staff will not accept this alternative method unless validation is performed every time for each location where this non-traditional approach is used. The staff concludes that use of this non-conventional sub-modeling approach is not advantageous. The staff requests that the topical report be revised to delete this alternative sub-modeling approach.

BWRVIP Response to NRC RAI BWRVIP194-EMCB-RAI-08

We concur that the sub-modeling approach currently described in Section 9.4.3.3 could be implemented in a manner that is arbitrary or non-unique, and agree that such implementations should be rejected. It is noted that such erroneous implementations can be realized in the displacement-based sub-structuring framework (e.g., by imposing what is considered a “reasonable” displacement field) as well as within a force-based sub-modeling framework (e.g., by specifying a force on qualitative grounds). In either case such methods would lack formality and precision, introduce a subjective element in the selection of the force or displacement, and make the determination of bias and uncertainty of the method difficult or impossible to quantify.

The assertions of non-uniqueness and arbitrariness, however, do not apply to the displacement-based sub-structuring (DSS) approach that can be implemented as part of an ANSYS analysis or to the reformulated sub-modeling approach (SM) discussed below. In a properly executed sub-model approach the forces and moments applied to the sub-model are uniquely determined from the limiting stress state in the global dryer. The associated limiting forces and moments are extracted from the global model at the sub-model boundaries and impressed upon a highly detailed solid element representation of the local weld geometry. The combined inertial and acoustic loads can either be extracted from the global model directly or else inferred (to linear accuracy) on the basis of d'Alembert's Principle. While the DSS technique is more commonly used and comprehended, the force-based SM approach is equally well grounded on a solid mathematical foundation and relies on elementary principles in structural mechanics (St. Venant's Principle and d'Alembert's principle) that have been well understood for over a century. An analogous equivalency in finite element modeling theory is found in the complementary principles of virtual displacements and virtual forces, the former being more commonly employed in finite element applications and the latter being formally equivalent and offering computational / analytical advantages in certain contexts.

The sources and magnitudes of errors in the force-based sub-modeling method (SM) should be quantified; this quantification can be done on both a theoretical basis and by benchmarking against high resolution simulations (HRS) involving the full steam dryer. The primary sources of error in the SM are as follows. First, there is a discretization error associated with finite mesh size at the sub-model boundary where the forces and moments from the global model are transferred. This error is present in the DSS method also and needs to be quantified. This error can also be controlled by sufficient mesh refinement if warranted. Another source of error in SM is in the linearization of inertial loads and impressed acoustic pressures. Finally, both SM and DSS are subject to errors associated with mesh discretization, though these errors tend to be small since the mesh spacing in the sub-model is so small. In both DSS and SM, the errors, once quantified, are accounted for by imposing an additional bias and uncertainty on the sub-model result.

Since a properly formulated force-based sub-modeling approach (SM) is neither arbitrary nor non-unique, the reasons cited in the RAI for rejecting the sub-modeling approach previously submitted are not applicable to the SM approach presented in this response. The SM approach is therefore valid as an effective means of analyzing complex weld geometries. As indicated above, any results obtained using either a SM- or DSS-based approach should be adjusted by the biases and uncertainties used to account for the associated errors and quantified on the basis of theoretical analysis and benchmarking against high resolution simulations of the steam dryer. Of course, direct application of HRS results is always an acceptable approach.

Consequently, Section 9.4.3.3 FEA Sub-Modeling at Welds will be replaced in its entirety by the following sections:

9.4.3.3.1 Displacement-Based Sub-Structuring (DSS) Approach

In order to keep computational costs at a feasible level, the steam dryer model is predominantly comprised of shell elements. These elements are well suited for structures such as the steam dryer, which consist of shell-like components and tend to produce conservative estimates of the stresses. In some cases, however, such as welded junctions involving multiple components, shell element models can overestimate the nominal stress intensities in the vicinity of the junctions. In such cases a more refined analysis, using solid elements to capture the 3-D stress distribution, is warranted. Therefore, to efficiently analyze complex structures such as steam dryers, a standard engineering practice is to first analyze the structure using a shell-based model. Then, if any locations with high stresses are identified, these regions are examined in greater detail using 3D solid elements to obtain a more accurate stress prediction. Direct application of high resolution simulations (HRS) using 3D solid elements results is always an acceptable approach.

For locations requiring supplemental calculations that cannot justify HRS to more accurately represent the member interactions, sub-modeling techniques are used. Sub-models are relied upon to expeditiously evaluate the changes in local stresses due to structural modifications or reinforcements and also conduct more refined stress evaluations in critical areas that take into account details pertaining to the 3D geometry, welds, and connections. The sub-modeling methodology used for the dryer acoustic analysis follows the same steps utilized for a static application, supplemented as necessary to address the acoustic (dynamic) response of the dryer. The approach, identified as a displacement-based sub-structuring approach (DSS for Displacement-Based Sub-Structure), is considered standard and available within ANSYS.

In this approach the sub-model is cut from the global model. The cut boundaries of the sub-model are then subjected to displacements extracted from the global model, and the same loads (in this case due to acoustic pressures) are imposed. The inertial terms are accounted for by assembling the harmonic responses developed over the complete frequency range.

The linearized stress intensities computed by the model are typically lower than those obtained with the shell-based FEA used to analyze the complete steam dryer. These reductions are represented by stress reduction factors (SRFs) which vary according to location due to their dependence upon the individual local geometry. SRFs are generally less than unity due to conservative stress estimates inherent in the shell-based weld stress evaluations at welds and junctions. For example, the discontinuity stresses computed in a shell model at a weld joint between two orthogonal members are often quite conservative, because the shell element depiction does not provide any credit for the stress distribution associated with the specific weld geometry. Once the SRFs are obtained, the stress intensities predicted by the global shell element-based analysis at these locations are first multiplied by these SRFs to obtain more accurate estimates of the linearized membrane and membrane+bending stresses. These are then multiplied by the weld factor before comparing against allowable stress limits to obtain the alternating ratios.

It should also be noted that in the DSS approach, while some discretization errors in the displacement map are incurred at the cut boundaries (because the global mesh is generally coarser than that of the sub-model), these errors decay with distance from the cut boundary and are usually inconsequential with regard to stress evaluations at the location of interest usually located near the center of the sub-model domain. This behavior is an expression of St. Venant's Principle which states that higher order details of the 3D stress distribution at a specific location are insignificant when examining the stress state away from that location.

The steps involved in the DSS sub-modeling approach are the following:



9.4.3.3.2 Force-Based Sub-Modeling (SM) Approach

While DSS is a viable approach for obtaining more accurate stresses at selected locations, it is also computationally expensive. An alternative method has been formulated that achieves a significant advantage in terms of computational cost, while simultaneously producing stress reduction factors that closely match those obtained by DSS or other high resolution calculation procedures. This approach, “force-based sub-modeling” (SM), when properly formulated, both is mathematically rigorous and produces a unique load definition. SM relies on the fact that if the sub-model is subjected to the same distributed body forces (i.e., inertial loads and any other loads such as acoustic pressures or damping forces), then identical stress states will be obtained if either: (1) the consistent solution displacements and velocities are prescribed on the perimeter – the DSS, or (2) the consistent solution forces and moments are impressed over the same perimeter – the SM. By “consistent” it is meant that the forces and displacements all correspond to the same solution (e.g., the solution obtained in the global model). Also, this statement of stress identity, while true mathematically, will not be satisfied exactly in practice due to various errors associated with finite mesh size as described below.

Like DSS, the SM method involves setting up a highly detailed mesh of the local geometry with explicit representation of the welds. Rather than analyzing the complete transient response, however, the sub-model is formulated to consider only the alternating stress state for the limiting case in the global (i.e., the complete dryer) model. The computational implementation essentially constitutes a static stress analysis – hence the significant reduction in computational cost – but one where dynamic effects are fully and explicitly accounted for via the inertial terms introduced as equivalent body forces in accordance with d'Alembert's Principle.

After the stress evaluation has been performed at the limiting conditions in the global model, the stress solution is post-processed in the same manner as in DSS. Thus the linearized stresses are extracted along paths located at and through the welds. The limiting linearized stress is then compared against the corresponding limiting value in the global model. The resulting ratio of limiting stresses constitutes the stress reduction factor (SRF) that is subsequently applied to the global model calculation. It is noted that in addition to the SRF, the applicable weld factors to account for local stress concentration and weld quality must also be imposed to obtain the weld stress that is compared against Code allowables.

It should be noted that a properly formulated SM produces a unique sub-model load definition. In this respect it differs from the alternative sub-modeling approach previously submitted. We agree that the previously submitted alternative sub-modeling approach may not produce unique load and boundary conditions. Instead, forces or displacements should be extracted from the global model as described in the SM approach described above to produce unique load and boundary conditions.

9.4.3.3.3 Bias and Uncertainties / Validation

Both DSS and SM are subject to discretization and interpolation errors that must be quantified and accounted for by means of a bias and uncertainty. The possible sources of error include:

1. Mesh discretization error within the sub-model or sub-structure. Although the mesh in the sub-model is generally finer than in the global steam dryer model, a finite error still remains and requires quantification. This error is present in both DSS and SM and can be estimated by refining the mesh and examining the change in the limiting linearized stress. The resulting stress error is accounted for by applying an appropriate bias.
2. Interpolation of displacements or forces/moments at the sub-model boundary. In DSS, displacements are extracted from a global model with mesh spacing that is coarse compared to that of the sub-model. In the SM approach, the forces and moments are extracted from the global model. In both cases, the transfer of information from the global mesh to the sub-model boundaries is subject to discretization and/or interpolation error that must be estimated. One way to estimate this error is use a global steam dryer model that has a finer mesh in the vicinity of the sub-model location. This approach reduces the associated interpolation error and produces improved stress estimates against which DSS and SM predictions can be compared. Another option is to compare DSS or SM results against ones obtained with a global model that utilizes a high resolution, solid element-based representation in the vicinity of the sub-model. In either case, the estimated error is accounted for by imposing the associated bias and uncertainties determined by such comparisons.
3. Discretization, interpolation and/or linearization errors identified with the distributed loads imposed over the sub-model, such as the inertial loads or acoustic pressure forces. These forces are separate from the perimeter forces or displacements. An estimation of the associated errors should be obtained on theoretical grounds or by comparison against alternate HRS. The resulting error is accounted for in the associated bias or uncertainty.

BWRVIP194-EMCB-RAI-09

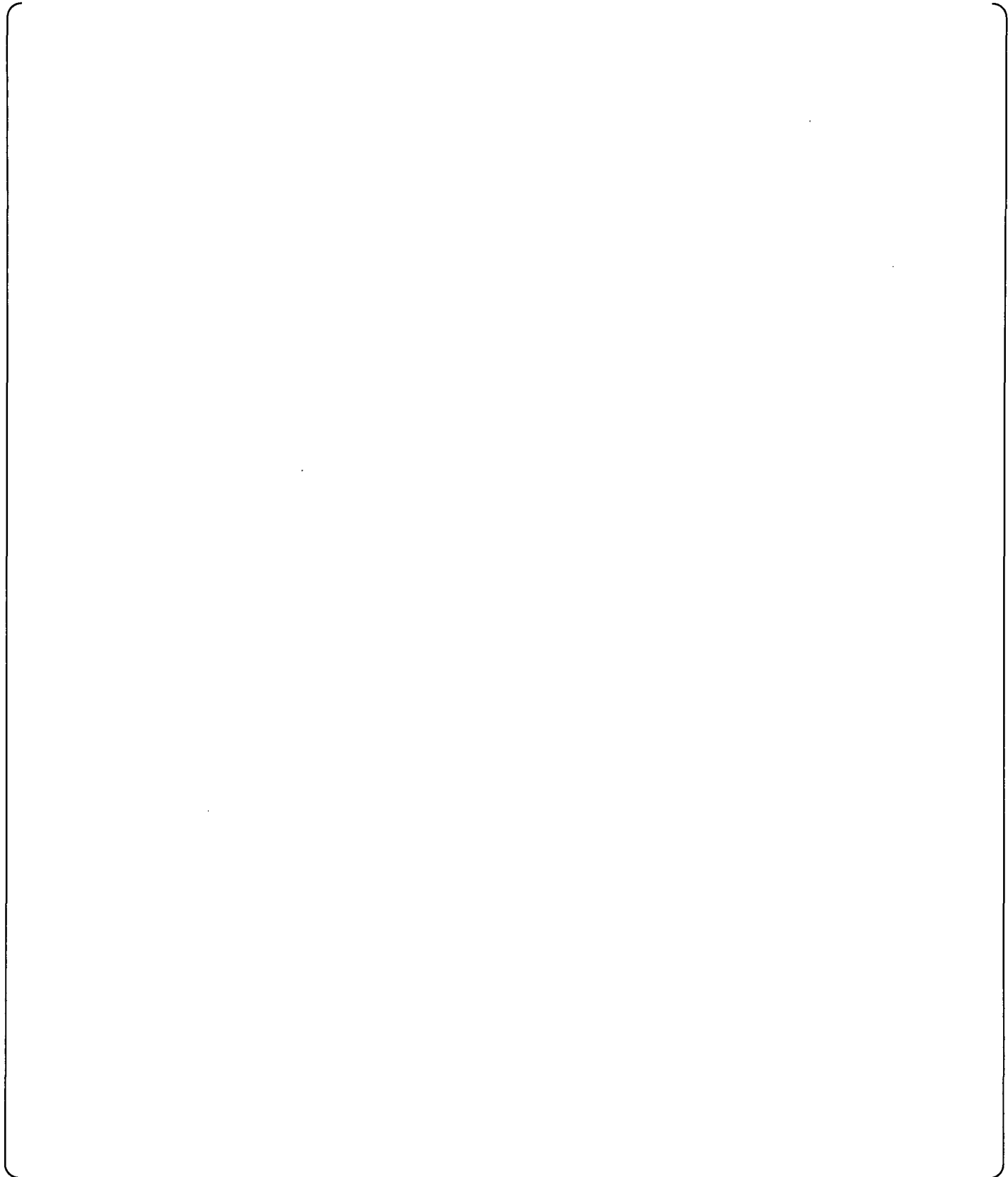
Section 6.3.2, Helmholtz Model Formulation, Pages 6-4 and 6-5: The topical report states that high resolution grid mesh is spaced 3 inches on the outer top plates, outer hoods, outer portions of the skirt and end plates closest to the MSLs, 6 inches on the first inner top plates, first inner hoods, sections near the center of the dryer, and 12 inches on the rest of the inner top plates, inside hoods, and center of the dryer.

Address how these spatial resolutions were established to be adequate. If resolutions are based on sensitivity studies, provide a discussion in support of these studies.

BWRVIP Response to NRC RAI BWRVIP194-EMCB-RAI-09

The first applications of the steam dryer analysis, to QC2 and Vermont Yankee, transferred two seconds of predicted time history dryer pressure data to an ANSYS model. The amount of transferred data became a problem for the vendor undertaking the structural analysis. For example, a 3-inch grid over the VY dryer would have generated approximately 1 GB of compressed data (2.6 GB uncompressed) that would have to be transmitted to the structural vendor. Since everything had to be done as quickly as possible (during power ascension), the two ways to transmit these data were by uploading to a backup site, or writing the data to CDs, which were then sent overnight. Time taken, data fidelity, and data reliability became immediate issues. At that time it was suggested that if the file size could be reduced, the transmittal would be smaller and therefore smoother.

a,c

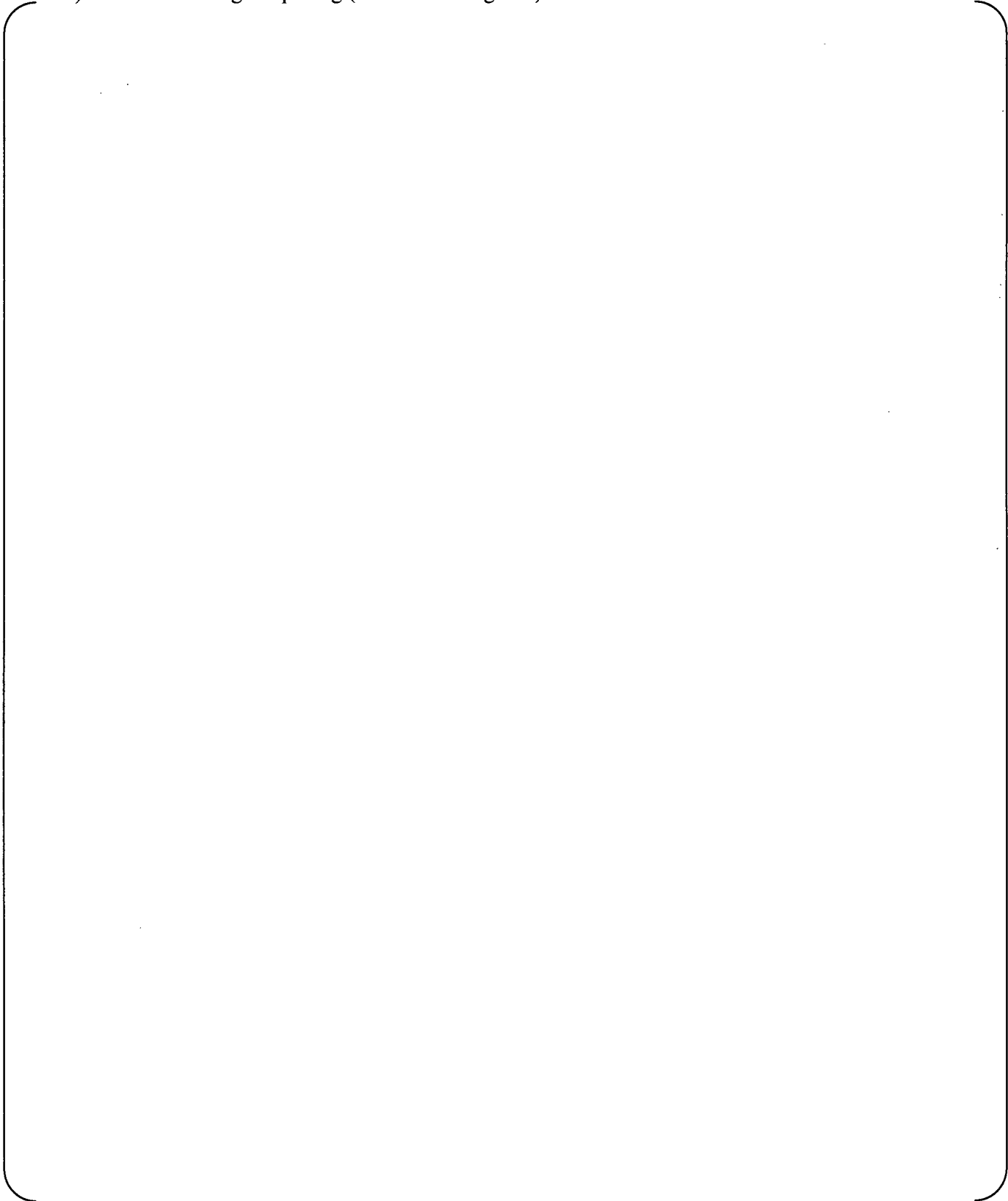


Westinghouse Non-Proprietary Class 3



a,c

Table RAI-9.1: Comparison of Alternating Stress Ratios between the original grid spacing (3, 6, and 12 inches) and the revised grid spacing (3 inches throughout).



a,c

BWRVIP194-EMCB-RAI-10

Pages v, 1-2, 3-3, 4-1, 7-1, 8-1, 9-1, 9-23, 9-26, 9-27, and 9-36: The topical report references the BWRVIP-181 and BWRVIP-182 reports, which are still under NRC review and have not been accepted as yet. References to unapproved topical reports should be removed, and necessary information provided as part of the BWRVIP-194 topical report.

BWRVIP Response to NRC RAI BWRVIP194-EMCB-RAI-10

The subject references will be retained in any revision to BWRVIP-194, as the NRC has accepted these reports, which are now identified as BWRVIP-181-A and BWRVIP-182-A.

BWRVIP194-EMCB-RAI-11

Section 9.4.3.1 Weld Fatigue Strength Reduction Factor, Page 9-32: The topical report addresses fatigue strength reduction factors (FSRF) for fillet and full penetration welds. The staff requests that the BWRVIP address the FSRF values for undersized welds and intermittent stitch welds that may be present in some dryer components.

BWRVIP Response to NRC RAI BWRVIP194-EMCB-RAI-11

Two changes will be made to the topical report in response to this RAI:

- A. Section 9.4.3.1 Weld Fatigue Strength Reduction Factor will be replaced in its entirety with the following:

[Redacted content] a,c

- B. Section 9.4.3.3 FEA Sub-Modeling at Welds will be renumbered 9.4.3.4, and Section 9.4.3.2 Comparison to Allowable Range of Alternating Stress Intensity S_a will be renumbered 9.4.3.3. A new Section 9.4.3.2 Fatigue Strength Reduction Factors at Undersized and Intermittent Stitch Welds will be inserted as follows:

9.4.3.2 Fatigue Strength Reduction Factors at Undersized and Intermittent Stitch Welds

[Redacted content] a,c

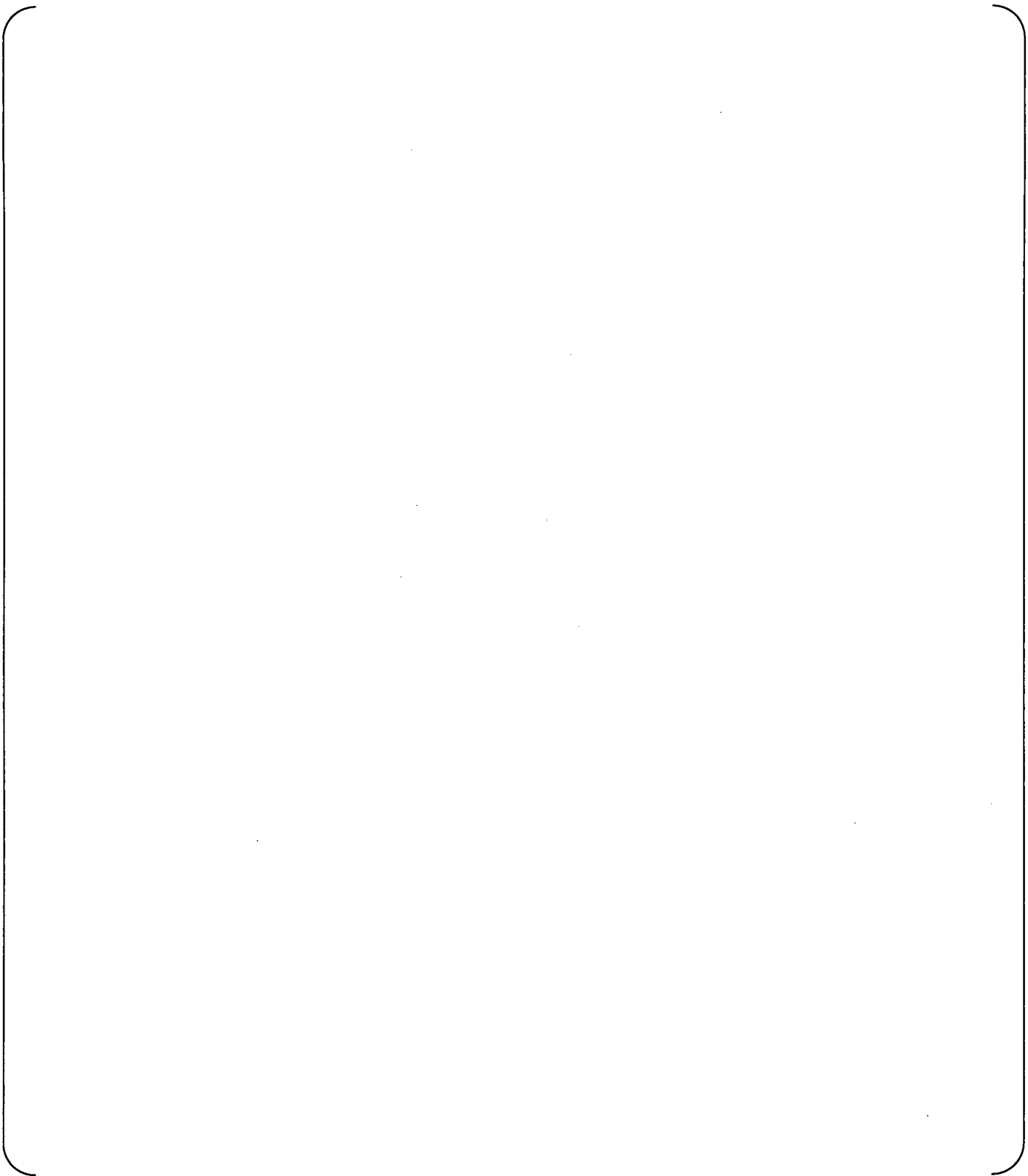




Figure 9-10: Schematic of simple in-line shell configuration loaded to produce stresses normal to the weld line.



a,c

Westinghouse Non-Proprietary Class 3



BWRVIP194-EMCB-RAI-12

Section 10.1, Page 10-2: The topical report provides an uncertainty for the accuracy of the ANSYS model solution, based on measurements from shaker tests conducted on the Hope Creek spare dryer. The uncertainty value accepted by the staff in the previous EPU applications is larger than the non-conservative lower uncertainty value in the topical report. The BWRVIP is requested to use the larger uncertainty value as shown in Table E-10 (page E-78), as opposed to the uncertainty value shown in Table E-11 (page E-78).

BWRVIP Response to NRC RAI BWRVIP194-EMCB-RAI-12



a,c

Table RAI-12.1: Damping set to 0.051%.

A large, empty rectangular frame representing a table. On the right side, there is a vertical bracket that spans the height of the table, with the text 'a,c' positioned to its right.

a,c

Table RAI-12.2: Damping optimized within $(1 \pm 0.37) \times 0.051\%$.

A large, empty rectangular frame representing a table. On the right side, there is a vertical bracket that spans the height of the table, with the text 'a,c' positioned to its right.

a,c

BWRVIP194-EMCB-RAI-13

[] a,c

BWRVIP Response to NRC RAI BWRVIP194-EMCB-RAI-13

A. In response to a previous plant RAI submittal, the NRC staff agreed to the lower damping value; this lower value will replace the larger value given in the topical report. Therefore, Section 9.2.4.2 Hydrodynamic Damping will be replaced in its entirety with the following:

[] a,c

B. A series of scale model experiments for steam dryers with []^{a,c} experimentally established variables or constants used in damping calculations. These tests, covered more fully in Appendix F.5, may be summarized as follows:

[] a,c

C. Figure E-52 (now Figure F-52) will be replaced by the following figure, which indicates the plate thickness τ :

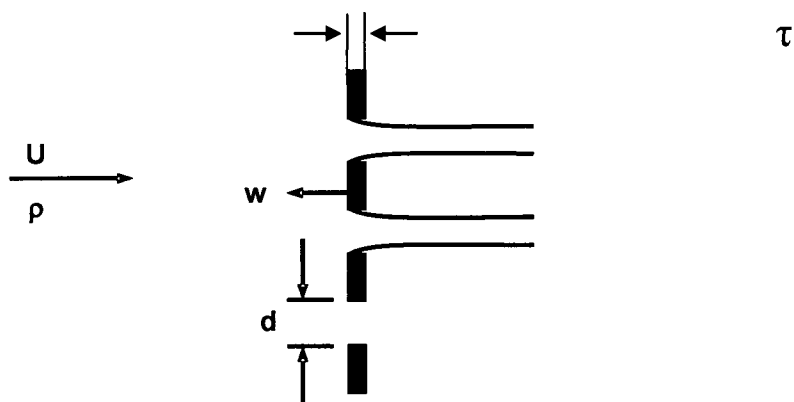


Figure F-52: Schematic of flow past a moving plate.

BWRVIP194-EMCB-RAI-14

Section 5.3: The topical report discusses the installation of strain gages around MSLs to define local fluctuating pressures. The topical report shall be revised to include a discussion on experience gained from strain gage failures due to improper installation, and cautions and recommendations to avoid such failures.

BWRVIP Response to NRC RAI BWRVIP194-EMCB-RAI-14

A new subsection will be added to Section 5 of BWRVIP-194, immediately following Figure 5-4. The content of this section is as follows:

5.3.1 Precautions to be Taken when Installing Strain Gages

In order to avoid a repetition of mistakes and previously encountered issues, a summary of the lessons learned from previous EPU strain gage installations is provided here:

- Use high-temperature strain gages capable of dynamic measurements. Gages that can be spot welded to the main steam piping provide a more secure installation. In order to minimize the chance of signal failure, gages with a built-in high temperature cable are preferable. Many plants have successfully used the Hitec Products HBWAK series (for example, the HBWAK-35-250-6-10FG). This gage has a 350 ohm nominal resistance and a built-in 10-foot long high temperature cable, which can be placed directly on the outside surface of the MSL.

- The wall thickness and pipe diameter at each strain gage location should be measured and documented. These measurements are used to compute the uncertainty of the dynamic pressure measurement.
- At each strain gage elevation, strain gage pairs should be oriented 180° apart, and wired to a single strain gage channel. One plant inadvertently connected strain gages that were only 45° apart into a single strain gage channel. The mistake was corrected prior to plant startup; however, the strain gage pairs should be clearly identified in the modification package to avoid confusion.
- Ensure that the surface of the pipe is smooth at the installation locations. Remove any visible paint residue or oxidization. Place gages away from longitudinal and circumferential welds, pits, or other irregularities, as these may affect the accuracy of the measurements.
- Strive to minimize sharp bends or kinks in the cabling, particularly the high temperature segments coming from the gages, to minimize the potential for shorted signals. All cables should be secured at the connectors, with a small amount of slack between the tie-off point and the piping to allot for thermal expansion. Do not use the high temperature cables to support weight, particularly that of bundled field cables.
- Strain gage assemblies (sensor, cable, connectors) should be prepared prior to the start of the outage, and tested for functionality prior to field installation. Care should be taken to avoid shorting the shield to the connector housing/shell inside the connector assembly. This approach greatly simplifies and expedites the installation process while in the radiation-controlled area. Using Amphenol or similar type connectors between the high temperature cable and the field cable simplifies and speeds up installation while saving dose. Field cable should be precut to the estimated length before being installed.
- Use low noise field cable. In EPU type applications, strain gages produce very low signals (in terms of voltage) and using low noise cabling is essential to maximizing signal-to-noise ratio.
- It is best to use female connectors on the lead wires from the strain gages. This approach simplifies the electrical functionality testing that must be performed after strain gage installation.
- Cable shield should be terminated inside the connector. Leaving it exposed on the outside could cause it to short when touching plant metallic parts, which in turn can cause ground loops.
- Ensure that only the high-temperature cable (leads connected directly to the strain gage) is installed under the piping insulation. One plant coiled the low-temperature cables under the piping insulation. Prior to plant startup, the strain gages for those channels appeared to be working correctly. However, upon plant startup, the low temperature instrument cable, in direct contact with the MSL, melted when exposed to the MSL operating temperatures, and all strain gage data were lost for those particular channels.

- Use caution when reinstalling piping insulation over the strain gages. Several plants have experienced gage shorts and failures when strapping the insulation down too tightly.
- If possible, avoid stringing cable in high-traffic areas where the potential for personnel to trip or tug on the field cable may exist. Strain gage assemblies are quite fragile and should not be altered after installation.
- Electrical resistances should be measured and documented after each step of the installation process, to verify that the connections were made correctly and to ensure that there are no shorts or open circuits in sensors or cables.
- Use a shielded instrumentation penetration to pass signals through the drywell wall. If an unshielded instrumentation penetration must be used, ensure that no high-voltage lines are located in the same penetration or near the strain gage cables. Several plants have routed strain gage cables through an unshielded electrical penetration containing high voltage cables; this environment caused excessive electrical noise in the signal, and resulted in a reduced signal amplitude resolution for the DAS.
- Run the shield wire from each field cable through its own penetration connector. Several plants have spliced these wires together at the penetration. This approach creates the potential for increased noise through a ground loop.
- When using CONE or similar type connectors at drywell penetration locations, it is highly recommended that the pins and sockets be cleaned prior to final installation, to avoid poor signal quality and potential disconnections.
- Label all cables during installation – one plant had to perform extensive troubleshooting due to misinterpretation of the strain gage pairs. The modification package should clearly identify which sets of strain gages and cables should be paired together.
- All cable between the strain gage connector and the primary containment penetration should be shielded, twisted-pair instrument cable. This cable should also be routed from the drywell penetration to the DAS.
- When running the cable between the strain gage connector and the DAS, avoid prolonged segments parallel to equipment power cabling, as this condition can induce unwanted electrical noise. For this reason, it is best to avoid cable trays. Where crossing a power line is necessary, attempt to do so in a perpendicular fashion.
- Field cables should be terminated at the DAS using Amphenol or similar type connectors allowing for easy decoupling. Field cables should be disconnected from the DAS if it is anticipated that data will not be recorded for an extended period of time.
- The DAS should be capable of turning power off to the gages. Leaving the gages powered by the DAS for long periods of time (days) should be avoided, as it may cause gage damage or burn-out.

- Care should be taken when moving the DAS enclosure. Some utilities share the DAS between units of the same plant and even between plants. Connections inside the DAS can be loosened due to the movement. A procedure should be developed to confirm continued DAS functionality after the move.
- The DAS cabinet should be lockable.
- Numerous pictures should be taken during installation, especially of the strain gage locations, to assist with future troubleshooting or questions that may arise during analysis.
- A known failure in a strain gage signal conditioning module resulted in a 1 Hz pulsing of the signal from the Wheatstone bridge. A redesign of the module by National Instruments corrected this problem. However, this incident points to the need to perform consistency checks on the power supply to ensure that a different form of electrical interference is not introduced into the signal, resulting in invalid data.

BWRVIP194-EMCB-RAI-15

Section 9.1.9: In this section the topical report briefly touches on the subject of steam dryer cracking and plant specific evaluations. The topical report should be revised to address loose parts evaluations, on a plant specific basis, as well as the potential for degraded components, with unknown structural conditions and inaccessibility for inspection, for the possibility of flutter vibrations or galloping under cross-flow. The supporting documentation should also contain an evaluation of any existing flaws in the steam dryer components and their impact on steam dryer operation at EPU conditions. A reference to Section 4.0 of BWRVIP-06-A topical report, for consideration of loose parts, and the BWRVIP-139 topical report, Steam Dryer Inspection and Flaw Evaluation Guidelines, should be incorporated into the BWRVIP-194 topical report.

BWRVIP Response to NRC RAI BWRVIP194-EMCB-RAI-15

Section 9.1.9 Consideration of Steam Dryer Cracking will be expanded, and a new Section 9.1.10 Consideration of Flutter Vibrations and Galloping under Cross Flow will be added to the topical report. These sections will replace Section 9.1.9 in its entirety with the following:

9.1.9 Consideration of Steam Dryer Cracking

The structural analysis methodology described in this report contains the inherent assumption that the steam dryer components are uncracked. It is impractical to postulate cracking of different sizes in each steam dryer component and assess the relative effect that these cracks have on the results of the stress analysis; therefore, any cracking identified during a dryer inspection must be evaluated on a plant specific basis. An evaluation of observed cracking should include the following considerations:

1. Potential for additional crack growth as a result of the suspected initiation mechanism and all relevant propagation mechanisms (IGSCC, fatigue); and
2. Effect of observed cracking on dynamic characteristics of the steam dryer.

The normal modes of a structure are generally not significantly affected by cracking unless there are a large number of cracks distributed throughout the structure or a crack is very large; nevertheless, a plant specific evaluation is considered appropriate to identify if the existence of cracking must be included in the stress analysis. The output of this evaluation will assist the utility in determining whether a repair must be applied.

Cracking identified prior to power uprate in BWR steam dryers should be evaluated in accordance with the guidance provided in BWRVIP-139-A. This evaluation generally includes determining the cracking mechanism (i.e. IGSCC or fatigue), considering crack growth and stability, assessing the impact of the flaws on the local and global dynamic characteristics of the steam dryer assembly, and considering potential generation and effects of loose parts. Flaw evaluations are used to determine whether further assessment is required, when/if repair of the indications will be implemented, or if there is sufficient justification to recommend that the indication requires no immediate remediation.

Each of the components of a steam dryer flaw evaluation is discussed in more detail below.

9.1.9.1 Determination of Cracking Mechanism

The cracking mechanism must be identified in order to properly consider flaw growth for the observed crack. The discussion contained in BWRVIP-139-A effectively details the evaluation recommended to determine and document the flaw initiation mechanism; those details are not repeated here.

9.1.9.2 Consideration of Crack Growth

To be evaluated effectively for disposition, the anticipated crack growth for flaws resulting from IGSCC should be determined for the applicable (or proposed) re-inspection interval. Note that such evaluations are not required by BWRVIP-139-A for IGSCC cracks that are less than eight inches in length and located in specific locations on the steam dryer that have not experienced significant crack growth based on field experience. A bounding industry IGSCC crack growth rate for un-irradiated stainless steel in BWR internals (5×10^{-5} in/hr) is provided in BWRVIP-139-A, and can be used for IGSCC indications in the steam dryer assembly. Fatigue crack growth must be considered for both fatigue cracks and for IGSCC, since cracks may initiate by IGSCC but subsequent crack extension may also be driven by fatigue, if the fluctuating loads are sufficiently large. Since the steam dryer assembly experiences turbulence-induced loads, as well as acoustic-induced loading during normal operation, the criterion used to predict fatigue crack growth is to compare the range of applied stress intensity factor ΔK_I with the threshold range of stress intensity factor for fatigue crack growth ΔK_{ITH} , in order to determine whether the plant specific fluctuating loads will result in an applied ΔK_I which exceeds ΔK_{ITH} . If $\Delta K_I < \Delta K_{ITH}$, then fatigue crack growth is not predicted to occur, and the necessary (i.e. minimal condition but not “sufficient” condition) requirement to leave the flaw in-service – “as is” – has been met. Conversely, if $\Delta K_I \geq \Delta K_{ITH}$, then fatigue crack growth is anticipated, crack growth becomes controlling and must be investigated.

Since the applied turbulent and acoustic loading will accumulate a large number of cycles over a typical fuel cycle (1.5 to 2 years), no specific fatigue crack growth increment is calculated; rather, if growth is predicted to occur in this time period, a plant specific flaw evaluation must assess whether the flaw will grow into a region of decreasing stress such that the flaw self-arrests. If flaw arrest can be demonstrated, then again the necessary condition that the flaw be left in place (i.e. use “as is”) has been met, and further justification must be provided if the final recommendation is to leave the flaw in place. If the flaw does not arrest, then the flaw will typically not be considered acceptable “as is”, requiring repair. Flaws which are identified to be initiated by fatigue, with no signs of IGSCC, do not need to consider IGSCC growth in the flaw evaluation.

9.1.9.3 Consideration of the Effect of Cracking on the Dynamic Characteristics of the Steam Dryer

Assessing whether the flaw will grow, or only grow a small amount before arresting, is not sufficient by itself (it does however meet the “necessary” condition). To meet the sufficiency requirement, the effect of the end-of-interval flaw size must be assessed with respect to the dynamic characteristics of the steam dryer assembly. Specifically, it must be determined whether the presence of the cracks will significantly change the response of the steam dryer assembly to the imposed loads. If the observed cracking will change the

response of the dryer to the applied loads, then the presence of the cracking must be included in the overall dryer stress analysis. Since the steam dryer assembly is built of numerous plates, the effect of cracking can often be assessed by evaluating the effect of the end-of-interval flaw size on the modal characteristics of the local region. If the end-of-interval crack is shown to have an insignificant effect on the normal modes of the local region, then it can be argued that the effect of the crack on the global response of the dryer is also insignificant.

9.1.9.4 Consideration of Loose Parts

Consideration of loose parts should be included in any flaw evaluation. The loose parts assessment in BWRVIP-06-A should be used as input and appropriately supported by the plant specific flaw evaluation.

9.1.10 Consideration of Flutter Vibrations and Galloping under Cross Flow

Flutter vibration and/or galloping of parts under cross-flow should be considered if the geometrical situation is such that the likelihood of such an event is possible, i.e. whether steady steam flow can cause oscillations of a cantilevered part, similar to the vibrations of power lines in crosswind. The cause of such galloping vibrations is negative aerodynamic damping arising under specific flow conditions. However, such adverse aerodynamic damping, when present, has to be sufficiently large to overcome the structural damping, which is conservatively set at 1%. However, in a typical example, the energy supplied to the system by aerodynamic forces is much less than 1% of the energy dissipated, which suggests that no galloping vibrations of a cantilevered part is possible.

In a worst case scenario, when the stitch weld attaching the cantilevered part to a dryer plate is inactive along the whole plate, if the part were hypothetically to disconnect from the plate, the stress ratios in the cantilevered part and its associated remaining welds at EPU conditions would be well above target levels. Therefore, no additional weld disconnection would occur.

Typically the weld connecting the cantilevered part to the plate is a stitch weld rather than a continuous weld. Therefore, any crack that may occur in a given stitch weld segment will, at most, propagate along the length of this segment. The crack is then naturally arrested, since further extension of the disconnection would require initiation and subsequent propagation of a new crack at the next stitch weld.

The galloping phenomenon described here is caused by the negative damping introduced by hydrodynamics. Another phenomenon, known as vortex shedding, can also produce instabilities. In this case the formation of a vortex street downstream of a bluff body structure induces fluctuating loads back onto the structure. But again, as before, no vortex shedding induced oscillations will occur either. In summary, even for extremely conservative hypothetical scenarios, no galloping occurs.

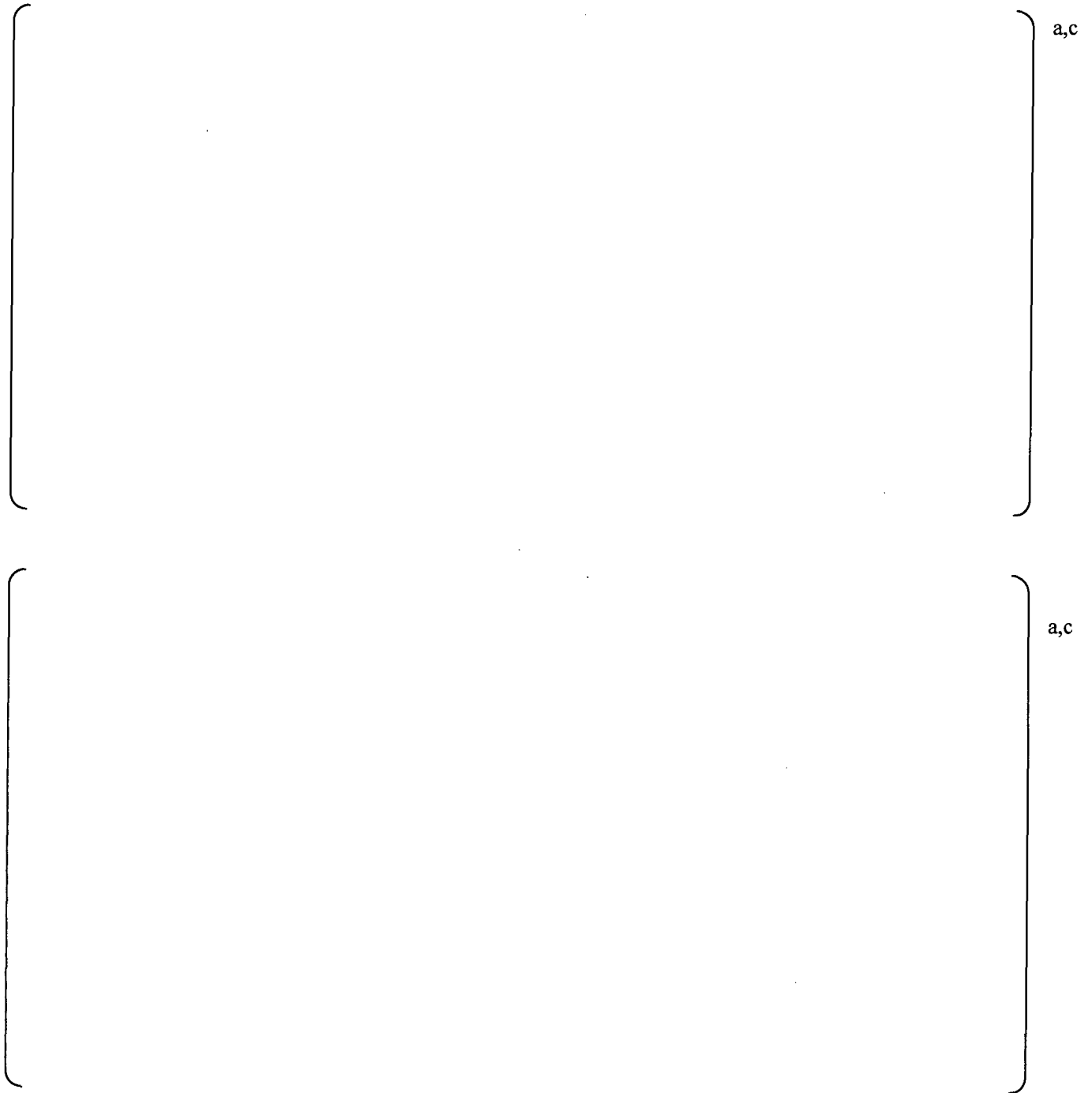


Figure 12-1: Subscale measurements of the effectiveness of ASB installation: before installation (top), after installation (bottom), with one ASB, filled with dampening material, on each standpipe. In this example the standpipe excitation frequency is between 200 and 210 Hz.

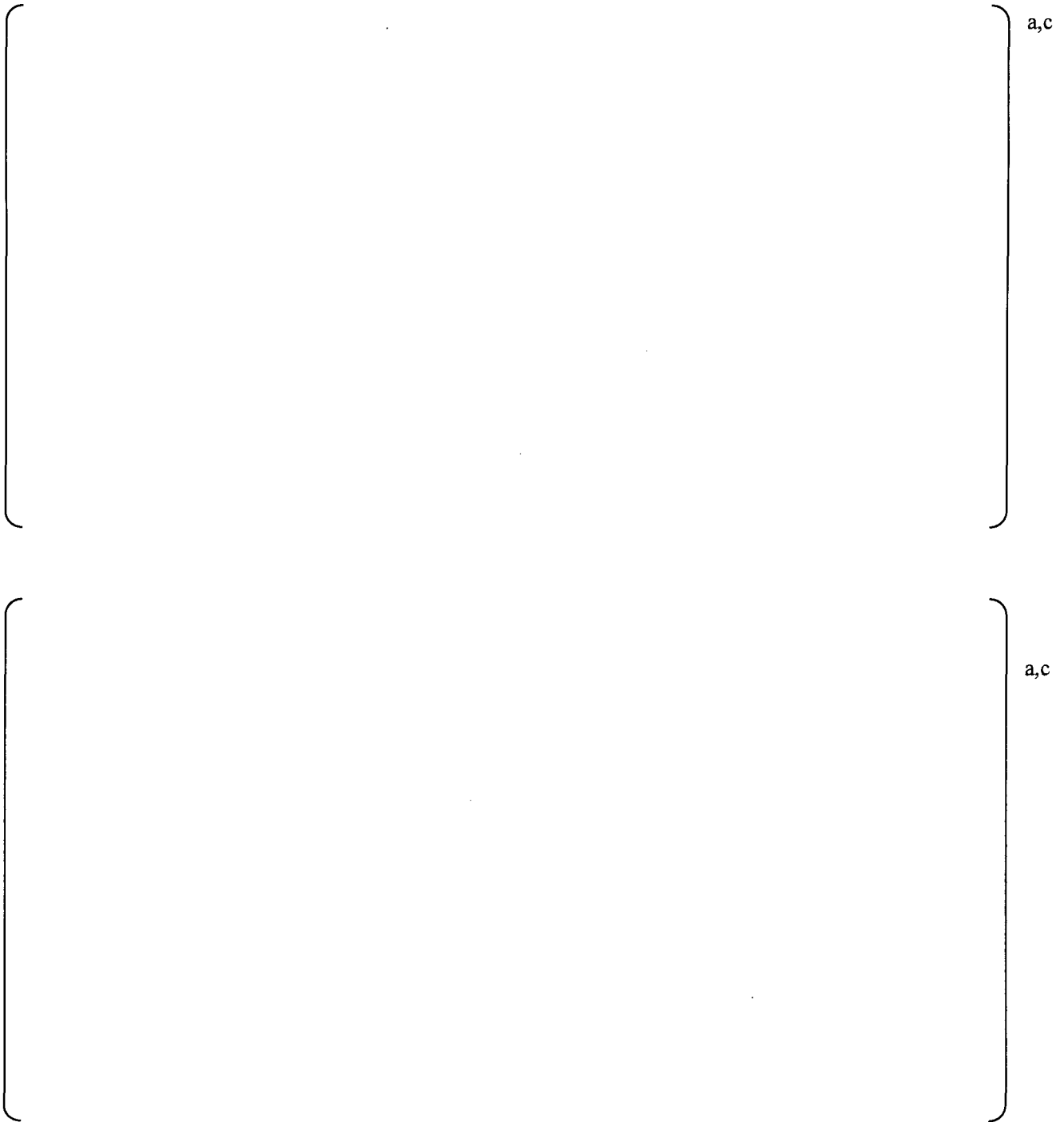


Figure 12-2: Subscale measurements of the effectiveness of AVS installation on blind standpipes: before installation (top), after installation (bottom). In this example the blind standpipe excitation frequency is between 200 and 230 Hz.

BWRVIP194-EMCB-RAI-17

In Item 2 of Section 5.9 of the topical report, strain gage signals or data sets with []^{a,c} are addressed. This RAI pertains to the filtering of []^{a,c} signals from the CLTP signals, []^{a,c} the hydrodynamic and acoustic loads on the steam dryer. In a recent conference call with a licensee on October 30, 2009, regarding the use of Rev. 4 of the Continuum Dynamics, Inc. Acoustic Circuit Model (ACM), with respect to the extended power uprate (EPU) application, the NRC staff was informed that during the benchmarking of the ACM parameters, by means of the Quad Cities Unit 2 (QC2) data, the []^{a,c} from the main steam line (MSL) strain gage signals used to estimate the steam dryer loads. Therefore, it is non-conservative to remove the []^{a,c} from main steam line (MSL) strain gage data prior to computing dryer loads using Rev. 4 of the ACM.

The BWRVIP is requested to address that steam dryer stress analysis results for EPU conditions shall be based on steam dryer loads determined []^{a,c}. In addition, the BWRVIP is requested to ensure that the minimum alternating stress ratio (SR-a) is not less than 2.0 for any dryer component for the projected EPU conditions.

BWRVIP Response to NRC RAI BWRVIP194-EMCB-RAI-17

The response to BWRVIP194-EMCB-RAI-01 discusses the replacement of the ACM Rev. 4 model with the ACM Rev. 4.1 model and the fact that steam dryer stress analyses for EPU conditions will be based on steam dryer loads determined []^{a,c} across the entire frequency spectrum. In ACM Rev. 4.1, applications of the model use EIC signals only for the purpose of identifying discrete and extraneous electrical interference spikes. The response to BWRVIP194-EMCB-RAI-03 addresses the NRC staff recommendation that the minimum alternating stress ratio be at least 2.0 for any dryer component for projected EPU conditions.

BWRVIP194-EMCB-RAI-18

The BWRVIP is requested to provide a detailed description (i.e., a step-by-step procedure) of how the QC2 MSL strain gage signals at OLTP were modified (both during and after data acquisition) before they were applied to the ACM Rev. 4 Code (whose results were used for benchmarking) to estimate acoustic loads on the instrumented QC2 dryer.

Additionally, the licensee is requested to provide the following information about any exclusion frequencies:

- a. Provide the amplitudes of the QC2 MSL strain gage signals for the exclusion frequencies (60, 120, and 180 Hz) at CLTP conditions before these frequencies were removed or filtered. Discuss which of these frequencies were treated as exclusion frequencies in modifying the QC2 signals.
- b. Provide the information on the QC2[]^{a,c}, and provide the amplitudes of the MSL strain gage signals at this frequency. Explain whether this frequency was treated as an exclusion frequency in modifying the QC2 signals.
- c. Explain whether any exclusion frequency filtering was also applied to the instrumented QC2 dryer pressure signals.

BWRVIP Response to NRC RAI BWRVIP194-EMCB-RAI-18

[]^{a,c}

Answers to the three items requested in the RAI are as follows:

a,c

BWRVIP194-EMCB-RAI-19

Section 5.9.1 of the topical report addresses noise removal by coherence filtering. This RAI pertains to the []^{a,c} signals from the MSL strain gage signals at OLTP, []^{a,c} the hydrodynamic and acoustic loads on the steam dryer. In a recent conference call with a licensee on 4 February 2010, on using Rev. 4 of the ACM, regarding their Extended Power Uprate (EPU) application, the NRC staff was informed that during the benchmarking of the ACM parameters, by means of the QC2 data, []^{a,c} the data used to estimate the steam dryer loads. Therefore, it is non-conservative to []^{a,c} the strain gage data prior to computing dryer loads using Rev. 4 of the ACM.

To be consistent with the ACM code benchmarking, the BWRVIP is requested to state that steam dryer stress analysis for EPU conditions shall be based on dryer loads []

[]^{a,c}. In addition, the BWRVIP is requested to ensure that the minimum alternating stress ratio (SR-a) is not less than 2.0 for any dryer component for the projected EPU conditions.

BWRVIP Response to NRC RAI BWRVIP194-EMCB-RAI-19

ACM Rev. 4 benchmarking []^{a,c}. In ACM Rev. 4.1, however, the QC2 main steam line signals at OLTP conditions were filtered with the steps identified in response to BWRVIP194-EMCB-RAI-01, including []^{a,c}. The approach used in the re-benchmark is identical to the approach to be used in plant applications of ACM Rev. 4.1. The response to BWRVIP194-EMCB-RAI-03 addresses the NRC staff recommendation that the minimum alternating stress ratio be at least 2.0 for any dryer component for projected EPU conditions.

BWRVIP194-EMCB-RAI-20

The staff, performing EPU reviews for three plants, recently became aware of procedures such as

[]^{a,c} that were not performed in ACM Rev. 4 benchmarking. In Section 5.9 of the topical report, BWRVIP is utilizing these methodologies that were not employed in ACM Rev. 4 benchmarking, based on the QC2 data. This is not only inconsistent with ACM Rev. 4 benchmarking but also would result in under-prediction of dryer loads. The BWRVIP is requested to address if ACM Code will be re-benchmarked, or will revise the topical report to eliminate the filtering of MSL strain gage signals. The BWRVIP is also requested to identify any further inconsistencies with the QC2 benchmarking procedure that the staff is unaware of. In addition, please describe the impact of those inconsistencies on the minimum alternating stress ratio for the projected EPU conditions.

BWRVIP Response to NRC RAI BWRVIP194-EMCB-RAI-20

ACM Rev. 4 has been replaced by ACM Rev. 4.1, re-benchmarked to the QC2 data with the steps described in response to BWRVIP194-EMCB-RAI-01, and used as well in plant applications to be conducted according to BWRVIP-194. Thus, with the use of ACM Rev. 4.1 there will be no inconsistencies between QC2 re-benchmarking and plant applications.

The revised bias and uncertainty values, comparing ACM Rev. 4 with ACM Rev. 4.1, are shown in Table RAI-20.1, and plotted in Figure RAI-20.1.

Table RAI-20.1: QC2 bias and uncertainty values for specified frequency intervals.



a,c

There are no inconsistencies in the use of ACM Rev. 4.1 between QC2 validation and plant application.

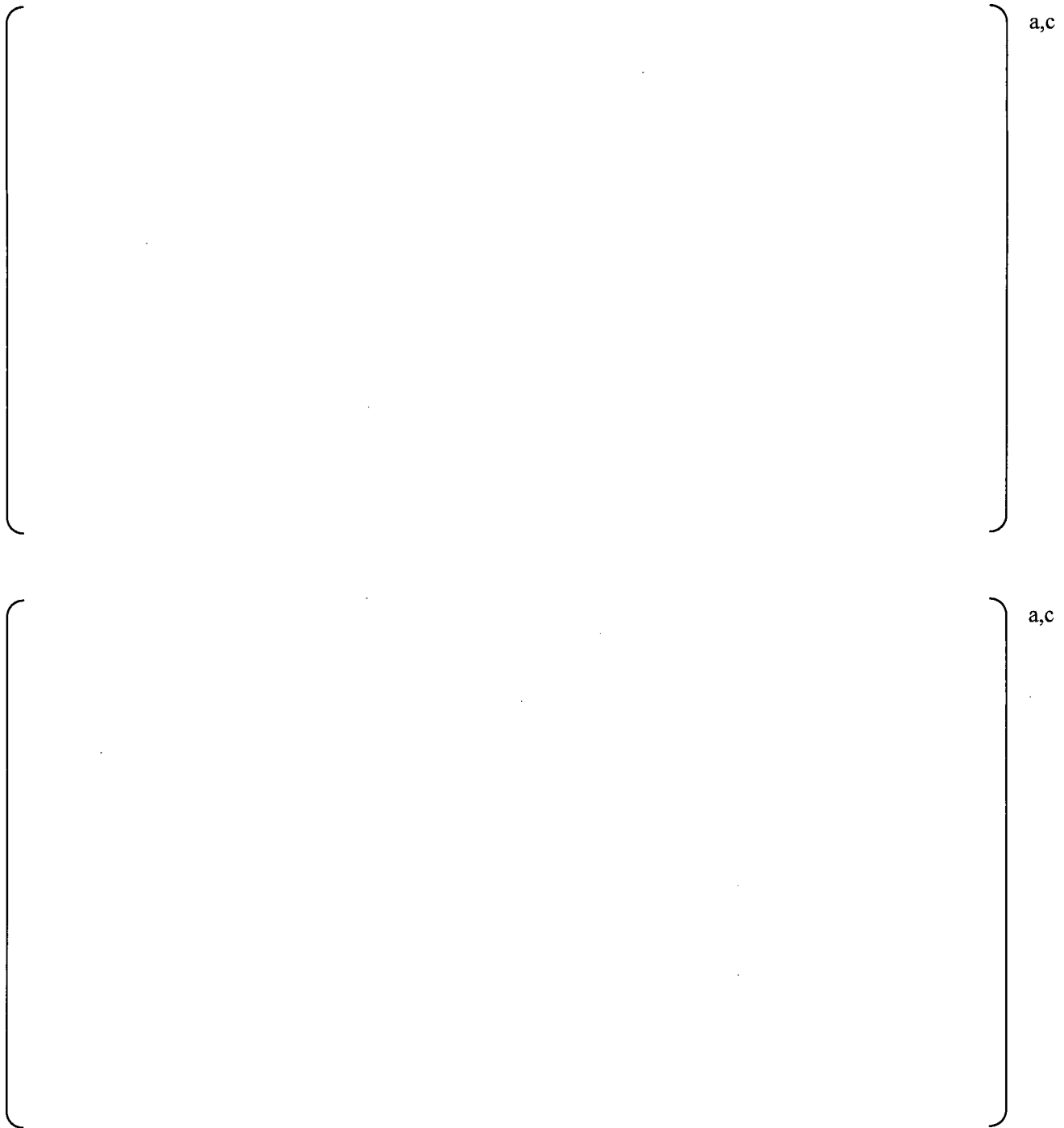


Figure RAI-20.1: Comparison of bias and uncertainty values between ACM Rev. 4 and ACM Rev. 4.1. Bias is shown in the upper figure, uncertainty in the lower: ACM Rev. 4 (in blue), ACM Rev. 4.1 (in red).

ADDITIONAL REVISIONS TO BWRVIP-194

In addition to the changes required to respond to the RAIs, the following changes to the topical report are planned:

- A. Step 3 of Section 3 Overview of Steam Dryer Evaluation Approach will be replaced in its entirety with the following:

Step 3: Conduct in-plant tests at CLTP

[] a,c

- B. Section 5.2 Uncertainty Associated with Axial Measurement Locations will be replaced in its entirety with the following:

5.2 Uncertainty Associated with Axial Measurement Locations

[] a,c



a,c

C. Appendix A Evaluation of Coherence Between MSL Fluctuating Pressure Measurements will be modified by replacing the paragraph between Equations (A.14) and (A.15) with the following paragraph, and ending the Appendix with the short paragraph after Equation (A.19):

Paragraph between Equations (A.14) and (A.15):



a,c

Paragraph after Equation (A.19):



a,c

D.Appendix F Application of Methodology to Predict Steam Dryer Fluctuating Pressure Loading from In-Plant Steam Dryer Pressure Measurements will be relabeled Appendix G and be replaced in its entirety by the following:

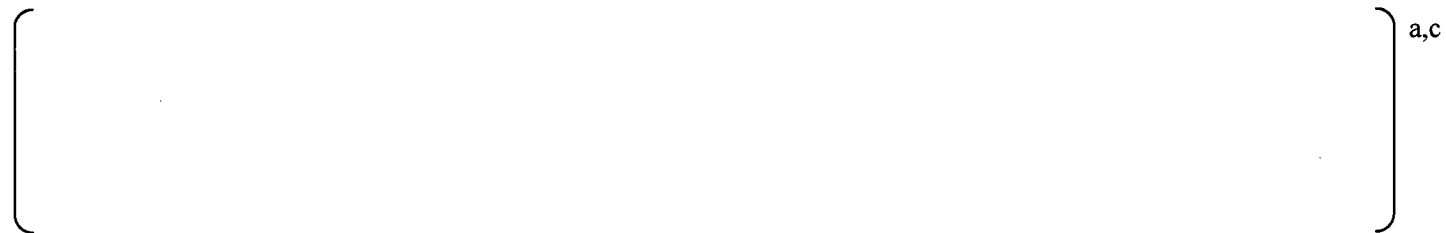
Appendix G: APPLICATION OF METHODOLOGY TO PREDICT STEAM DRYER FLUCTUATING PRESSURE LOADING FROM IN-PLANT STEAM DRYER PRESSURE MEASUREMENTS

An instrumented dryer, such as the replacement QC2 dryer, offers an alternative way of predicting the pressure loading on the dryer when pressure transducer data are collected at measured power levels. The solution approach includes the use of the Helmholtz results (discussed in Section 6.3) and a least squares analysis involving applicable data. This appendix summarizes the approach and presents comparisons with the QC2 OLTP data set.

G.1 Approach



G.2 Solution



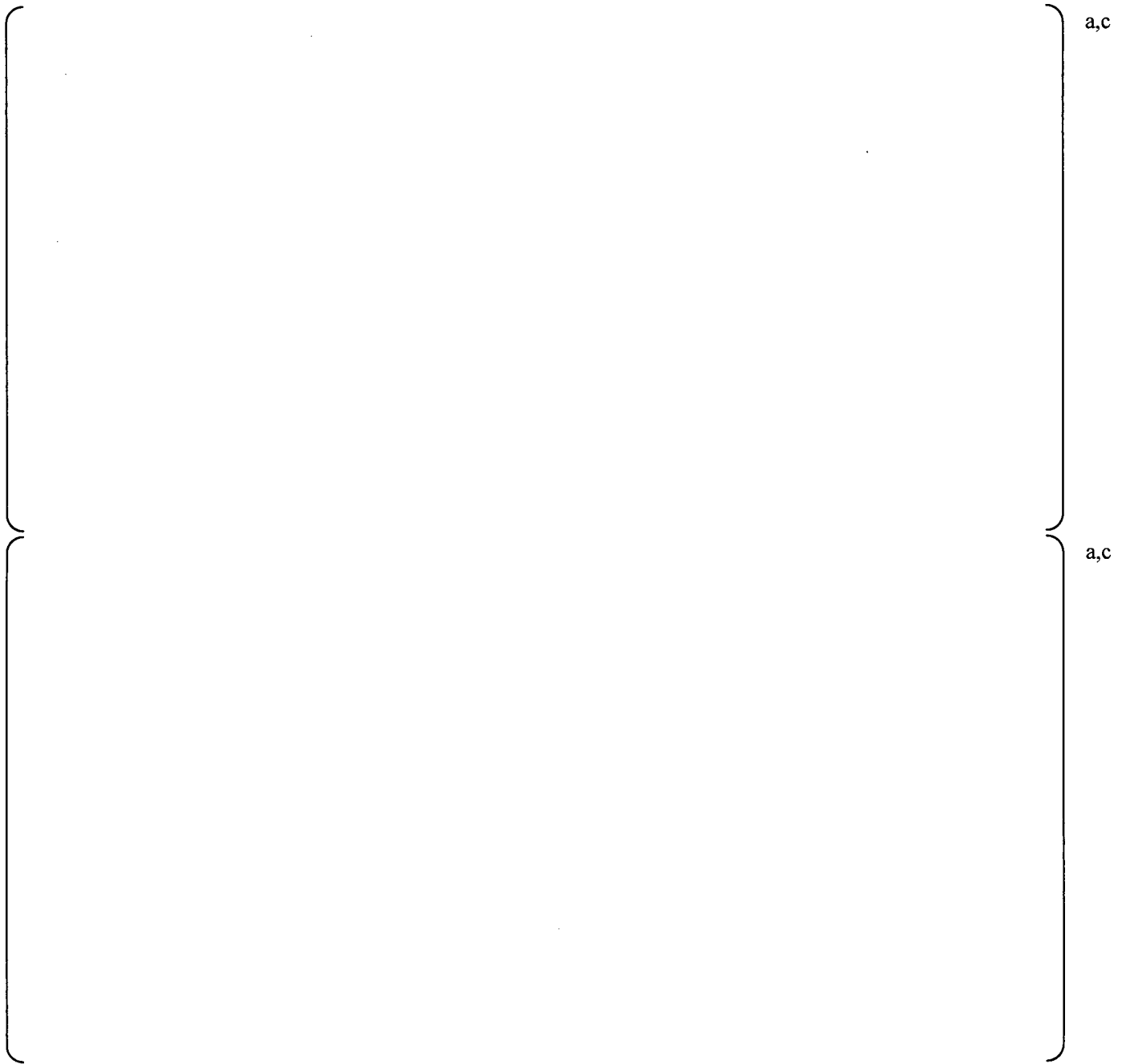


Figure G-1: Least squares predictions at 790 MWe at the dryer pressure sensors: peak maximum (top) and peak minimum (bottom) pressure levels, with data (blue) and predictions (red).

Table G-1: QC2 bias and uncertainty values for specified frequency intervals.



The table area is mostly empty, with a large right-side bracket indicating a specific section or reference. The label 'a,c' is positioned to the right of the bracket.

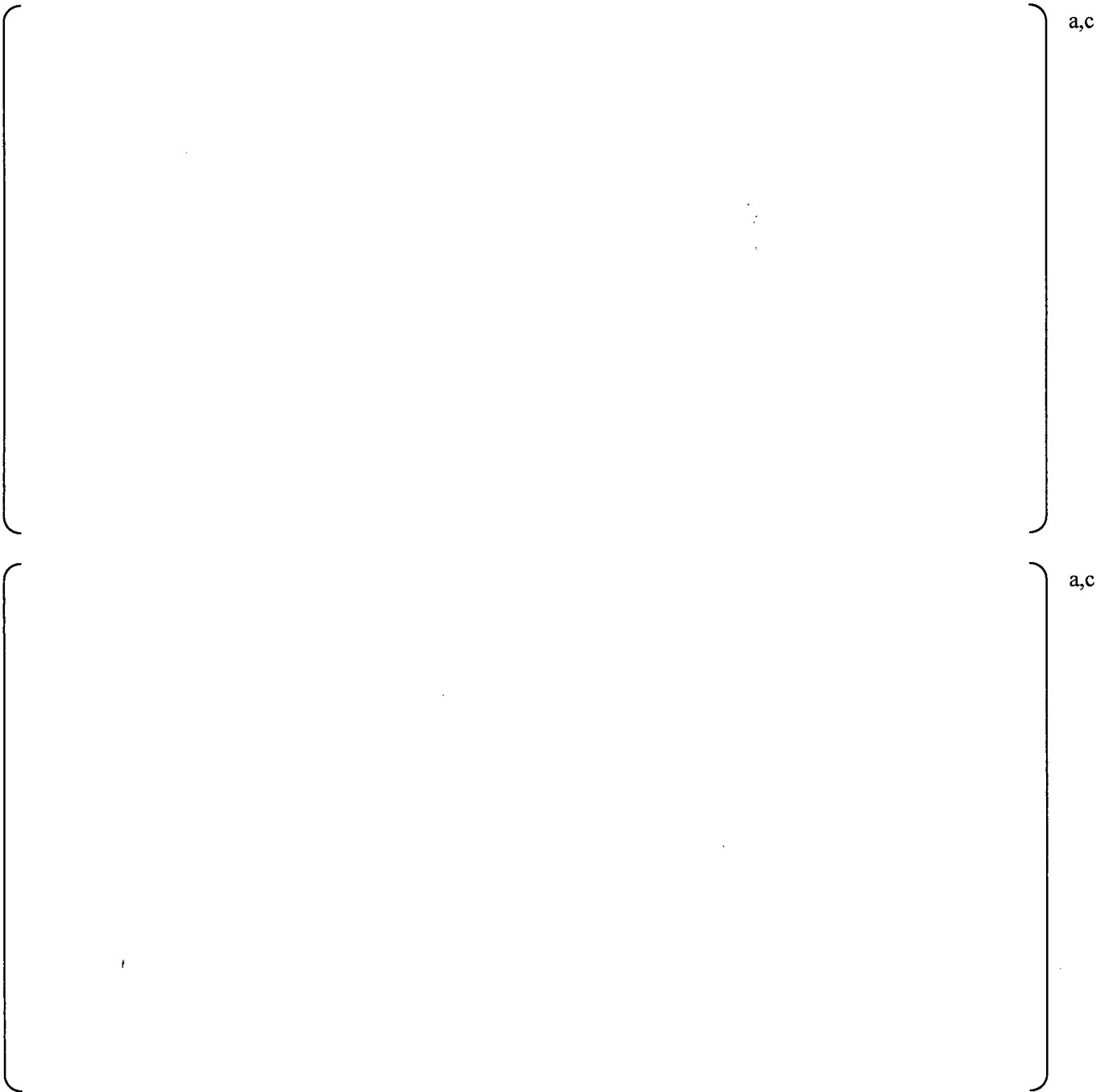


Figure G-2: Least squares predictions at 790 MWe at the dryer pressure sensors: peak maximum (top) and peak minimum (bottom) pressure levels, with data (black), predictions (blue), and predictions with bias and uncertainty added (red). Sensors P13, P14, P16, P23, and P27 are inside the dryer, while P26 is on a mast above the dryer.

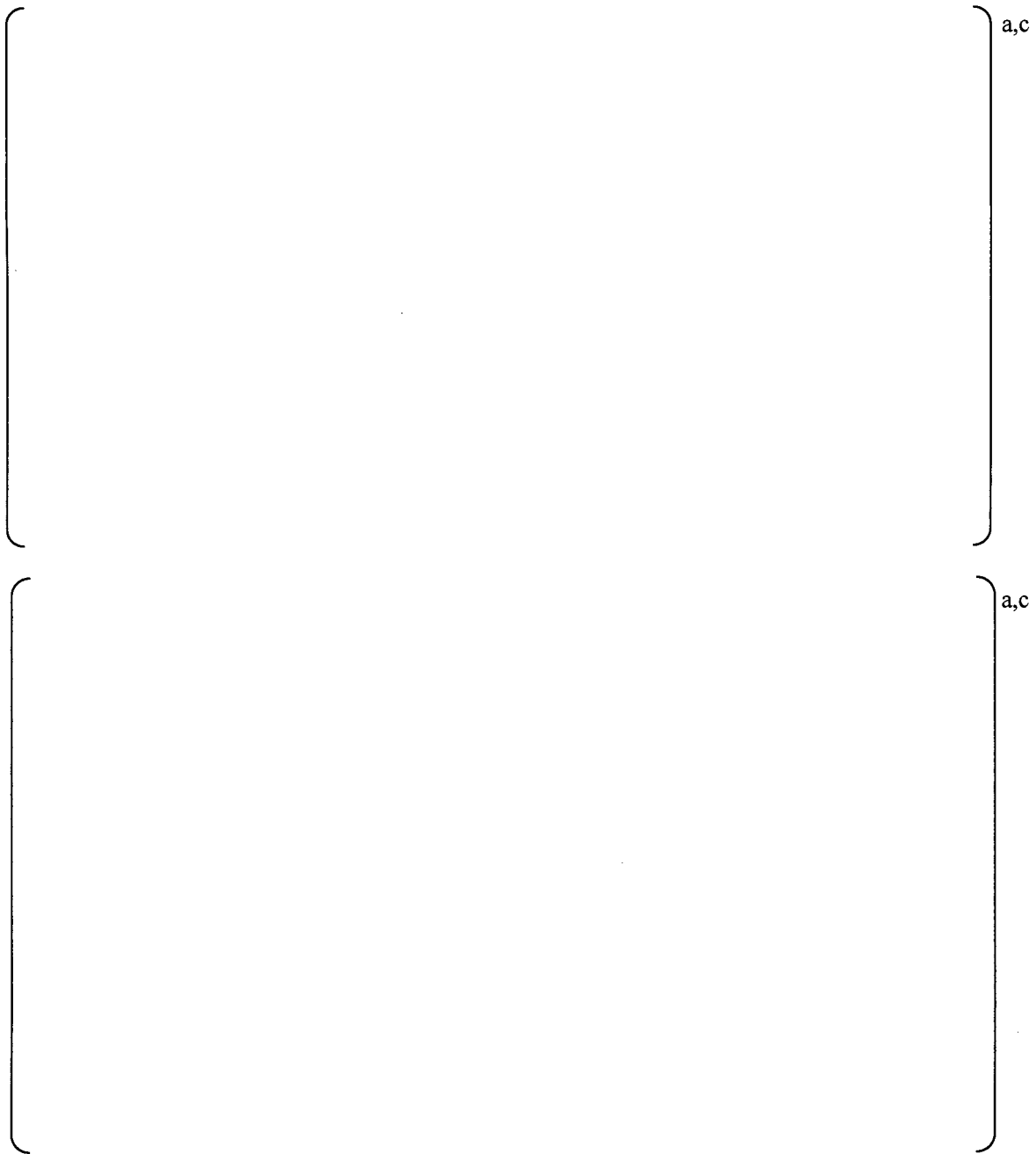


Figure G-3: Comparison between measured and predicted peak pressures at the 27 pressure sensors in QC2 at 790 MWe, without (top) and with (bottom) bias and uncertainty added to the predicted load. The lines are the one-to-one boundaries. [

]a,c

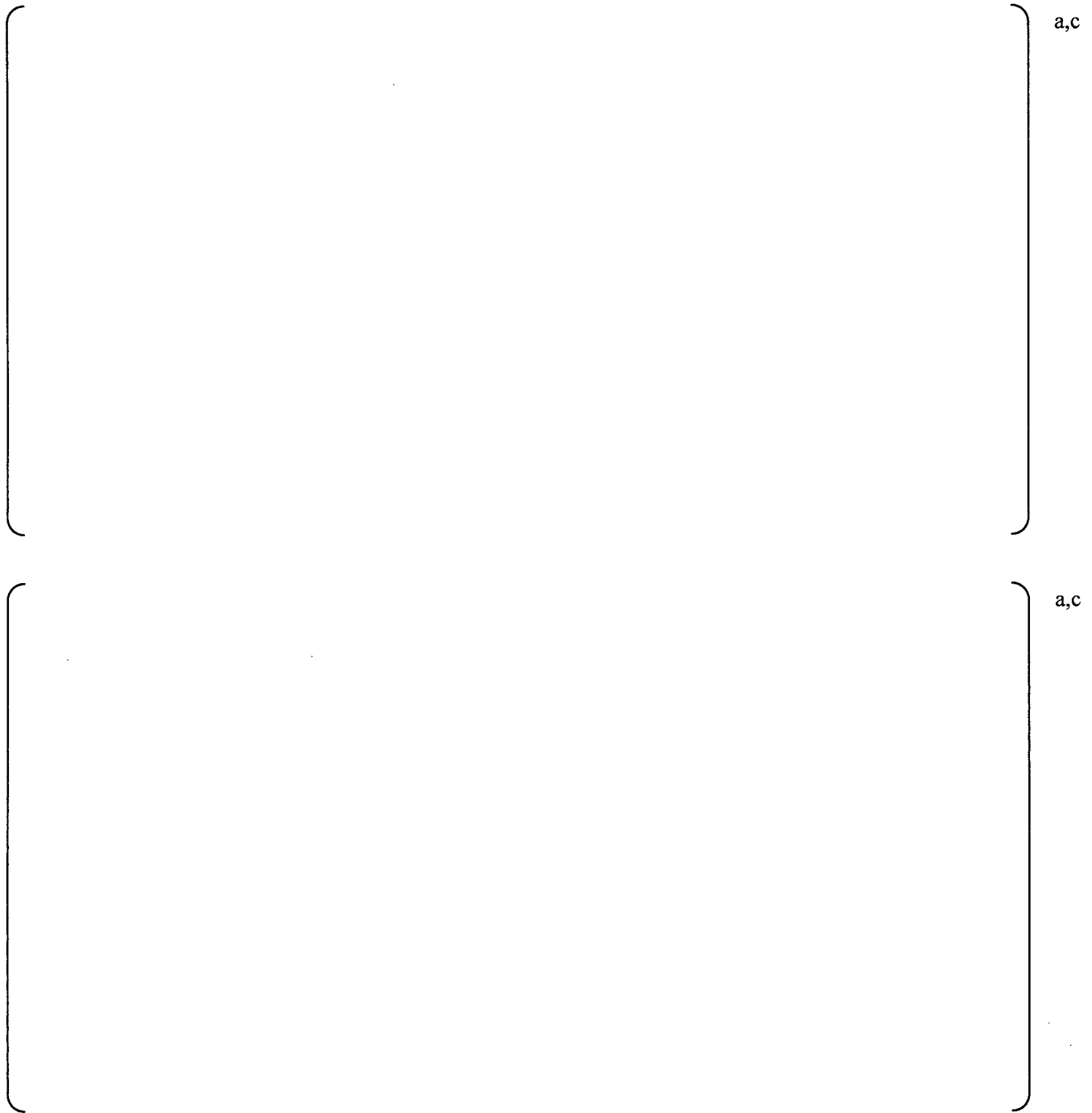


Figure G-4: PSD comparison at 790 MWe for pressure sensor data (black curves) and least squares predictions with bias and uncertainty added (red curves), for P1 (top) and P2 (bottom).

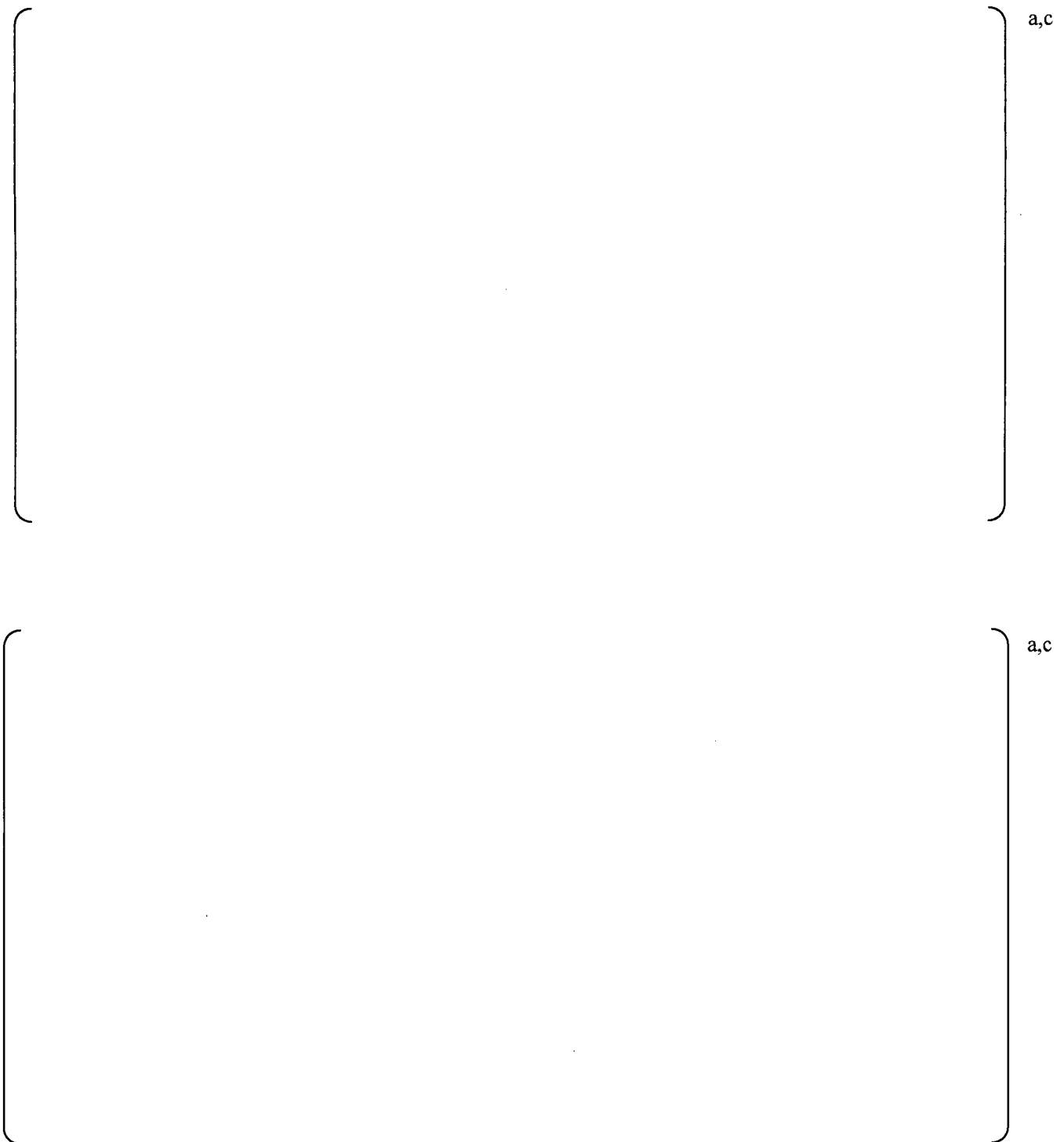


Figure G-5: PSD comparison at 790 MWe for pressure sensor data (black curves) and least squares predictions with bias and uncertainty added (red curves), for P3 (top) and P4 (bottom).

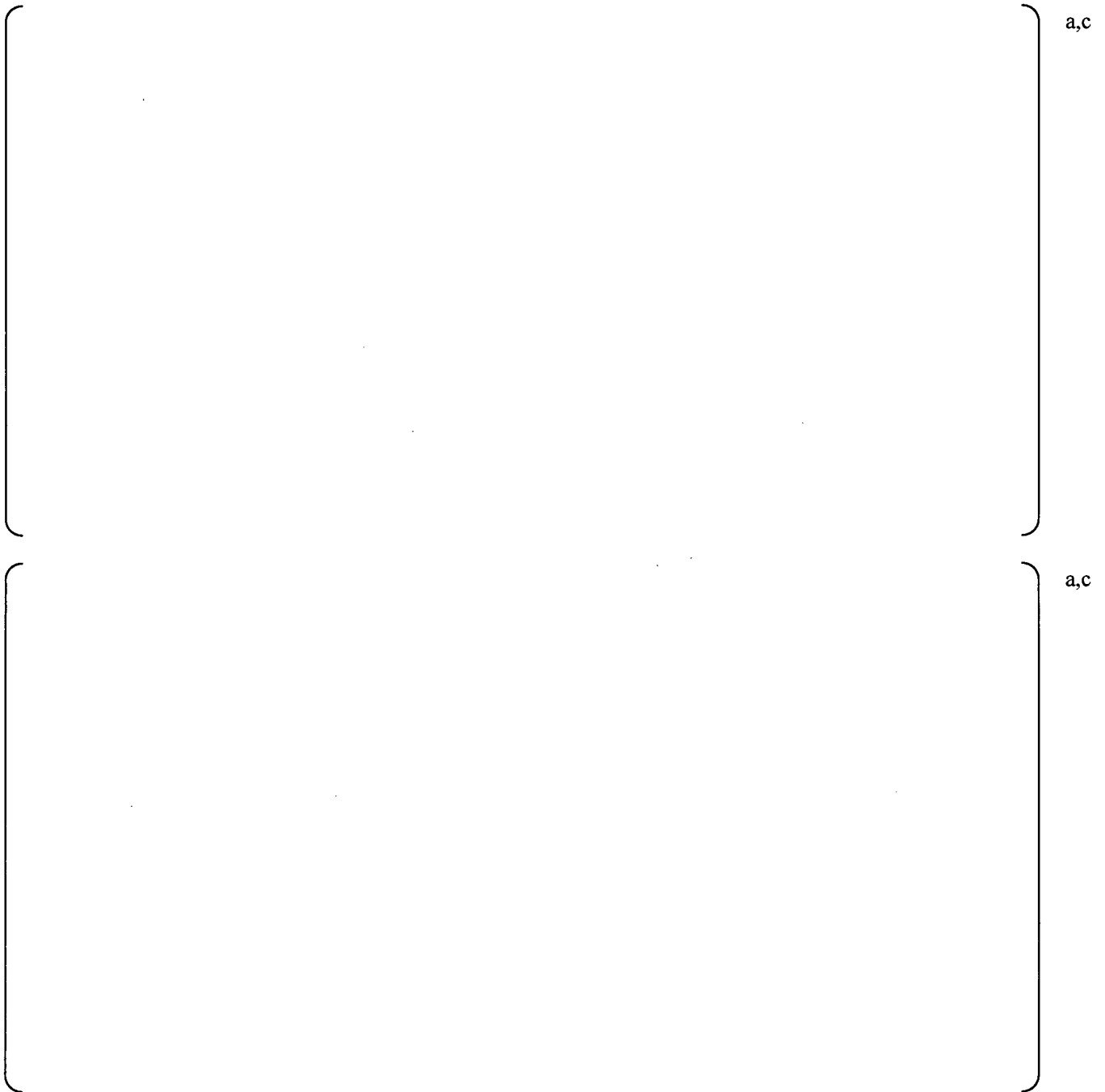


Figure G-6: PSD comparison at 790 MWe for pressure sensor data (black curves) and least squares predictions with bias and uncertainty added (red curves), for P5 (top) and P6 (bottom).

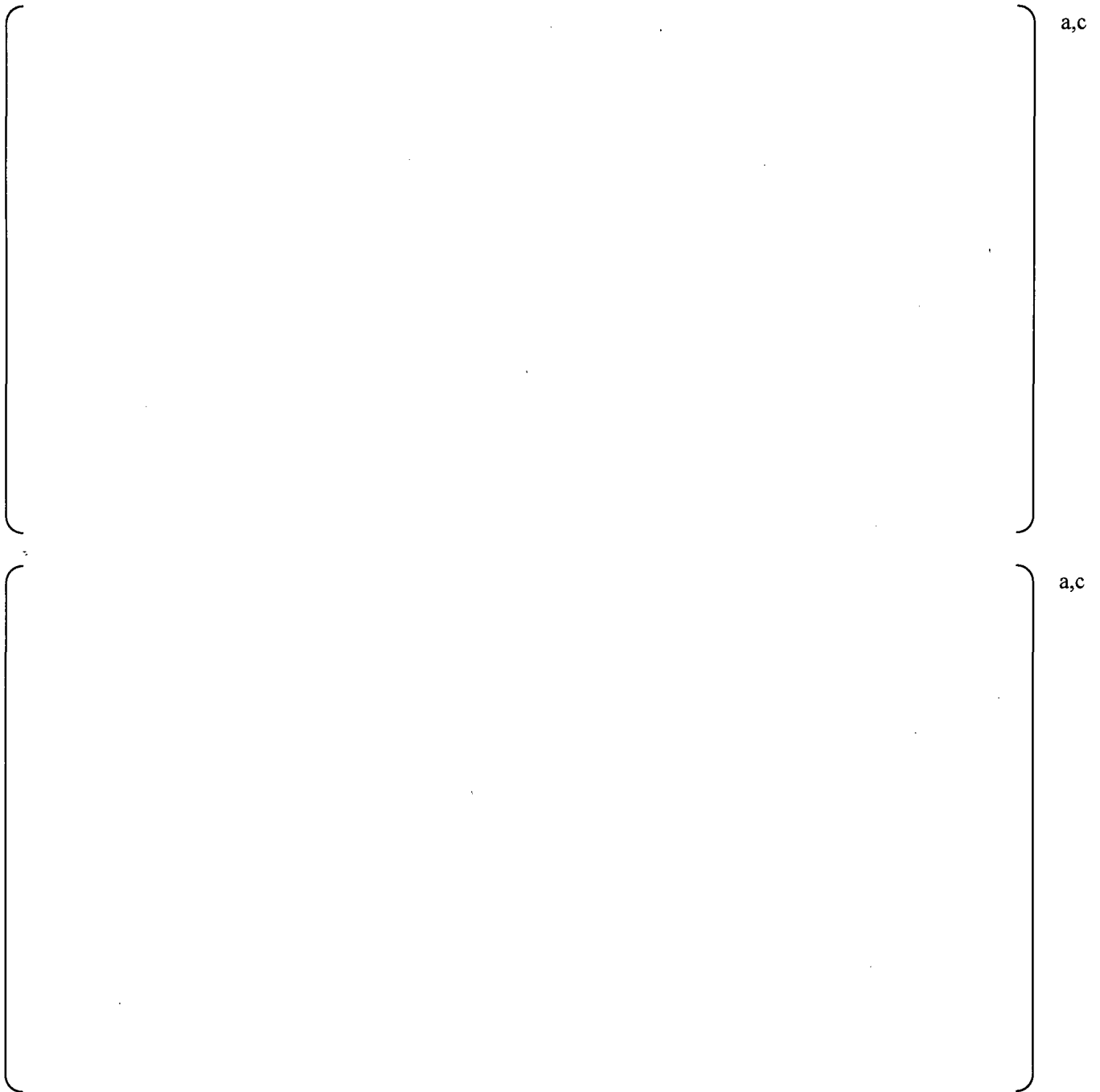


Figure G-7: PSD comparison at 790 MWe for pressure sensor data (black curves) and least squares predictions with bias and uncertainty added (red curves), for P7 (top) and P8 (bottom).

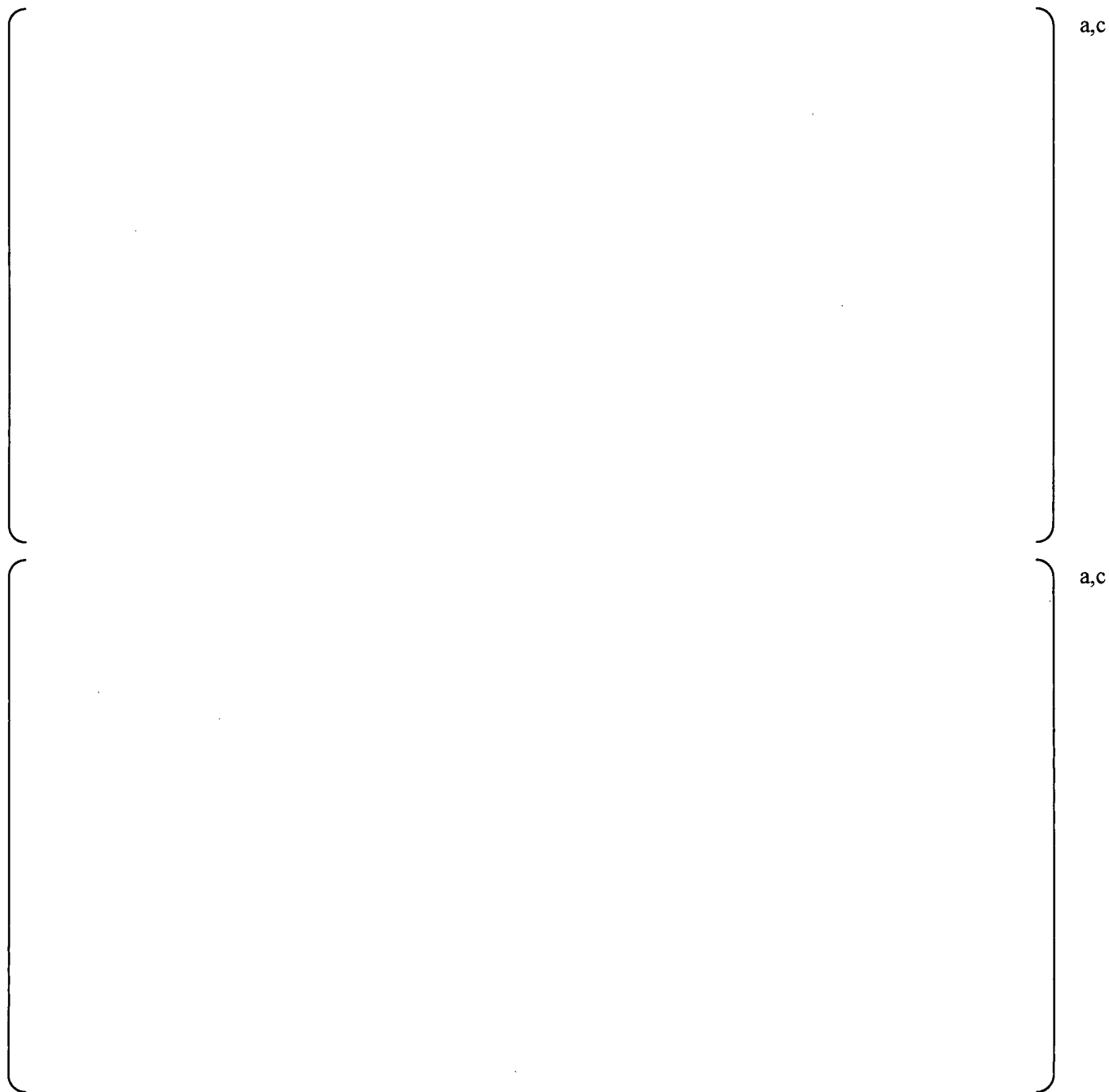


Figure G-8: PSD comparison at 790 MWe for pressure sensor data (black curves) and least squares predictions with bias and uncertainty added (red curves), for P9 (top) and P10 (bottom).

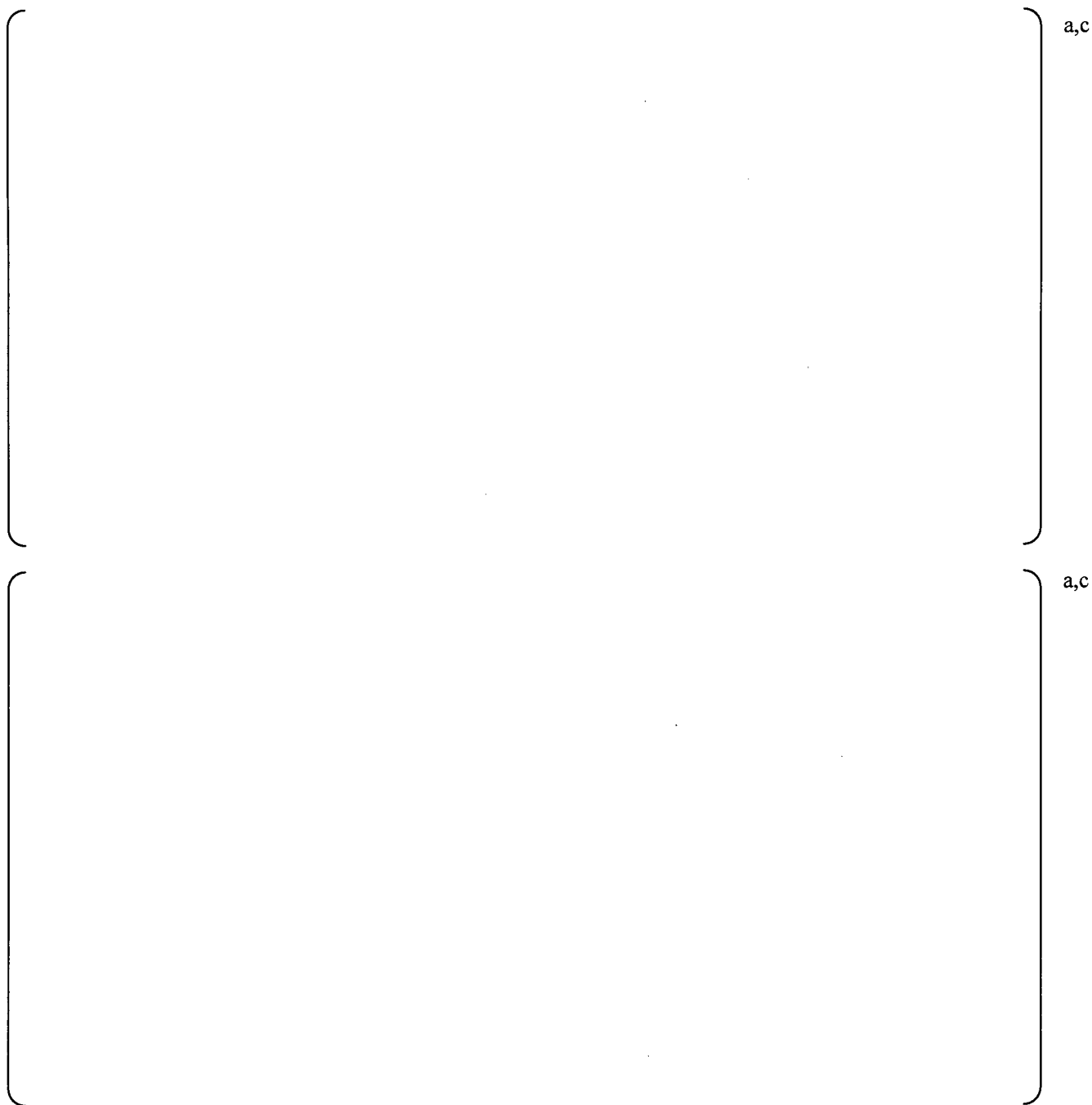


Figure G-9: PSD comparison at 790 MWe for pressure sensor data (black curves) and least squares predictions with bias and uncertainty added (red curves), for P11 (top) and P12 (bottom).

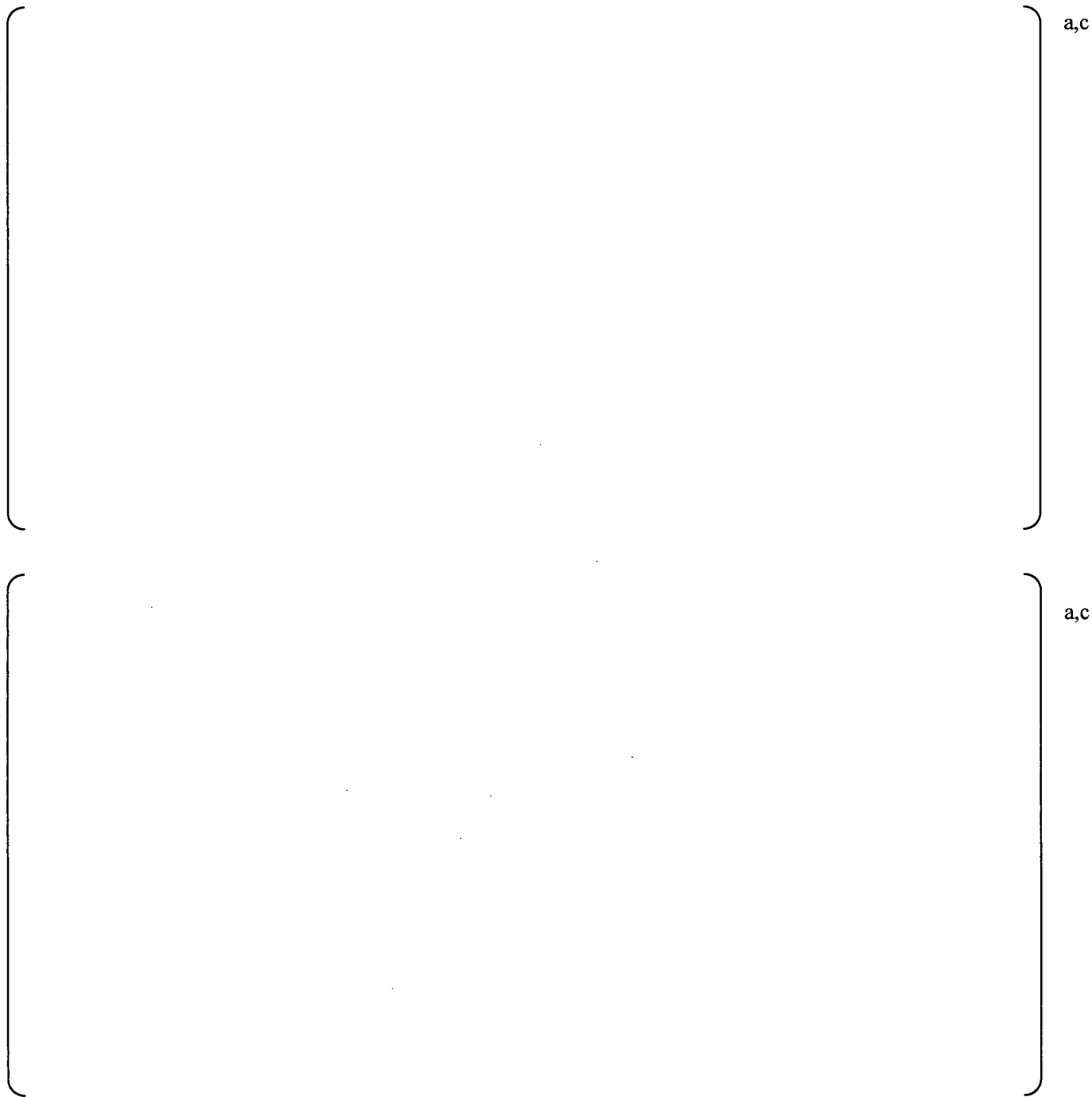


Figure G-10: PSD comparison at 790 MWe for pressure sensor data (black curves) and least squares predictions with bias and uncertainty added (red curves), for P13 (top) and P14 (bottom).

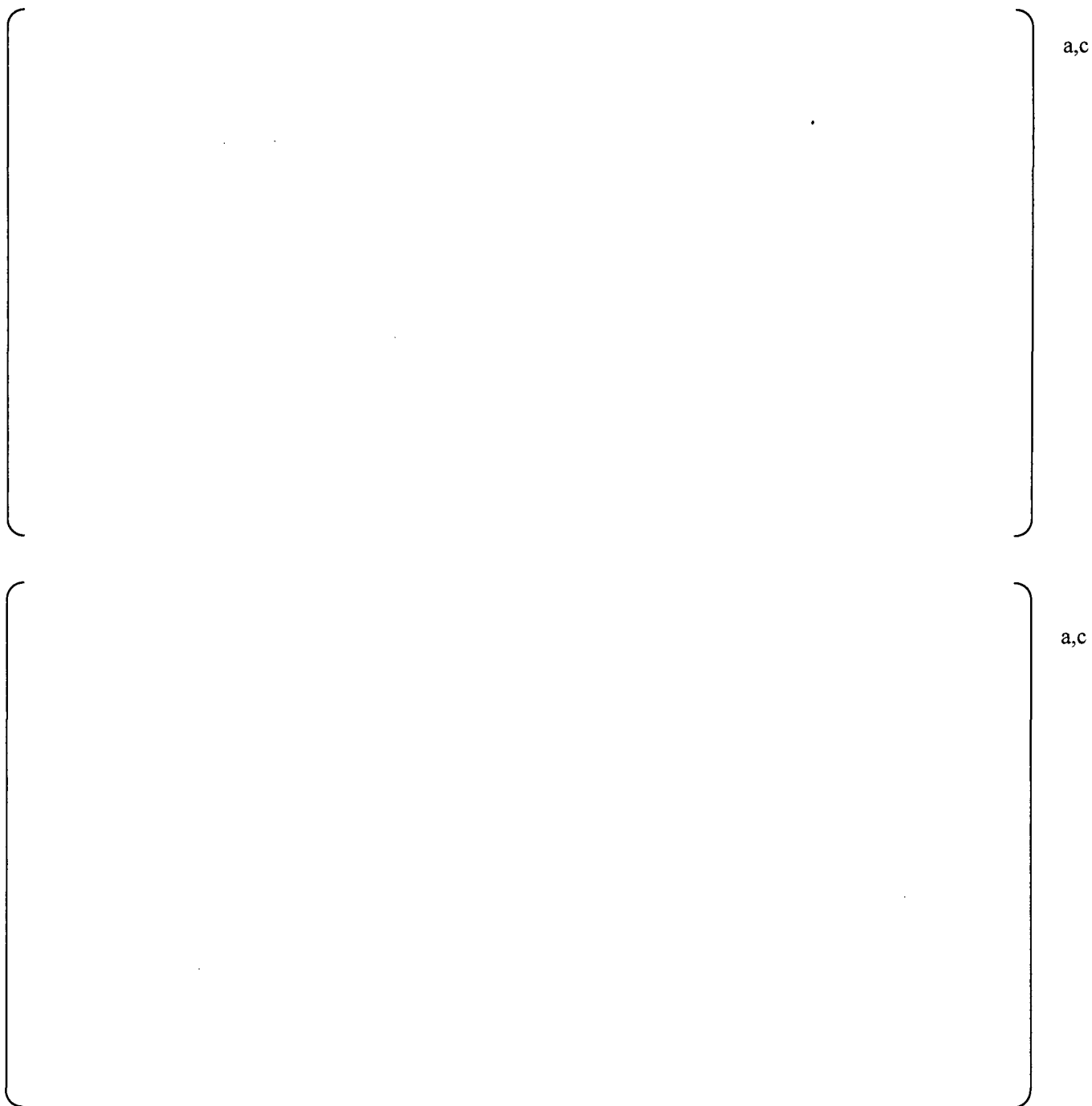


Figure G-11: PSD comparison at 790 MWe for pressure sensor data (black curves) and least squares predictions with bias and uncertainty added (red curves), for P15 (top) and P16 (bottom).

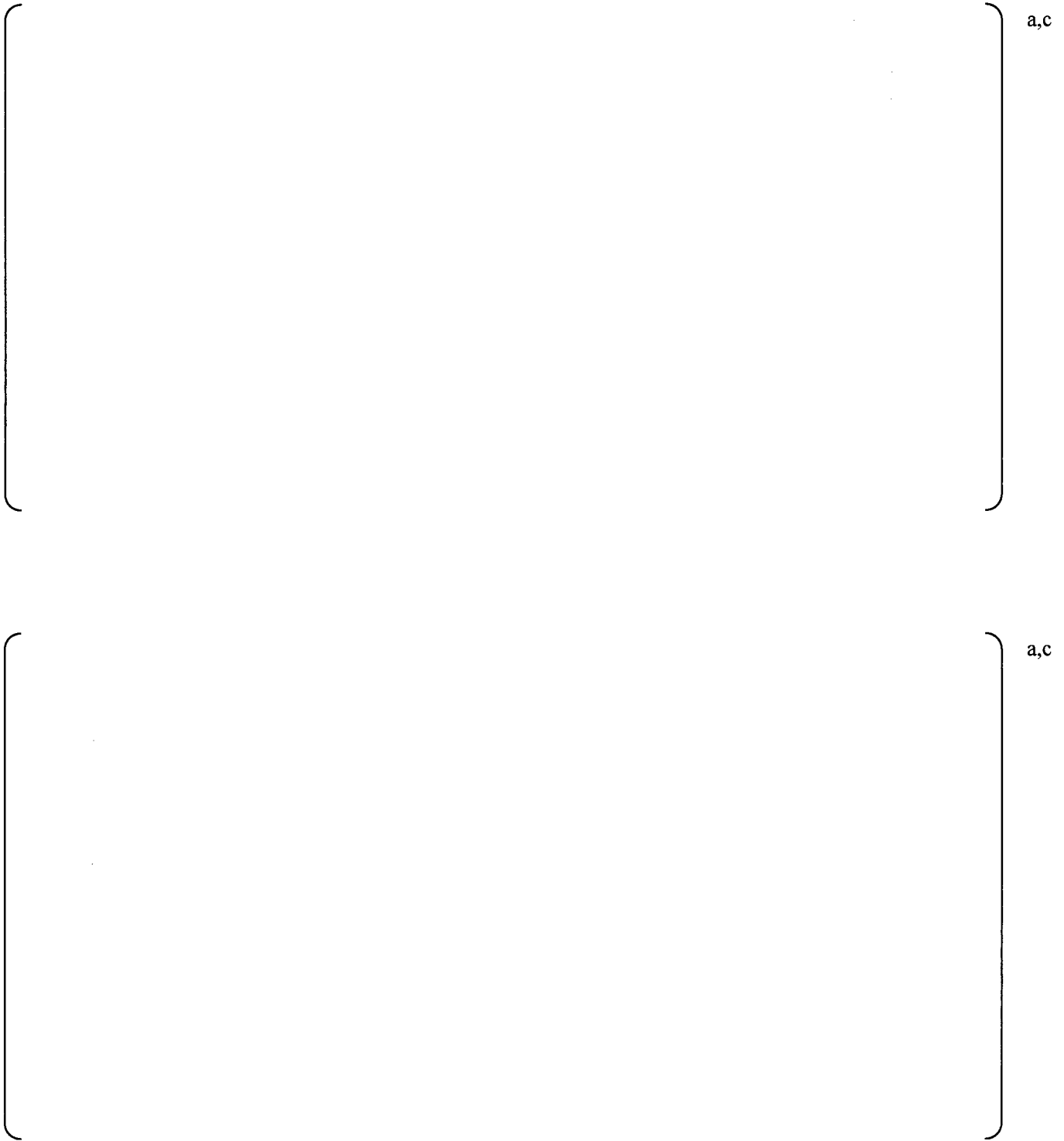


Figure G-12: PSD comparison at 790 MWe for pressure sensor data (black curves) and least squares predictions with bias and uncertainty added (red curves), for P17 (top) and P18 (bottom).



Figure G-13: PSD comparison at 790 MWe for pressure sensor data (black curves) and least squares predictions with bias and uncertainty added (red curves), for P19 (top) and P20 (bottom).



Figure G-14: PSD comparison at 790 MWe for pressure sensor data (black curves) and least squares predictions with bias and uncertainty added (red curves), for P21 (top) and P22 (bottom).



Figure G-15: PSD comparison at 790 MWe for pressure sensor data (black curves) and least squares predictions with bias and uncertainty added (red curves), for P23 (top) and P24 (bottom).

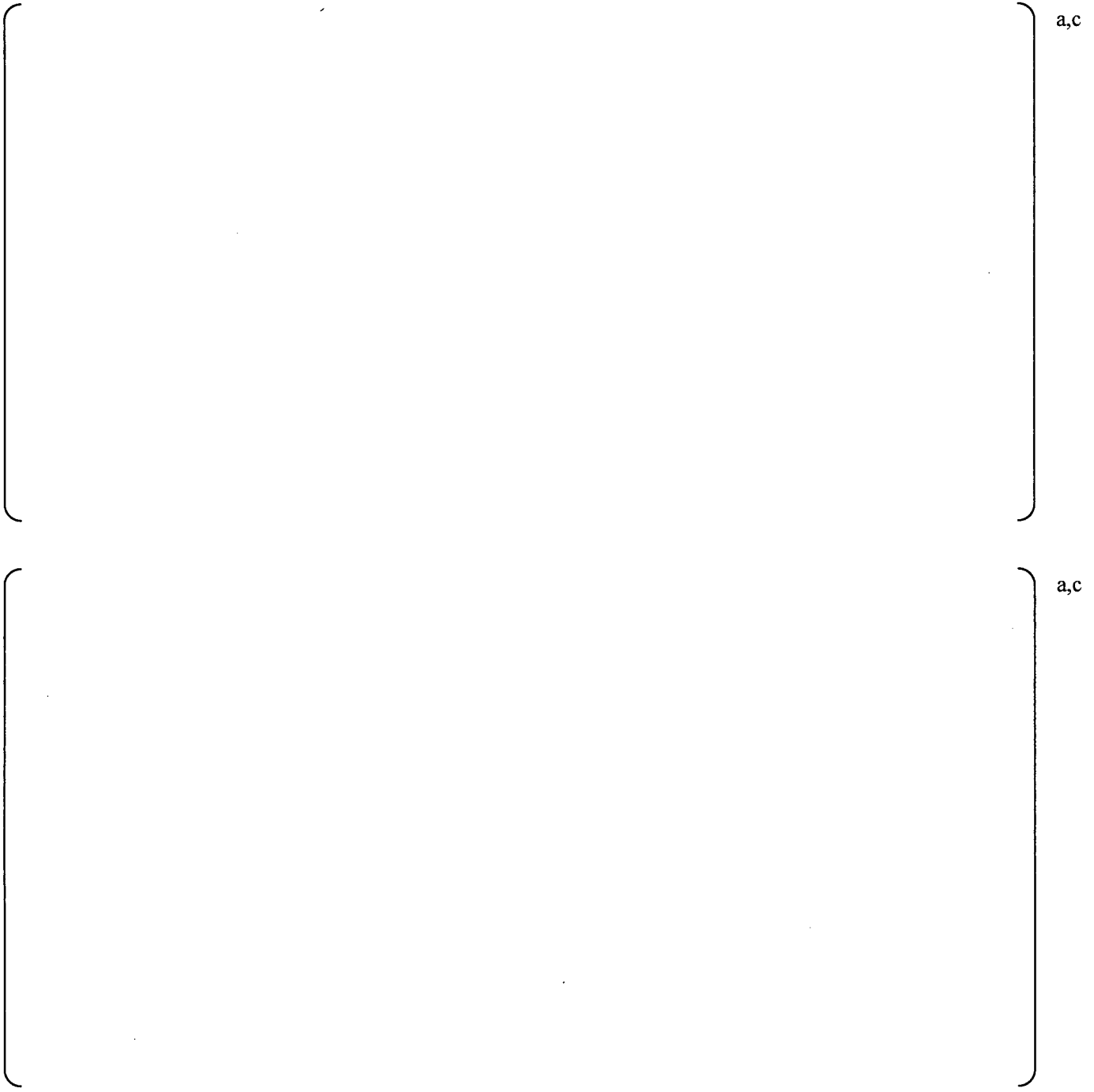


Figure G-16: PSD comparison at 790 MWe for pressure sensor data (black curves) and least squares predictions with bias and uncertainty added (red curves), for P25 (top) and P26 (bottom).



Figure G-17: PSD comparison at 790 MWe for pressure sensor data (black curves) and least squares prediction with bias and uncertainty added (red curves), for P27.

G.3 References

G.1 LAPACK Driver Routine (Version 3.0). 31 October 1999. University of Tennessee, University of California at Berkeley, NAG Ltd., Courant Institute, Argonne National Laboratory, and Rice University.

G.2 Anderson, E., Z. Bai, C. Bischof, J. Demmel, J. Dongarra, J. Du Croz, A. Greenbaum, S. Hammarling, A. McKenney, S. Ostrouchov, and D. Sorensen. 1992. LAPACK Users Guide. Society for Industrial and Applied Mathematics (SIAM): Philadelphia, PA.